

BUBBLE DYNAMICS IN BARBOTAGE AND BOILING

A Thesis

Presented to

The Faculty of Graduate Studies

The University of Manitoba

In Partial Fulfillment

of the Requirements for the Degree

Master of Science



by

NARAYANASWAMY SUBASH

February, 1973

ABSTRACT

Because of the importance of boiling heat transfer, there has recently been an increased interest in the simulation of boiling in an effort to improve our understanding of the boiling phenomenon. The present study is a further effort in this direction and compares, in more detail than heretofore attempted, the bubble dynamics in barbotage and boiling.

For the first time, bubble growth rates, under constant-pressure-supply conditions in pool barbotage and determined using high-speed cine photography, were reported. Distilled water, acetone and hexane were used as the test liquids and air as the injected gas. Bubble departure volumes and frequencies were determined by the stroboscopic method for a wide range of air flow rates for these three test liquids. This information was used in a quantitative comparison of the bubble growth rates, departure sizes and frequencies in pool barbotage and saturated pool boiling. This comparative study showed the following:

(i) The experimental bubble growth rates in saturated pool boiling lie between the growth rates determined for the two extreme cases in barbotage, viz, the

constant-volume case and the constant-pressure-supply case.

(ii) The bubble departure sizes in pool barbotage and saturated pool boiling are comparable in magnitude in the static regime (i.e., very low gas flow rates in barbotage and very low heat fluxes in boiling).

(iii) Barbotage frequency data obtained from the present work and from the literature overlap with boiling frequency data for a wide range of bubble departure diameters.

(iv) Both the barbotage data and the available boiling data indicate that in general, bubbling frequencies decrease with increasing orifice (or cavity) sizes.

As part of the above study, a theoretical analysis of the problem of bubble growth under constant-pressure-supply conditions was performed. The theoretically predicted growth rates were found to be in good agreement with the experimental data. Finally, a theoretical study to predict bubble departure sizes in boiling (in uniformly-superheated liquids) was performed on the basis of a simple model developed in barbotage, with encouraging results.

ACKNOWLEDGEMENTS

This study was carried out under the direction of Professor G.E. Sims whose advice and support were invaluable.

Thanks are due to Mr. Oscar Tonn and Mr. Sherif Barakat for helpful discussions and to Mr. L. Wilkins of the Mechanical Engineering Machine Shop for his help in building the experimental apparatus.

Finally, the support provided by the National Research Council of Canada through Operating Grant A5185 is gratefully acknowledged.

TABLE OF CONTENTS

	Page
ABSTRACT	iii
ACKNOWLEDGEMENTS	v
TABLE OF CONTENTS	vi
LIST OF FIGURES	x
LIST OF TABLES	xiv
NOMENCLATURE	xvi
CHAPTER 1 INTRODUCTION	1
1.1 Background	1
1.2 Scope of Present Investigation	3
CHAPTER 2 REVIEW OF LITERATURE ON BUBBLE DYNAMICS IN BOILING AND BARBOTAGE	6
2.1 Barbotage Bubble Dynamics	6
2.1.1 Introduction	6
2.1.2 Bubble growth rate	7
2.1.3 Frequency and departure size	12
2.2 Nucleate Boiling Bubble Dynamics	22
2.2.1 Introduction	22
2.2.2 Bubble growth rate	24
2.2.3 Bubble departure size	25

Table of Contents	(Continued)	Page
	2.2.4 Frequency	28
	2.3 Barbotage as an Analog of Boiling	31
CHAPTER 3	EXPERIMENTAL INVESTIGATION TO DETERMINE BUBBLE GROWTH RATES UNDER CONSTANT- PRESSURE CONDITIONS	35
	3.1 Introduction	35
	3.2 Apparatus	35
	3.2.1 Description of apparatus	35
	3.2.2 Selection of experimental liquids	39
	3.2.3 Photographic and strobo- scopic apparatus	40
	3.3 Procedure	41
	3.3.1 Growth rate determination	41
	3.3.2 Calculation of instantaneous volume of a bubble	45
	3.3.3 Bubbling frequency and departure volumes	45
	3.4 Results and Discussion	46
	3.4.1 Photographic observations	46
	3.4.2 Bubble frequency data	50
	3.4.3 Bubble volume data	50
	3.4.4 Bubble growth data	58

Table of Contents (Continued)		Page
CHAPTER 4	COMPARISON OF BARBOTAGE AND NUCLEATE BOILING BUBBLE DYNAMICS	72
	4.1 Comparison of Bubble Growth Rates	72
	4.2 Bubble Departure Size	77
	4.3 Bubble Frequency	81
CHAPTER 5	THEORETICAL ANALYSIS OF THE PROBLEM OF BUBBLE GROWTH UNDER CONSTANT-PRESSURE- SUPPLY CONDITIONS FROM A SUBMERGED ORIFICE	83
	5.1 Theoretical Formulation of the Problem	83
	5.2 Method of Solution	86
	5.3 Results and Discussion	87
CHAPTER 6	APPLICATION OF BARBOTAGE THEORY TO BOILING FOR THE PREDICTION OF DEPARTURE DIAMETERS	104
	6.1 Background	104
	6.2 Development of the Model	106
	6.3 Evaluation of V_{EXP}	108
	6.4 Evaluation of V_{FIN}	112
	6.4.1 Detachment stage	112
	6.4.2 Solution of equation of motion	114

Table of Contents	(Continued)	Page
	6.4.3 Growth constant	114
	6.5 Results and Discussion	115
CHAPTER 7	SUMMARY AND CONCLUSIONS	122
REFERENCES		125
APPENDICES		130
	APPENDIX A - Forces Acting on a Bubble Forming at an Orifice (or a Nucleating Cavity)	131
	APPENDIX B - Physical Properties of Water, Acetone and Hexane	134
	APPENDIX C - Calculation of Bubble Volume	135
	APPENDIX D - Method for Finding the True Flow Rate of Air Through the Orifice	138
	APPENDIX E - Bubble Growth Rate Data	140
	APPENDIX F - Further Discussion of Bubble Growth Rates	167
	APPENDIX G - Growth Equation $R^* = \theta^n$ Used for Barbotage Data	176
	APPENDIX H - Equation of Motion for an Expanding Bubble	179

LIST OF FIGURES

Figure		Page
2.1	Bubbling regimes in barbotage	15
2.2	Data for bubble frequency vs diameter from literature	30
3.1	Schematic of experimental set-up	36
3.2	Details of container assembly and orifice plate	38
3.3	Arrangement of photographic equipment	42
3.4	Cine pictures of bubbles of Category I	47
3.5	Cine pictures of bubbles of Category II	48
3.6	Frequency data for air-water system	51
3.7	Frequency data for air-acetone and air- hexane systems	52
3.8	Bubble volume as a function of mean air flow rate for air-water system	56
3.9	Bubble volume data for air-acetone and air-hexane systems	57
3.10	Bubble growth data in water (air flow rate - $4.07 \text{ cm}^3/\text{sec}$)	59
3.11	Bubble growth data in water (air flow rate - $32.5 \text{ cm}^3/\text{sec}$)	60
3.12	Bubble growth data in water (air flow rate - $60.5 \text{ cm}^3/\text{sec}$)	61
3.13	Bubble growth data in acetone (air flow rate - $8.64 \text{ cm}^3/\text{sec}$)	62
3.14	Bubble growth data in acetone (air flow rate - $19.65 \text{ cm}^3/\text{sec}$)	63

Figure	Page
3.15 Bubble growth data in acetone (air flow rate - 32.4 cm ³ /sec)	64
3.16 Bubble growth data in hexane (air flow rate - 8.1 cm ³ /sec)	65
3.17 Bubble growth data in hexane (air flow rate - 15.6 cm ³ /sec)	66
3.18 Bubble growth data in hexane (air flow rate - 30.4 cm ³ /sec)	67
4.1 Growth rate results for barbotage and boiling	76
4.2 Comparison of measured and calculated values of D_d/D_o	80
4.3 Comparison of frequencies in barbotage and boiling	82
5.1 Theoretical bubble growth curve for E = 0.0	88
5.2 Theoretical bubble growth curve for E = 0.001	89
5.3 Theoretical bubble growth curve for E = 0.005	90
5.4 Theoretical bubble growth curve for E = 0.008	91
5.5 Theoretical bubble growth curve for E = 0.01	92
5.6 Comparison of experimental and theoretical bubble growth rates for water - air flow rate 4.07 cm ³ /sec	94
5.7 Comparison of experimental and theoretical bubble growth rates for water - air flow rate 32.5 cm ³ /sec	95
5.8 Comparison of experimental and theoretical bubble growth rates for water - air flow rate 60.5 cm ³ /sec	96
5.9 Comparison of experimental and theoretical bubble growth rates for acetone - air flow rate 8.64 cm ³ /sec	97
5.10 Comparison of experimental and theoretical bubble growth rates for acetone - air flow rate 19.65 cm ³ /sec	98

Figure	Page
5.11 Comparison of experimental and theoretical bubble growth rates for acetone - air flow rate 32.4 cm ³ /sec	99
5.12 Comparison of experimental and theoretical bubble growth rates for hexane - air flow rate 8.1 cm ³ /sec	100
5.13 Comparison of experimental and theoretical bubble growth rates for hexane - air flow rate 15.6 cm ³ /sec	101
5.14 Comparison of experimental and theoretical bubble growth rates for hexane - air flow rate 30.4 cm ³ /sec	102
6.1 Mechanism of bubble formation	107
C.1 Enlarged bubble outline for volume calculations	136
E.1 Bubble growth profiles - W-L-3	158
E.2 Bubble growth profiles - W-M-3	159
E.3 Bubble growth profiles - W-H-3	160
E.4 Bubble growth profiles - A-L-2	161
E.5 Bubble growth profiles - A-M-3	162
E.6 Bubble growth profiles - A-H-1	163
E.7 Bubble growth profiles - H-L-2	164
E.8 Bubble growth profiles - H-M-3	165
E.9 Bubble growth profiles - H-H-3	166
F.1 Bubble growth curves of Category I and Category II bubbles (water)	168
F.2 Bubble growth curves of Category I and Category II bubbles (acetone)	169
F.3 Bubble growth curves of Category I and Category II bubbles (hexane)	170

Figure		Page
F.4	Bubble growth curves corresponding to the two departure criteria (water)	171
F.5	Bubble growth curves corresponding to the two departure criteria (acetone)	172
F.6	Bubble growth curves corresponding to the two departure criteria (hexane)	173

LIST OF TABLES

Table		Page
2.1	Comparison of Eqn. 2.8 with experimental data of Howell and Siegel and Hatton and Hall	27
3.1	Conditions for bubble formation experiments	44
3.2	Bubble volume and frequency data for air-water system	53
3.3	Bubble volume and frequency data for air-acetone system	54
3.4	Bubble volume and frequency data for air-hexane system	55
3.5	Growth exponents for barbotage bubbles, obtained in present work	71
4.1	Growth exponents for bubbles in saturated pool boiling of water at atmospheric pressure	75
6.1	Properties of water and water vapour	116
6.2	Properties of acetic acid	117
6.3	Theoretical growth parameters for acetic acid	118
6.4	Theoretical growth parameters for water	119
6.5	Bubble properties at break-off in uniformly-superheated liquids	120
E.1	Bubble growth data for water	142
E.2	Bubble growth data for acetone	148
E.3	Bubble growth data for hexane	153

Table		Page
F.1	Values for bubble growth exponent n for the two cases discussed in Appendix F	175
G.1	Growth exponents for barbotage bubbles obtained by the two methods discussed in Appendix G	178

NOMENCLATURE

a	Bubble growth constant	
A	Area	cm ²
c	Speed of sound in gas	cm/sec
C _d	Drag coefficient	(dimensionless)
C	Coefficient of discharge	(dimensionless)
C _g	Specific heat of gas	cal/gm °C
C _L	Specific heat of liquid	cal/gm °C
D	Diameter	cm
f	Frequency of bubbling	$\frac{1}{\text{sec}}$ or $\frac{1}{\text{min}}$
g	Gravitational acceleration	cm/sec ²
h _{fg}	Latent heat of vaporisation	cal/gm
k	Thermal conductivity of liquid	$\frac{\text{cal}}{\text{sec cm } ^\circ\text{C}}$
K	Orifice constant	(dimensionless)
L	Length of orifice channel	cm
M	Virtual mass of bubble	gm
M'	Velocity of approach factor	(dimensionless)
n	Bubble growth exponent	(dimensionless)
N _C	Dimensionless group	(see Eqn. 2.1)
N _R	Dimensionless group	(see Eqn. 2.2)
p	Pressure	gm/cm sec ²
Δp	Pressure difference	gm/cm sec ²
q	Heat flux	cal/cm sec ²

Q	Mean (volumetric) air flow rate	cm ³ /sec
r'	Radius	(see Eqn. H.1.)
R	Radius (without subscript, radius of bubble)	cm
R*	R/R ₀	
T	Saturation temperature	°C
ΔT	Superheat (T _s - T _{sat}) required to form bubbles	°C
T _A	Growth time	sec
t	Time	sec
t*	Dimensionless time	$t \left(\frac{\sigma}{\rho_L R_0^3} \right)^{1/2}$
U _∞	Departure velocity of bubble	cm/sec
v	Velocity	cm/sec
v _{fg}	Difference in specific volume between liquid and vapour phases	cm ³ /gm
V	Volume	cm ³
x	Distance moved by bubble base	cm

Greek Symbols

ρ	Density	gm/cm ³
μ	Dynamic viscosity	gm/cm sec
γ	Ratio of specific heats at constant pressure, and constant volume for gas	
ν	Kinematic viscosity	cm ² /sec
β	Growth constant	(see Eqn. 6.17)
σ	Surface tension	dynes/cm
α	Thermal diffusivity of liquid	cm ² /sec
∇	Gradient	

ϕ	Velocity potential
∞	At a large distance
θ	Contact angle or t/t_d
ψ	Constant associated with the virtual mass of a bubble

Subscripts

b	Bubble
c	Chamber
crit	Critical
d	Departure
eq	Equivalent
e	Relating to expansion stage
EXP	At the end of the expansion stage
f	Formation
fg	Evaporation
FIN	Final
g	Gas
M	Quasi-static
mix	Mixture
o	Orifice
s	Surface (or wall)
sat	Saturation
TRANS	Translation
v,vap	Vapour
w	Waiting

CHAPTER 1

INTRODUCTION

1.1 Background

Boiling heat transfer is an extremely important method of heat removal, particularly in systems, such as nuclear reactors and liquid propellant rocket motors which involve high heat flux densities. However, boiling is a complex phenomenon.

The complexity arises out of the fact that boiling is a process in which several interdependent phenomena occur simultaneously. Thus, bubble growth depends on heat transfer, while the heat transfer depends, among other things, on agitation due to bubble growth and motion. In addition, the process depends on such stochastic factors as nucleation, distribution of bubbling sites, and their condition at the start of boiling. It is obvious that in order to gain a full understanding of this process an analytic approach (the word 'analytic' is used here to mean 'resolving into constituent parts'), in which the interactions between the component phenomena are severed, is desirable. In particular, one would like to separate the phenomena of heat transfer and bubble growth those

being the ones whose interaction is largely reciprocal). One would also like to exercise independent control over the location of the bubbling sites and over the nucleation process, thus removing the stochastic aspects of the situation.

With the above in mind, several authors have sought to improve the understanding of heat transfer across bubble-stirred boundary layers by simulating nucleate boiling using "barbotage" or electrolysis to produce bubbles on the heat transfer surface. The term "barbotage" as used here is defined as the bubbling of a gas through a drilled or porous surface into a liquid in which the gas is essentially insoluble. Barbotage systems are attractive for the study of bubble-stirred boundary layers, because, in contrast with boiling, the bubble generation rate is independent of the rate of heat transfer and can be accurately controlled and measured. Further, in boiling, there are heat transfer mechanisms involving both latent heat effects and heat transfer through the liquid [33]; in barbotage, in general, only heat transfer through the liquid is present. This is an advantageous simplification which could aid in the understanding of bubble-stirred boundary layers.

When considering barbotage as an analog of boiling, various aspects may be examined. These may be purely hydrodynamic or may include heat transfer. Zuber [46], Wallis [41] and Kudirka [22] have noted the similarities in

appearance of the bubbling flow regimes in barbotage and saturated nucleate pool boiling; the similarity of initiation [41] and of growth rates and growth times have also been pointed out. Several investigators [1,33,42] have used barbotage systems to simulate the boiling critical heat flux. Some investigators [1,34] have concentrated on heat-transfer coefficients, comparing these coefficients in boiling and barbotage and examining in considerable detail the heat transfer mechanisms in these two systems.

Because of this very considerable interest shown in the simulation of boiling by barbotage systems, the time appeared opportune to examine and compare, in more detail than here-to-fore attempted, the hydrodynamics of bubbles in barbotage and boiling. The investigation presented in this thesis was undertaken for this purpose. The hydrodynamic quantities examined included bubble growth rates, departure diameters and frequency of bubbling. The study concentrated exclusively on 'pool' barbotage and 'pool' boiling systems.

1.2 Scope of Present Investigation

The present investigation can be divided into four main parts:

(i) In order to make a quantitative comparison of the bubble growth rates in barbotage and boiling, experimental data were needed. While data for saturated pool

boiling (especially of water) were available in abundance from the literature, a survey of barbotage literature indicated that no such results were available to date. It was, however, quite evident that at least in one extreme case of pool barbotage, namely, the "constant-flow-rate case"[†], the growth rate can be theoretically predicted with confidence, since in this case, the volume of the bubble increases linearly with time. The other extreme case, namely, the "constant-pressure-supply case"[†] is more complex because of the unsteady nature of gas flow into the bubble during its formation time. It was therefore decided to conduct experiments for this case to determine the growth rate. Distilled water, acetone and hexane were used as the experimental liquids and air was the injected fluid. The experimental conditions for this study are summarised in Table 3.1, Chapter 3. Other important hydrodynamic quantities obtained with the experimental apparatus are the frequency of bubbling and bubble departure size. The experimental results are presented in Figs. 3.6 through 3.18.

(ii) The above experimental results were used for a quantitative comparison with the corresponding hydrodynamic quantities in boiling. The main results of such a comparative study are shown in Figs. 4.1, 4.2 and 4.3.

[†] See Chapter 2, Review of Literature.

(iii) A theoretical analysis was made to predict the bubble growth rate for the aforesaid constant-pressure-supply case. The analysis developed herein applies to the dynamic growth of an idealized gas bubble under the influence of gas injection through an orifice without any heat or mass transfer into the bubble from the surrounding liquid. The liquid is assumed to be inviscid in the analysis. The theoretical equation derived is Eqn. 5.3 while its comparison with the experimental results is presented in Figs. 5.6 through 5.14.

(iv) A theoretical analysis was made to predict the bubble departure size in nucleate boiling, in uniformly-superheated liquids, on the basis of the 'two stage' bubble formation theory proposed by Kumar *et al.* [23] for barbotage. This material is presented in Chapter 6.

CHAPTER 2

REVIEW OF LITERATURE ON BUBBLE DYNAMICS IN BOILING AND BARBOTAGE

2.1 Barbotage Bubble Dynamics

2.1.1 Introduction

The injection of a gas into a liquid through a submerged orifice results, under certain conditions, in the periodic formation of discrete gas bubbles of approximately equal volume. The study of the formation of such bubbles has been the subject of numerous investigations [23] particularly because of the importance of that phenomenon in connection with distillation, absorption, extraction and other mass and energy transfer processes. Such investigations have been concerned principally with the determination (theoretical and experimental) of the departure size of the bubbles produced under various liquid and gas flow conditions. This is because of the importance of knowing the size of the bubbles rising through the liquid in the evaluation of the overall mass or energy transfer rates for the bubbling process. However, the study of the motion of the gas-liquid interface, during the formation of a bubble under different liquid and gas

flow conditions has received limited attention to date [7,8,26] and the state of knowledge in this area is far from satisfactory.

The ensuing review of the available literature is confined to bubble formation studies from submerged orifices and made under two separate headings, namely, 'bubble growth rate' and 'frequency and departure size'.

2.1.2 Bubble growth rate

"Bubble growth rate" can be defined as the change in size (normally radius or volume) of a bubble with time during its formation. This change in size, resulting from the motion of the gas-liquid interface during formation of a bubble, can, in general, be considered to be governed by the fluid dynamic and interfacial forces due to:

- (i) momentum of the injected gas stream,
- (ii) inertia of the displaced liquid,
- (iii) drag on the interface associated with the motion of the liquid relative to the bubble,
- (iv) buoyancy, and
- (v) interfacial tension.

The system variables such as the gas injection rate, the liquid and gas physical properties, the liquid depth, the orifice size and shape and the local acceleration due to gravitational action which have been observed to influence the bubble formation process derive their importance from their effect upon the aforementioned

forces governing the motion of the interface.

Because of the inherent instability of the interface that is generated during the gas injection, the gas flow is periodically interrupted by the termination of the formation of one bubble followed by the initiation of the formation of the succeeding bubble. It has been found [14] that the pulsating character of the flow imposed by the periodic formation of discrete bubbles produces an interaction or coupling of the bubble formation mechanism with the flow of gas. Thus, in addition to the variables directly associated with the forces governing the motion of the interface during the formation of a bubble, the fluid dynamic characteristics of the entire gas supply system up to the exit plane of the orifice can also have a significant influence upon the process of bubble formation. Such parameters include the length/diameter ratio of the orifice channel and the volume of the ante-chamber[†] supplying gas to the orifice.

An accurate evaluation of the dynamic forces acting at the interface requires an adequate knowledge of the flow of gas into the bubble. Unfortunately, the aforementioned coupling and the incomplete understanding of the interfacial phenomena involved have caused considerable difficulty in accurately defining the flow into a bubble for a given system, and as stated earlier, very little work

[†] The volume of the ante-chamber is defined as the volume between the orifice and that point in the gas stream where a large pressure drop occurs.

has been done in this regard. This work is briefly discussed below after some preliminary observations regarding the two limiting cases encountered in barbotage systems.

As indicated in Sec. 1.2, there are two limiting cases of gas flow into a bubble during its formation, which may be reasonably well defined. One case, commonly referred to as the "constant flow rate" case, pertains, as the name implies, to bubble formation in which the rate of gas flow into a bubble is essentially constant. Such has been found to be the case, for example, for bubble formation at the tip of a long capillary tube. The flow rate of gas is governed by the pressure drop in the capillary, and perhaps some controlling device upstream of the capillary. Nevertheless, the pressure fluctuations which result from bubble formation at the tip of the capillary or at the orifice are not transmitted upstream. The flow is essentially independent of the bubble formation process and, as such, there is no coupling. The bubble growth rate in the above case can be easily established, since by definition, the volume of the bubble increases linearly with time.

The other limiting case of flow, referred to as the "constant pressure supply" case, pertains to bubble formation at an orifice which is supplied with gas from an antechamber at constant pressure. That case is approximated, in practice, when an orifice is supplied with gas by a very

large ante-chamber. The rate of gas flow for such a system has been found to vary throughout the formation period [7,8] as the result of a variation of the pressure drop across the orifice. Such a system can be considered to be one for which the flow is independent of the ante-chamber volume.

Davidson and Schüler [7,8] were the first to propose a theory for the mechanism of bubble formation for the above case. They set up an 'orifice equation' which describes the instantaneous flow of gas into the bubble and introduced it into the general force balance equation for the bubble in order to predict the departure size. Reasonable agreement was obtained between experiment and theory for the departure size but no results were given comparing the theoretical and experimental growth rates.

Any actual bubble formation system will probably operate under conditions between the aforementioned limiting cases of flow and, therefore, will exhibit, to some extent, a coupling of the bubble formation mechanism with the gas supply system.

Hughes *et al.* [14] have derived two dimensionless groups to characterize the influence of the gas supply system upon bubble formation by considering the acoustical capacitance of the ante-chamber and the resistance to flow of the orifice channel. They are:

$$N_c = \frac{g(\rho_L - \rho_g)V_c}{A_o \rho_g c^2} \quad (2.1)$$

$$N_R = \frac{L}{D_o} \quad (2.2)$$

where,

g = acceleration due to gravity

ρ_L = liquid density

ρ_g = gas density

V_c = the ante-chamber volume

A_o = orifice cross-sectional area

c = the velocity of sound in gas

L = the length of the orifice

D_o = the orifice diameter.

Values of the ante-chamber volume which make $N_c \ll 1$ approximate the condition of constant flow rate whereas those which make $N_c \gg 1$ approximate the condition of constant-pressure-supply. The influence of the orifice channel, on the other hand, has been found to be significant only in the case of capillaries, when $N_R > 100$. Though not thoroughly tested, the parameters N_c and N_R have provided one means of characterising the gas injection systems for at least the two limiting cases of flow.

L'Ecuyer and Murthy [26] made an analytical investigation of the problem of bubble formation from a submerged orifice, in the presence of heat transfer into the bubble.

The equations of continuity, momentum and energy along with the equation of state of the gas in the bubble were solved numerically for specified flow conditions. Their bubble growth rate predictions were reasonably close to their experimental values. However, their analysis is applicable only to systems exhibiting a coupling of the bubble formation mechanism with the gas supply system. This severe limitation is a result of the form of their continuity equation for the rate of mass flow into the bubble, since it requires a knowledge of the ante-chamber pressure fluctuations during a bubble cycle. The authors resorted to experiment for obtaining this information but it is evident that this form of the equation is inapplicable for the case of a constant pressure ante-chamber.

A simple theoretical analysis was made in the present work for the special case of bubble formation under constant-pressure-supply systems and is presented in Chapter 5.

2.1.3 Frequency and departure size

The frequency of bubble generation (i.e., the number of bubbles generated per second from an orifice) and the departure volume of a bubble (also called the 'terminal bubble volume') are closely related in barbotage systems. Either may be considered the principal dependent variable in bubble formation studies. The more readily controlled independent variable is the rate of flow of gas through the system. In many cases, the instantaneous rate of gas flow

into a bubble is different from the mean gas flow rate and therefore also becomes in such instances, a dependent variable. For convenience, references hereafter to gas flow rate implies the mean flow rate. Because of the dependence of the forces due to liquid inertia, viscous drag and buoyancy upon the volume or the volumetric growth rate of the bubble, the volumetric gas flow rate has been employed consistently in the literature for describing the rate of gas injection. The important factors, then, which might be expected to affect the terminal volume (and hence the frequency) are:

- (i) gas flow rate,
- (ii) physical properties of the liquid,
- (iii) physical properties of the injected gas,
- (iv) effect of the motion of the liquid relative to the bubble,
- (v) liquid depth above the orifice, and
- (vi) the size, material and geometry of the orifice.

The effect of each of the above is briefly discussed below.

Gas flow rate:

The influence of the mean volumetric gas flow rate, Q , hereinafter referred to simply as the "gas flow rate", upon the terminal bubble volume can be divided into three regimes [14,40] characterising the operative forces, namely:

- (a) "static"
- (b) "dynamic"
- (c) "turbulent interaction"

These regimes are depicted qualitatively in Fig. 2.1.

At very low gas flow rates ($<1 \text{ cm}^3/\text{sec}$) the bubble formation process is essentially static, with the terminal volume V_d of the bubbles being determined by a balance between the static forces due to buoyancy and surface tension. Thus, V_d is given approximately by

$$V_d = \frac{\pi D_o \sigma}{g(\rho_L - \rho_g)} \quad (2.3)$$

where σ is the surface tension of the liquid. For a given orifice and liquid, V_d is reported to be essentially independent of variations in gas flow rate [40] although the value that has been measured is somewhat different from that predicted by the above equation. Next, it will be noted that V_d is related to the gas flow rate, Q , by

$$V_d \cdot f = Q \quad (2.4)$$

and therefore, the frequency of formation, f , varies linearly with the gas flow rate in the static regime.

As the gas flow rate is increased, the dynamic forces become operative in governing the rate of growth of a bubble and its terminal volume. Thus, in the dynamic regime, there is a range of gas flow rate for which both

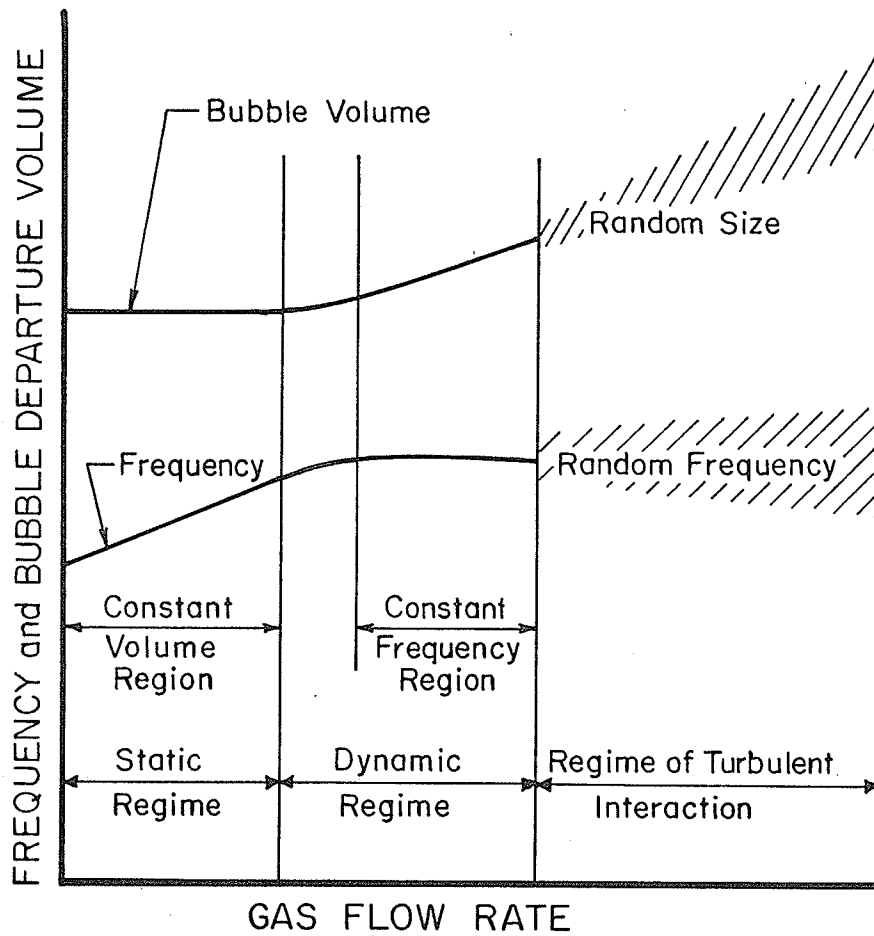


Fig. 2.1 Bubbling regimes in barbotage

V_d and f increase with the flow rate [5]. At some value of gas flow rate, the frequency becomes approximately constant and a further increase in Q results in a linear increase in V_d as indicated by Eqn. 2.4. Both the static and dynamic regimes may be said to yield regular bubble formation, that is, the periodic formation for a given flow rate.

In the dynamic regime, the occurrence of a constant frequency of formation above a particular value of the gas flow rate has been attributed as largely due to viscous retardation and/or coalescence of the bubbles at the orifice. In very viscous liquids, the constant frequency condition occurs at much lower frequencies than in relatively inviscid liquids.

When the gas flow rate is increased further, the formation of bubbles is characterised by a randomness both in the size as well as in the frequency of formation. It is this regime of flow that is referred to as the turbulent regime [28].

Of course, the lines of demarcation between the static, dynamic and turbulent regimes are not sharp, and the actual flow rates at which transitions occur from one regime to another are apparently dependent upon the physical properties of the liquid and the orifice size.

Liquid physical properties:

The physical properties of the liquid which influence

the formation process are the density, the surface tension, and the dynamic viscosity.

In the static regime, the terminal bubble volume should vary inversely with the liquid density (since $\rho_L \gg \rho_g$) as indicated by Eqn. 2.3. This trend has been verified within the limitation of some variation of other properties of the liquid in addition to the density. In the dynamic regime, however, the liquid inertia force, which is proportional to the liquid density tends to retard the bubble at the orifice, thus increasing the final bubble volume. The net effect of those two opposing trends has been experimentally observed to cause the terminal bubble volume to vary approximately as ρ_L^{-n} where n varied from 1/10 to 1/3. Density effects are thus relatively small. For very viscous liquids the dynamic inertia force does not come into effect as early as the viscous drag force, and consequently in such liquids, V_d varies as $\rho_L^{-3/4}$ for low gas flow rates in the dynamic regime.

The surface tension force on the bubble is particularly important in the static regime and it has been found that V_d varies directly as σ as would be expected from Eqn. 2.3.

In the dynamic regime, the latest experimental evidence indicates [23] that for the constant-flow-rate case, the surface tension has a large influence on the bubble volume at low and medium flow rates but becomes

insignificant as the flow rate increases. At constant-pressure conditions, recent works (reviewed in [23]) indicate that the surface tension variation has negligible effect for small orifice diameters or high flow rates and for higher orifice diameters, the influence is more pronounced at small flow rates.

The influence of liquid viscosity arises from the viscous drag force acting on the interface. There should be no influence of viscosity on the terminal bubble volume in the static regime and that fact has been demonstrated [3,40]. In the dynamic regime, recent work by Kumar *et al.* [23] indicates that

- (a) the effect of viscosity on bubble volume is large at higher flow rates, and
- (b) the effect of viscosity is large for liquids of low surface tension and where orifices of small diameter are used.

Gas properties:

There has been no systematic study of the influence of gas properties. The gas density appears in the analysis either in the virtual mass term or in the buoyancy term (see Chapter 6). It is generally omitted from the analysis on the assumption that it is negligible when compared with the liquid density. The viscosity of the gas has again little influence on the bubble volume. It should however, be mentioned here that the dimensionless parameter N_c ,

defined in Eqn. 2.1, indicates that the gas density and the acoustic speed in the gas may be important in characterising the type of flow into the bubble resulting for a given system. For a perfect gas:

$$\rho_g c^2 = \gamma p_c \quad (2.5)$$

where γ is the ratio of the specific heats and p_c the chamber pressure. Therefore, N_c is dependent upon the specific heat ratio for the gas and the pressure of the gas in the ante-chamber.

Liquid motion:

The forces acting on the bubble as a result of motion of the liquid relative to the bubble can arise from induced or forced liquid motion. For the present work, there is interest only in the induced convective motion.

Considering a liquid essentially at rest with respect to the orifice, there is motion of the liquid which is induced as a result of the growth and rise of the gas bubbles. Evidently, a liquid bath of infinite size would minimize the effect of such induced liquid motion. In the use of the liquid containers of finite dimensions, it has been found that there is no significant change in the size of the bubbles formed for container diameters greater than approximately 8 bubble diameters [40]. The effect of the induced liquid motion upon the bubble volume was observed to be significant when the orifice projected upwards into the

liquid bath. The liquid could consequently move upwards at the base of the bubble causing an additional force on the bubble which tends to reduce the bubble volume by as much as 10 per cent. When the orifice was surrounded with a ring of a diameter 1.5 times that of the bubble diameter, it was found to reduce the effect of induced liquid motion to a minimum and the ring therefore acted as an anti-circulation device.

Liquid Depth:

It has been shown [7,8] that the depth of the liquid does not influence the bubble volume or frequency provided the depth is at least equal to 2 or 3 bubble diameters.

Orifice:

The observations made below are applicable to wetted nozzles.

In the static regime, the effect of orifice diameter is such that the volume of the bubble is directly proportional to it. At higher flow rates also, the bubble volume has been reported to be a strong function of the orifice diameter [5,28]. Recently Kumar *et al.* [23], found that the effect of the orifice diameter on bubble volumes becomes negligible at high flow rates.

One of the variables associated with the orifice is the geometry of the opening. Most of the investigation has been confined to circular orifices. Krishnamurthy *et al.* (given in [23]) recently conducted experiments with orifices

of non-circular geometries. The bubble volume obtained by using a standard circular orifice of arbitrary diameter was compared with two sets of orifices of other geometries (triangular, square, etc.) chosen to have either (a) perimeters or (b) areas equal to that of the standard. Work confined to low flow rates ($<0.05 \text{ cm}^3/\text{sec}$) indicated that the bubble volumes obtained from the circular orifice did not correspond exactly with those from the non-circular orifices whether compared on an equal perimeter or equal area basis. The results for orifices of equal area were the closest. At higher flow rates up to $200 \text{ cm}^3/\text{sec}$ Ramakrishnan *et al.* [23] found that an orifice of a non-circular geometry gave bubble volumes equal to those obtained from a circular orifice of same area.

Theoretical prediction of bubble departure size:

For the two limiting cases (see Sec. 1.2), in pool barbotage systems, some theoretical models [7,23] have been proposed for predicting the bubble departure volume by evaluating the interfacial forces acting on the bubble. They differ mainly in their treatment of the different forces and the assumption used for a departure criterion. Appendix A shows the general method used by investigators in formulating the different forces. For a thorough treatment of the different models for barbotage systems Ref. 23 should be consulted.

2.2 Nucleate Boiling Bubble Dynamics

2.2.1 Introduction

It was stated in Chapter 1 that the phenomenon of nucleate boiling is of great interest mainly because of the unusually high heat-transfer coefficients associated with it. Good descriptions of the process as well as summaries of all but recent work, may be found in Jakob [21] and Westwater [44]. In brief, the phenomenon may be described as follows.

Heat is applied to a liquid, usually through a submerged surface. If the rate at which heat is supplied is sufficiently high, the liquid adjacent to the surface will become superheated, and eventually bubbles of vapour will form at certain sites on the surface. Unless the bulk of the liquid is strongly subcooled, each bubble grows by evaporation of more liquid into it, until an equilibrium of upward and downward forces is reached. It then rises to the free surface of the liquid and escapes to the atmosphere above it. If the liquid is substantially subcooled, the bubbles collapse through condensation before leaving the surface. Soon after the bubble has departed or collapsed, a new one forms at the same site, and the process repeats itself. It is usually observed that the number of active sites increases with the heat flux. At a sufficiently high heat flux, however, individual active sites can no longer be maintained, and the boiling process ceases to be nucleate.

The resulting "transition" and "film" boiling phenomena are characterised by considerably-reduced heat-transfer coefficients and are of interest only because of the danger of "burn-out" that they present. The various phases of the nucleate boiling process have received in the literature treatments ranging from theoretical to completely empirical. The phenomenon of nucleation is still poorly understood, although there has been broad agreement among various investigators on the following points:

(i) Nucleation tends to take place around certain favoured "nucleation" sites. These points may consist of patches of impurities, gas absorbed at faults in the crystal lattice, or surface defects such as pits and scratches.

(ii) If a bubble exists in a cavity, it is subject to an excess pressure due to surface tension effects. The actual value of this pressure depends on the cavity geometry and the contact angle. Further, this excess pressure relates to a superheat given by the Clausius-Clapeyron relation:

$$\Delta T = \frac{T v_{fg}}{h_{fg}} \Delta P \quad (2.6)$$

where

ΔT = superheat,

T = saturation temperature,

v_{fg} = difference in specific volume between vapour

and liquid phases,

Δp = the excess pressure, and

h_{fg} = the enthalpy of evaporation.

(iii) The surface characteristics and the nucleating cavity size are important factors controlling bubble nucleation and also departure size.

2.2.2 Bubble growth rate

Following nucleation, the bubble starts growing. Equations for bubble growth under the influence of its internal pressure alone, in the absence of heat transfer, were first derived by Lord Rayleigh [47], but the results do not fit the data for boiling. On the other hand, when the heat required for evaporating liquid into the bubble is taken into account, as for instance by Plesset and Zwick [30], Forster and Zuber [10], Dergerabedian [6], Griffith [13], and Han and Griffith [15], equations which fit the experimental data reasonably well are obtained. Of these works, the first four treat the case of spherical bubbles in uniformly-superheated infinite liquids, while the fifth treats bubbles originating from a constant-temperature wall, i.e., bubbles growing in a temperature gradient. Although the equations obtained fit the experimental data reasonably well, the underlying assumptions cannot always be justified. For instance, the work of Lummis [27], Hsu and Schmidt [16], and Moore and Mesler [29]

shows considerable fluctuations in wall temperature. Recently, Cooper and Vijuk [4] and Dzakowic and Frost [9] have continued analysis for vapour bubble growth from a wall, incorporating the combined effects of conduction of heat to or from the bulk fluid and conduction of heat from the heater wall through a thin liquid layer (the "microlayer") beneath the bubbles. The results illustrate that vapour bubble growth rate based upon liquid microlayer evaporation are similar to those given by existing theory and that microlayer evaporation may represent the major portion of vapour volume in a bubble nucleated at a heated surface.

2.2.3 Bubble departure size

It has generally been recognised that the phenomenon of bubble departure is essentially hydrodynamic in nature. As in barbotage systems, the departure volume is obtained by considering the interaction and equilibrium of the forces acting on the bubble. Fritz [12] derived the earliest expression for the diameter D_d of a bubble departing from a horizontal surface using his experimental results.

$$D_d = 0.0208 \theta \left[\frac{\sigma}{g(\rho_L - \rho_V)} \right]^{\frac{1}{2}} \quad (2.7)$$

where the contact angle θ is defined as the angle made by the interface with the solid surface, and is measured in degrees.

Other equations have been derived since, e.g., [17,25], most of them taking into account such forces as inertia, drag, etc. which were neglected by Fritz. The general method of formulating these forces are very similar to those of barbotage systems shown in Appendix A, and differ only in their detailed evaluation. Recently both Hatton and Hall [17] and Howell and Siegel [18] observed that nucleating cavity size may be an important factor influencing departure size. Hatton went on to propose an elaborate analysis for bubble departure, which agreed well with his results. A simple equation that fits the data of Howell and Siegel, and Hatton and Hall reasonably, is that of Zuber who considered the equilibrium of buoyancy and surface tension forces acting on a bubble generating from an orifice of radius R_o at low gas flow rates in barbotage:

$$D_d = \left[\frac{12R_o \sigma}{g(\rho_L - \rho_V)} \right]^{1/3} \quad (2.8)$$

Table 2.1 compares the experimental results obtained by Howell and Siegel as well as Hatton and Hall for different nucleating cavity sizes with the theoretical results obtained from Eqn. 2.8 by taking R_o to be the nucleating cavity radius. It is seen that the agreement between the computed and experimental values is reasonably good with the rms deviation being 22 per cent and the equation

Table 2.1 Comparison of Eqn. 2.8 with experimental data of Howell-Siegel and Hatton-Hall.

Diameter of Drilled Site cm	Bubble Diameter D_d (Experimental) cm	Bubble Diameter D_d (Equation 2.8) cm	$\frac{\text{Predict}}{\text{EXP}}$
0.1048†	0.296†	0.330†	1.120†
0.0772†	0.267†	0.290†	1.080†
0.0530†	0.232†	0.269†	1.160†
0.0290†	0.198†	0.218†	1.110†
0.0191†	0.192†	0.191†	0.995†
0.0097	0.124	0.152	1.225
0.0125	0.153	0.164	1.070
0.0080	0.128	0.142	1.110
0.0060	0.122	0.130	1.068
0.0049	0.107	0.098	0.915

† After Howell-Siegel
others After Hatton-Hall

generally overpredicting by 8.5 per cent on the average. It should, however, be noted that the above equation is applicable only to the static regime in barbotage and boiling (i.e., when the bubble formation rate is very low) when the inertia forces are relatively small compared with the static forces.

A further analysis of the problem of bubble departure is continued in the present work which takes into account the generally-neglected phenomenon of 'necking' (formation of a short neck connecting the bubble to the wall at departure). This is presented in Chapter 6.

2.2.4 Frequency

The frequency of bubble formation at a nucleation site is determined by two time periods; namely, the bubble growth period t_f and the waiting period t_w , which is the time required for a bubble nucleus to be conceived after the departure of the previous bubble. The frequency is given by

$$f = \frac{1}{t_w + t_f} \quad (2.9)$$

According to Jakob's early observation [21], these two time periods are approximately equal. However, more recent observations [15,18] have indicated that the waiting period may not be equal to the growth period. In fact, the equality case may be the rare exception. Some investigators,

e.g., [15], have tried to predict the waiting period by an analysis of a simplified model of the thermal layer near the heated wall, with limited success.

In nucleate boiling literature, expressions relating frequency, f , and the departure diameter, D_d , appear in abundance; a recent excellent review is available by Ivey [20]. The relationship $U_\infty = fD_d$, where U_∞ is the bubble rise velocity (i.e., the velocity at departure) was frequently used over the entire range of bubble diameters. Ivey [20] pointed out, after a detailed analysis of the experimental data, that a single relationship only approximately correlates f with D_d for all diameters encountered in boiling. The f vs D_d graph that he plotted from available data is given in Fig. 2.2. Ivey classified the experimental data into three separate regions and proposed three different correlations which fit the experimental data in each region. More experimental data and analysis are required before any valid conclusions can be drawn in regard to the above correlations. Very little experimental data are available for the case of nucleation from cavities of known geometry and size, the importance of which Hatton and Hall [17] have demonstrated. Their results for a constant heat flux, but different cavity sizes, are included in Fig. 2.2.

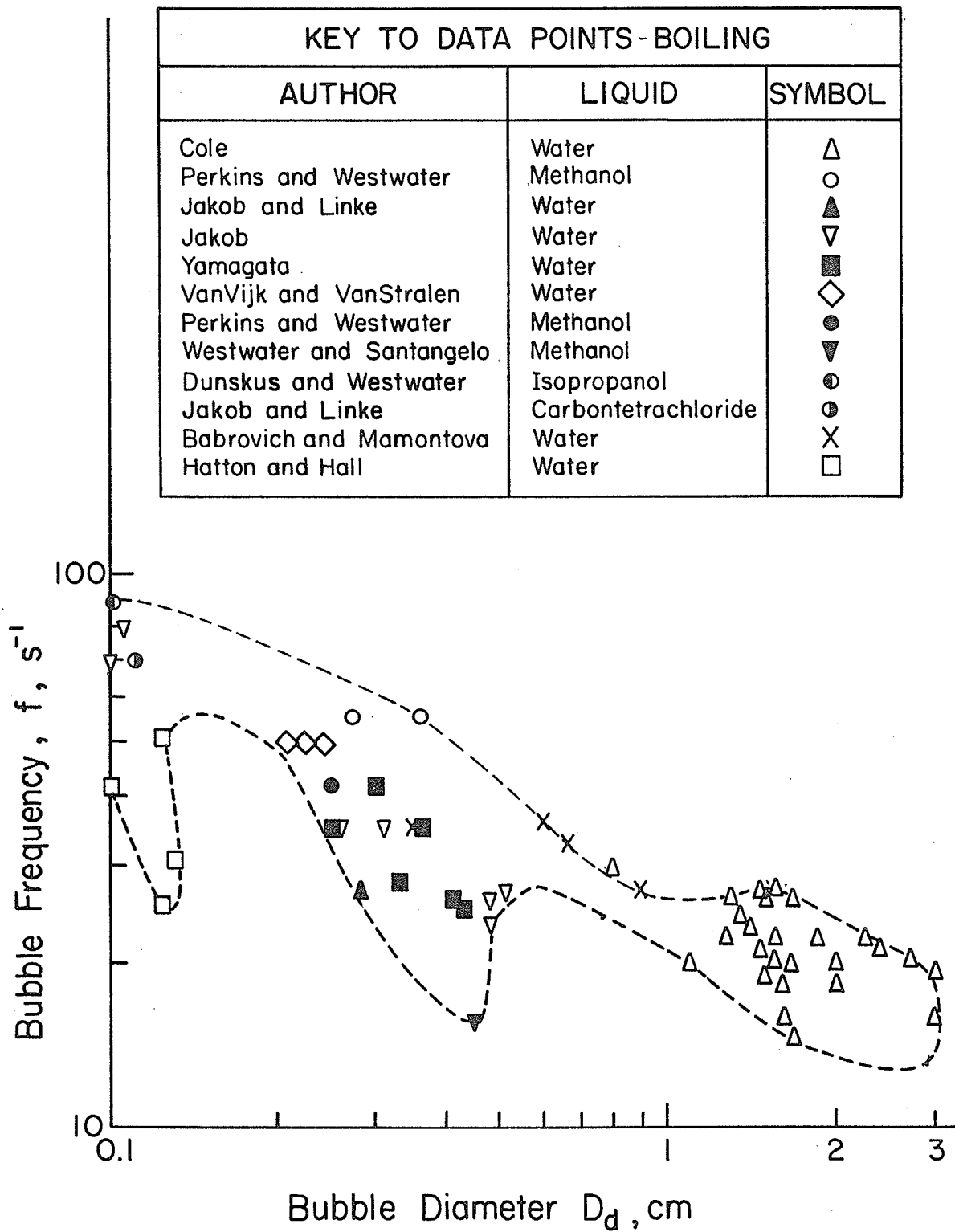


Fig. 2.2 Data for bubble frequency vs diameter from literature

2.3 Barbotage As An Analog of Boiling

In this section the existing literature comparing the bubble dynamics in boiling and barbotage will be reviewed. Zuber [46] was among the first to note the similarity in appearance of the bubbling flow regimes in barbotage and saturated nucleate pool boiling. He considered Davidson and Amick's [5] description of the appearance of barbotage bubbles forming at an orifice under constant-flow-rate conditions and noted that the description fitted well the bubble formation in Yamagata and Nishikawa's [45] experiments in nucleating boiling.

Zuber used the similarity to predict the frequency of bubble emission in nucleate boiling. He assumed that the velocity at departure of bubbles in nucleate boiling of water at saturation temperature could be adequately described by the Peebles and Garber equation (given in [46]) for barbotage bubbles:

$$U_{\infty} = 1.18 \left[\frac{\sigma g (\rho_L - \rho_V)}{\rho_L^2} \right]^{1/4} \quad (2.10)$$

where U_{∞} is the departure velocity, and ρ_V the vapour density. He further assumed that the velocity of the centre of gravity of bubbles remains a constant while growing and departing, and the growth and waiting periods are equal. These assumptions lead to the following:

$$\frac{D_d}{t_f} = U_\infty = 1.18 \left[\frac{\sigma g (\rho_L - \rho_V)}{\rho_L^2} \right]^{1/4} \quad (2.11)$$

$$D_d \cdot f = \frac{t_f}{t_w + t_f} 1.18 \left[\frac{\sigma g (\rho_L - \rho_V)}{\rho_L^2} \right]^{1/4} \quad (2.12)$$

$$= \frac{1.18}{2} \left[\frac{\sigma g (\rho_L - \rho_V)}{\rho_L^2} \right]^{1/4} \quad (2.13)$$

For any given liquid temperature and pressure, the right-hand side reduces to a constant. Zuber plotted the experimental results available then and found agreement with the above equation.

Zuber further attempted to predict the bubble departure diameter in nucleate boiling at low heat-transfer rates by relating the thermal layer thickness to the cavity radius in Eqn. 2.8. The resulting equation for the bubble diameter is

$$D_d = \left[\frac{6\sigma}{g(\rho_L - \rho_V)} \frac{k\Delta T}{q} \right]^{1/3} \quad (2.14)$$

where

k = thermal conductivity of the liquid,

q = the heat flux density, and

ΔT = the wall superheat.

The above equation was compared by Zuber with the experimental data of Zmola, of Fritz and Ende, and of Jakob and Linke; the computed values were found to be of the same order as the experimental data.

Wallis in his report [41] presented an excellent case

for using barbotage systems to study boiling. He pointed out that the nucleation phenomena in boiling and barbotage are described by the same basic equations. In both cases the excess pressure Δp , required inside the bubble for nucleation is given by

$$\Delta p = \frac{2\sigma}{R_0} \quad (2.15)$$

where R_0 is the orifice or cavity radius.

In boiling, Eqn. 2.6 further relates this excess pressure to the superheat. Wallis next compared bubble growth rates in barbotage and boiling. He proposed a correlation for Staniszewski's [39] data for bubble growth rates in boiling which indicated a linear volumetric growth rate during the major part of a bubble's history. This correlation was compared with Siemes and Kauffmann's [36] equations for bubble growth rates in barbotage (constant-flow-rate case). He found that the equations have the same basic form, namely,

$$V_d = V_M + T_A \frac{dV_d}{dt} \quad (2.16)$$

where V_d is the volume of bubble, V_M is the quasi-static volume, i.e., the critical volume required for further growth, and T_A is the growth time. He also observed that the departure times in each case were in agreement and individual variations can be explained by statistical arguments.

While the above works were concerned mainly with the hydrodynamic aspects in boiling and barbotage, several investigators have since dealt with the thermodynamic aspects. Some investigators [1,33,42] have used barbotage systems to simulate the boiling critical heat flux. Others (reviewed recently by Sims and Duffield [34]) have compared heat-transfer coefficients in pool barbotage and saturated nucleate pool boiling. These coefficients were based on time and area means and were found to be comparable in magnitude in boiling and barbotage. Bard [2] measured the heat-transfer coefficients to the liquid phase as a function of time and distance from the bubbling site in barbotage. From the results obtained, he concluded that in boiling, the chief contribution of bubble-induced agitation to the promotion of heat transfer from the heating surface occurs around the time of bubble detachment.

CHAPTER 3

EXPERIMENTAL INVESTIGATION TO DETERMINE BUBBLE GROWTH RATES UNDER CONSTANT-PRESSURE CONDITIONS

3.1 Introduction

It has been mentioned in Chapter 1 that, though some investigators [7,8,23] have studied bubble formation from a submerged orifice under constant-pressure conditions, no one has reported in what fashion the bubble radius varies with time under these conditions. The purpose of the present experimental investigation is to obtain quantitative data regarding this variation and also to measure departure diameters and frequency of bubbling for the liquids studied. Transparent liquids were employed to permit the use of high-speed cine photography for recording the sequence of bubble formation and to calculate instantaneous bubble volumes from the films.

3.2 Apparatus

3.2.1 Description of apparatus

Figure 3.1 illustrates schematically the principal experimental apparatus utilised for the periodic formation of gas bubbles by the injection of a gas into a

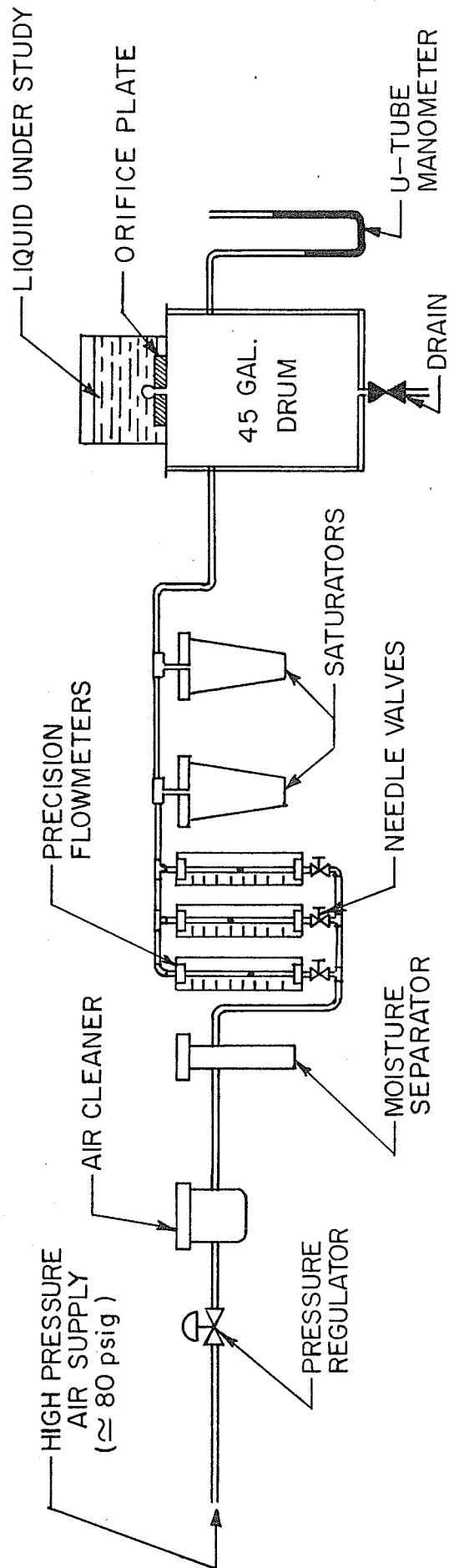


Fig. 3.1 Schematic of experimental set-up

liquid. Air from a high pressure source enters a pressure regulator which reduces the pressure to a steady value of 5 psig (350 gm/cm^2). The air then passes through a filter and a gas drier (Fisher Scientific Company), which effectively remove the oil particles and moisture that may be present in the air. Next, the air passes through one of three flow meters (Brooks Instrument Canada Ltd., Model No. 1560) which have built-in needle valves to accurately control the flow. The flow meters for measuring the mean flow rates were carefully selected to cover a wide range of flow rates ($0 - 700 \text{ cm}^3/\text{sec}$) and were installed parallel to each other. The air then flows through two bubblers which saturate it with the liquid under study, and finally enters a 45-gallon drum (the ante-chamber) from which it passes through an orifice into a rectangular liquid bath, containing the experimental liquid. Details of the assembly comprising the container, the orifice plate and the drum are shown in Fig. 3.2. The liquid container was made by bonding four glass plates of identical dimensions to the four sides of a $3/16$ in. (0.48 cm) thick brass plate which formed the bottom of the liquid bath. The inside dimensions of the container were $9\frac{1}{2}$ in. x $9\frac{1}{2}$ in. x 8 in. (24.1 cm x 24.1 cm x 20.4 cm). The choice of a rectangular container in lieu of a cylindrical one was to avoid the refractive effects due to curvature of the glass while performing high-speed photography.

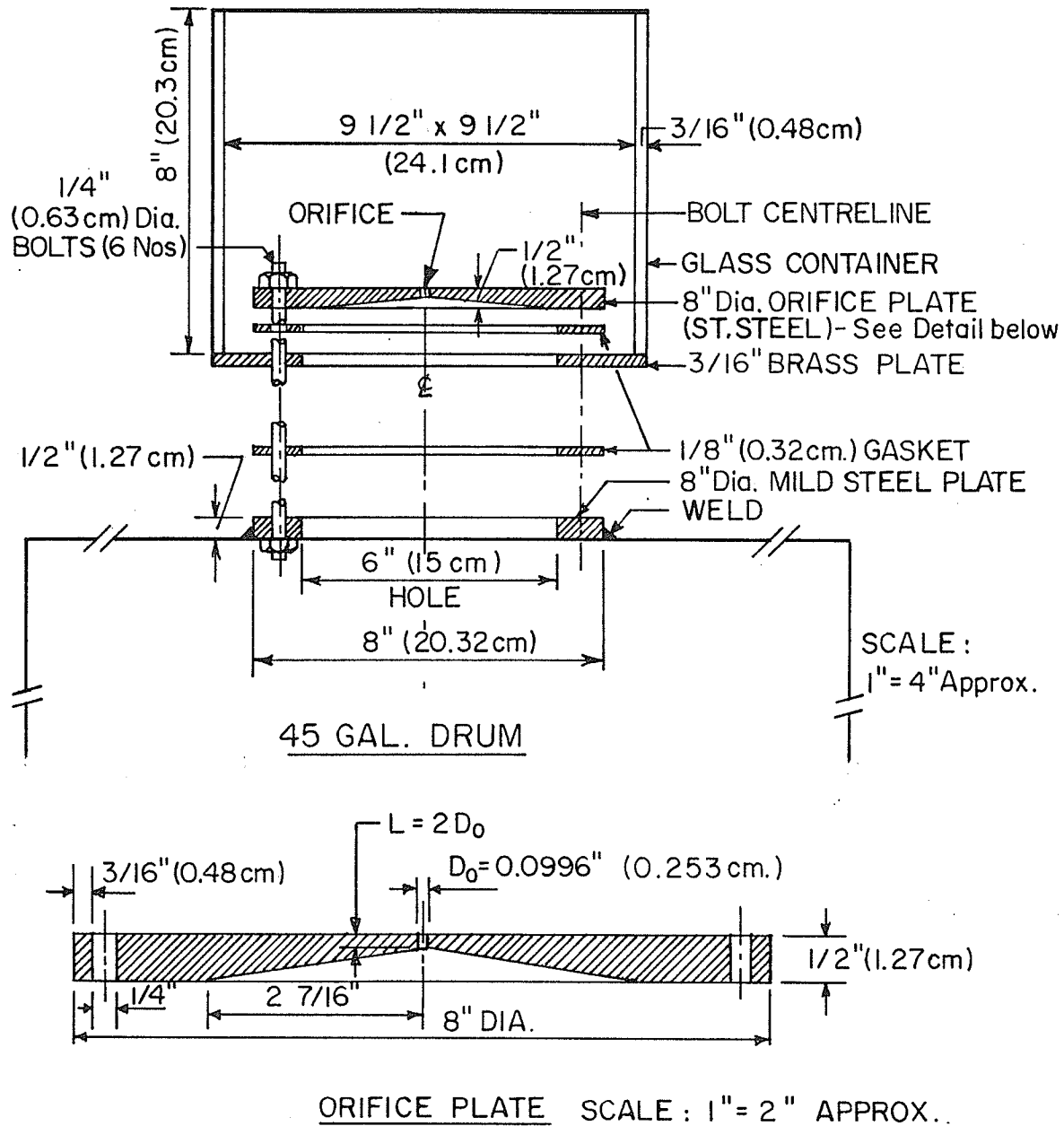


Fig. 3.2 Details of container assembly and orifice plate

The orifice plate was made of stainless steel. The diameter of the plate was 8 in. (20.4 cm) and the thickness $\frac{1}{2}$ in. (1.27 cm). An orifice of 0.253 cm (0.0996 in) diameter was drilled in the centre of the plate. This value of the orifice diameter was chosen to facilitate comparison with the experimental data for departure volumes given by Satyanarayan *et al.* [48] who used an orifice of equal diameter.

The injected air leaves the orifice in the form of bubbles and these bubbles rise through the liquid. Pressure inside the drum is measured by using a vertical U-tube liquid manometer, containing Meriam oil (sp. gr. 0.827). Liquid level in the container above the orifice is measured by a scale suspended vertically above the orifice. The container is open to atmosphere. All experiments were conducted at room temperature (72°F).

3.2.2 Selection of experimental liquids

A survey of the boiling literature indicated that sufficient experimental results were available for saturated pool boiling of water at atmosphere pressure, which could be used for comparing bubble growth rates. The main criterion for the selection of a liquid for the barbotage study was consequently influenced by the fact that the physical properties of the liquid at room temperature should be close to those of water at the boiling point at

atmospheric pressure. Availability of such a liquid renders the boiling and barbotage bubble growth results directly comparable with minimal influence by any parameter involving liquid physical properties. One such liquid which was readily available was acetone. Both the kinematic viscosity and density of acetone at 72°F and atmospheric pressure are approximately equal to those of boiling water at atmospheric pressure; the other two liquids used for the present study were distilled water and hexane. Growth rate studies for the two additional liquids served to provide data for a larger research program envisaged; as well, the use of water allows one to check at least some of the measurements obtained (breakoff diameters and frequency) with existing data in the literature.

The physical properties of all three liquids discussed are presented in Appendix B.

3.2.3 Photographic and stroboscopic apparatus

High-speed motion pictures of the bubble formation process, taken at the level of the orifice, provided a technique for investigating the details of the formation of an air bubble. Pictures were taken with a Hycam Model 41-0004, 16 mm motion picture camera in the range 500 to 2000 frames per second, using Kodak 4-x reversal 100 ft rolls of film. The frame speed could be accurately obtained from 100 or 1000 cycles/sec light "blips" placed on the film edge by a Millimite timing light

generator (Model 13-0001). The camera was normally located at about four feet from the orifice plane and was focussed on the orifice. Two 650W lamps were used in conjunction with a ground glass screen to provide illumination for the photography. The actual location of the lamps and the screen to provide optimum illumination, resulting in sharply defined bubble profiles was determined by trial and error. The optimum arrangement is illustrated in Fig. 3.3.

In order to determine the true volume of a bubble from a magnified image, some known reference measurement at the orifice level was necessary to obtain a "scale factor". For this purpose, before taking the photography of the bubbles, a scale whose actual width was known was suspended above the orifice, vertically, and its image recorded at a very low framing speed.

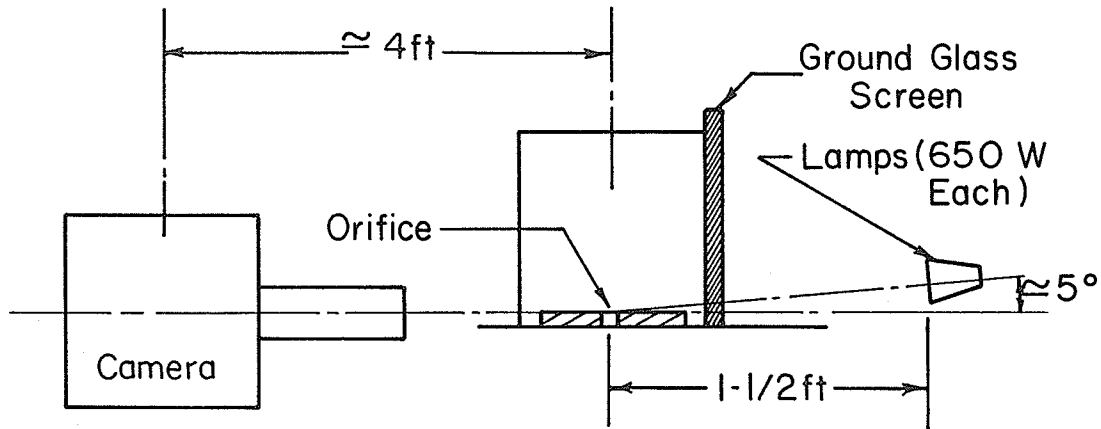
Frame by frame projection of the photographs enabled an accurate determination of the bubble volume, and the formation time of a bubble. A motion picture analyser (L-W Super Sports Model 900) with a variable frame speed was used for this purpose.

Determination of bubble frequency was done with a stroboscope (General Radio Company, Strobotac type 1538-A).

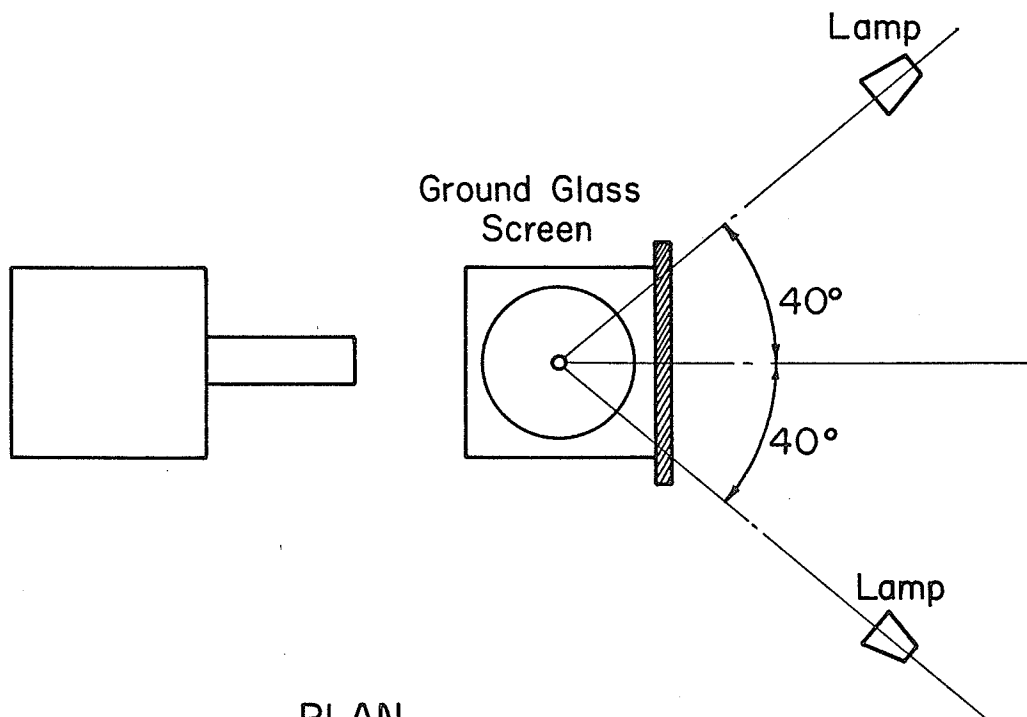
3.3 Procedure

3.3.1 Growth rate determination

As was mentioned earlier, growth rate



ELEVATION



PLAN

Fig. 3.3 Arrangement of photographic equipment

measurements were obtained using distilled water, acetone and hexane as experimental liquids and air as the injected gas. The conditions under which the experiments were run are summarised in Table 3.1. An experimental run was conducted as follows:

- (i) The liquid container was washed with soapy water and then rinsed thoroughly with distilled water. A clean rag was used for wiping the container dry.
- (ii) The air supply to the ante-chamber was turned on so that there was steady air flow through the orifice. This precaution was necessary to prevent liquid leaking through the orifice while the container was being filled.
- (iii) The liquid container was filled with the desired liquid to a depth of about 12 cm (≈ 5 in) above the orifice.
- (iv) The air flow rate was adjusted by means of the needle valve to set the ante-chamber pressure at any desired value.
- (v) Allowing a short interval of time to ensure steady state operation, the values of the gas flow rate, ante-chamber pressure and the liquid head above the orifice were recorded.
- (vi) High-speed motion pictures of the bubbles were taken.

Table 3.1. Conditions for bubble formation experiments.

Liquid	Air Flow Rate cm ³ /sec	Orifice Diameter = 0.253 cm	
		High Speed Cine Film for Growth Rate, Bubble Volume, and Frequency	Stroboscopic Observations for Frequency and Bubble Volume
water	4.07	x	
	27.00		x
	29.40		x
	32.50	x	
	34.60		x
	40.00		x
	50.40		x
	60.50	x	x
71.50		x	
acetone	8.64	x	
	14.25		x
	18.10		x
	19.65	x	
	25.60		x
	32.30	x	x
	39.60		x
hexane	8.1	x	
	11.8		x
	13.0		x
	15.0		x
	15.6	x	
	16.2		x
	19.5		x
	22.7		x
	28.7		x
	30.8	x	
34.8		x	

3.3.2 Calculation of instantaneous volume of a bubble

The high-speed motion pictures taken as described above provided a means for recording the sequence of the formation of a bubble. A frame-by-frame projection of such pictures enabled one to obtain a two-dimensional picture of the bubble at any instant during its formation. Because of the expected axial symmetry of a bubble forming at a smooth, vertically oriented orifice, it was assumed justifiable to calculate the volume of the bubble from the two dimensional profile obtained by photography. The procedure for computing the volume of a bubble is illustrated in detail in Appendix C.

An equivalent radius R_{eq} , i.e., the radius of a sphere of equal volume, can be obtained from the above calculated volume from the following equation:

$$R_{eq} = \left[\frac{3 \times V_{measured}}{4\pi} \right]^{1/3} \quad (3.1)$$

3.3.3 Bubbling frequency and departure volumes

The use of a stroboscope for bubble frequency measurements is not uncommon. Knowing the frequency f bubble departure volumes V_d can be calculated from the following equation:

$$V_d = Q/f \quad (3.2)$$

where Q is the flow rate through the orifice. Wherever flow rates are quoted in this thesis, unless otherwise noted, the flow rates are for the mixture of air (measured with one of the rotameters) saturated with the vapour of the test liquid; these flow rates are loosely termed "air flow rates", "flow rates", "mean air flow rates" or "mean flow rates". A sample calculation showing the method used to determine the flow rate through the orifice is given in Appendix D.

Departure volumes were calculated by the above method for each liquid at different mean flow rates.

3.4 Results and Discussion

3.4.1 Photographic observations

Two types of bubbles were encountered in the experimental investigation and they could be categorised as follows:

Category I: Bubbles which start as a hemisphere left behind by a departed bubble.

Category II: Bubbles which first appear as a meniscus at the orifice at the end of a discrete time interval after the previous bubble has departed.

Typical sequences of bubbles in both categories obtained from cine pictures are shown in Figs. 3.4 and 3.5. The variation in the physical properties of the test liquids



Fig. 3.4 Cine pictures of bubbles of Category I

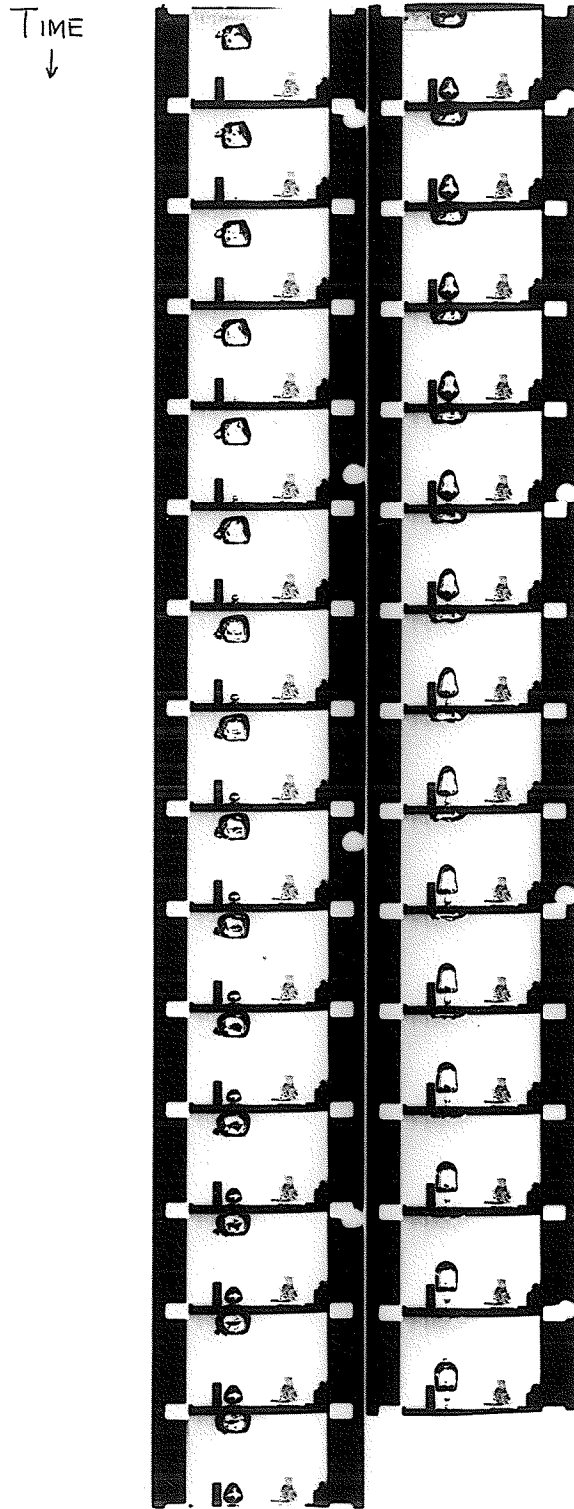


Fig. 3.5 Cine pictures of bubbles of Category II

did not appear to have any significant influence on the shapes of the bubbles in either category. Also, it is evident that there is no significant difference in shapes between the two categories of bubble.

A typical sequence starts with either an approximately hemispherical interface left behind by a departed bubble, or a small meniscus appearing at the orifice after a time interval. As the bubble size increases, due to mass flow into the bubble, the shape changes to that of a pear, with the vertical axis growing faster than the horizontal axis. As the bubble size increases further, a stage is reached when the upward forces acting on the bubble have increased sufficiently to start lifting the bubble off the surface. A small neck starts forming which connects the bubble to the orifice. The neck has the shape of a short cylindrical stem in the beginning, but gradually develops into a secondary bubble. This secondary bubble starts penetrating and rising through the bigger bubble as they move together upwards. Finally, the connection between the secondary bubble and the orifice is severed due to the upward acceleration, and the bubbles start moving freely, leaving behind at the orifice an hemispherical interface which either disappears into the orifice or starts growing. In course of time, the secondary bubble gets completely enveloped by the bigger bubble which rises through the liquid as a single unit.

The photographs indicate that the sequence of events described above is a periodic process. It is well known that the life cycle of a bubble is characterised by two time periods, namely the "waiting time" t_w and the "formation time" t_f . The "waiting time", as defined here, is the time interval between the departure of a bubble and the first appearance of the next bubble at the orifice. The "formation time" refers to the period of growth of a bubble between its first appearance and its detachment from the orifice. It is clear that the frequency of bubble emission is then given by $f = \frac{1}{t_w + t_f}$. It may be mentioned here that for bubbles under Category I, the waiting time t_w is obviously zero.

3.4.2 Bubble frequency data

The frequency of bubble formation in the three liquids were determined by stroboscopic examination and are given for increasing mean flow rates in Figs. 3.6 and 3.7. Tabulated values are given in Tables 3.2 to 3.4.

For water-air system, the frequency increases slightly with increasing mean flow rate within the range covered, whereas for acetone and hexane, it tends to be almost a constant, the increase in flow rate being accommodated by an increase in volume of bubbles.

3.4.3 Bubble volume data

Figures 3.8 and 3.9 present the variation of

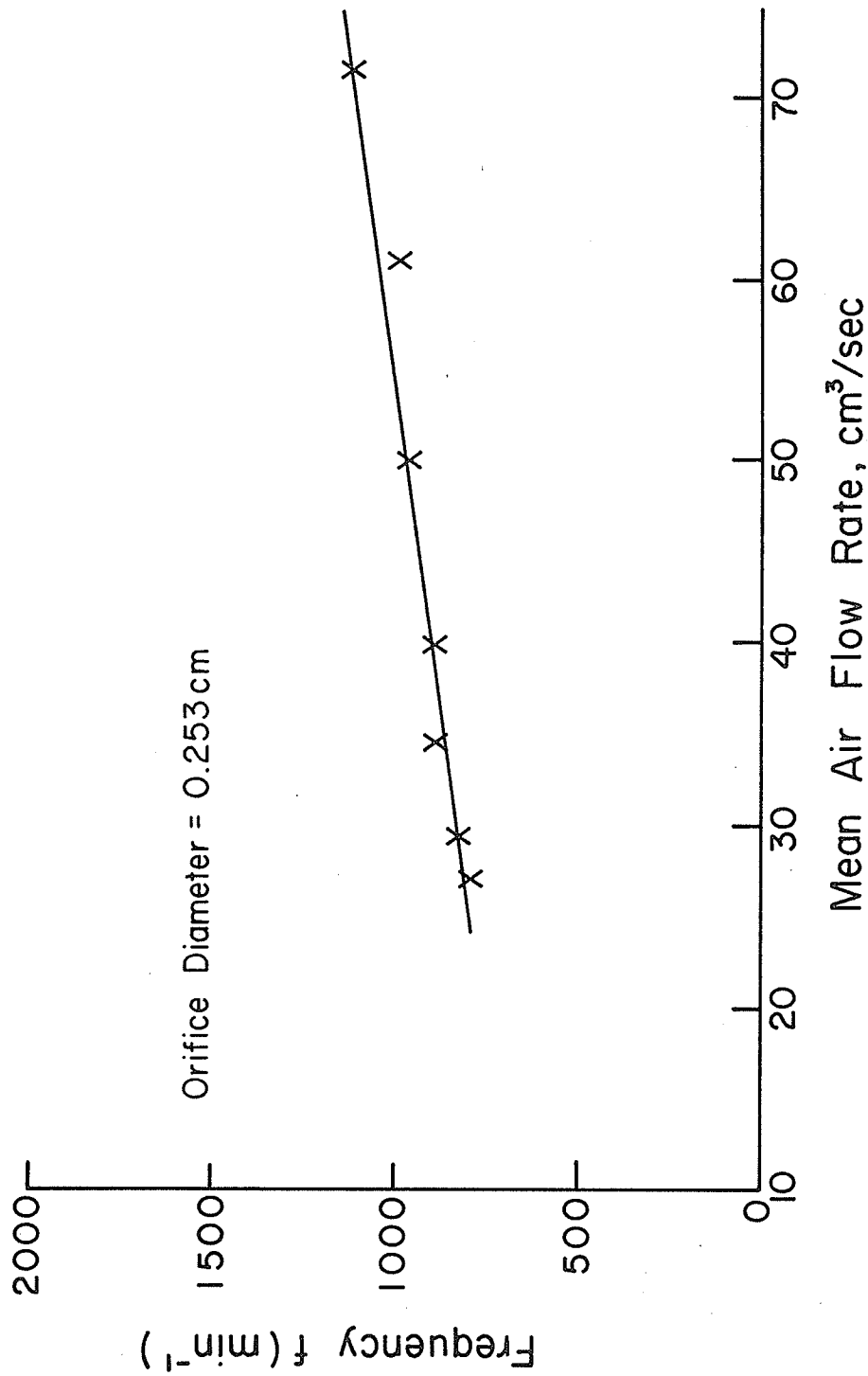


Fig. 3.6 Frequency data for air-water system

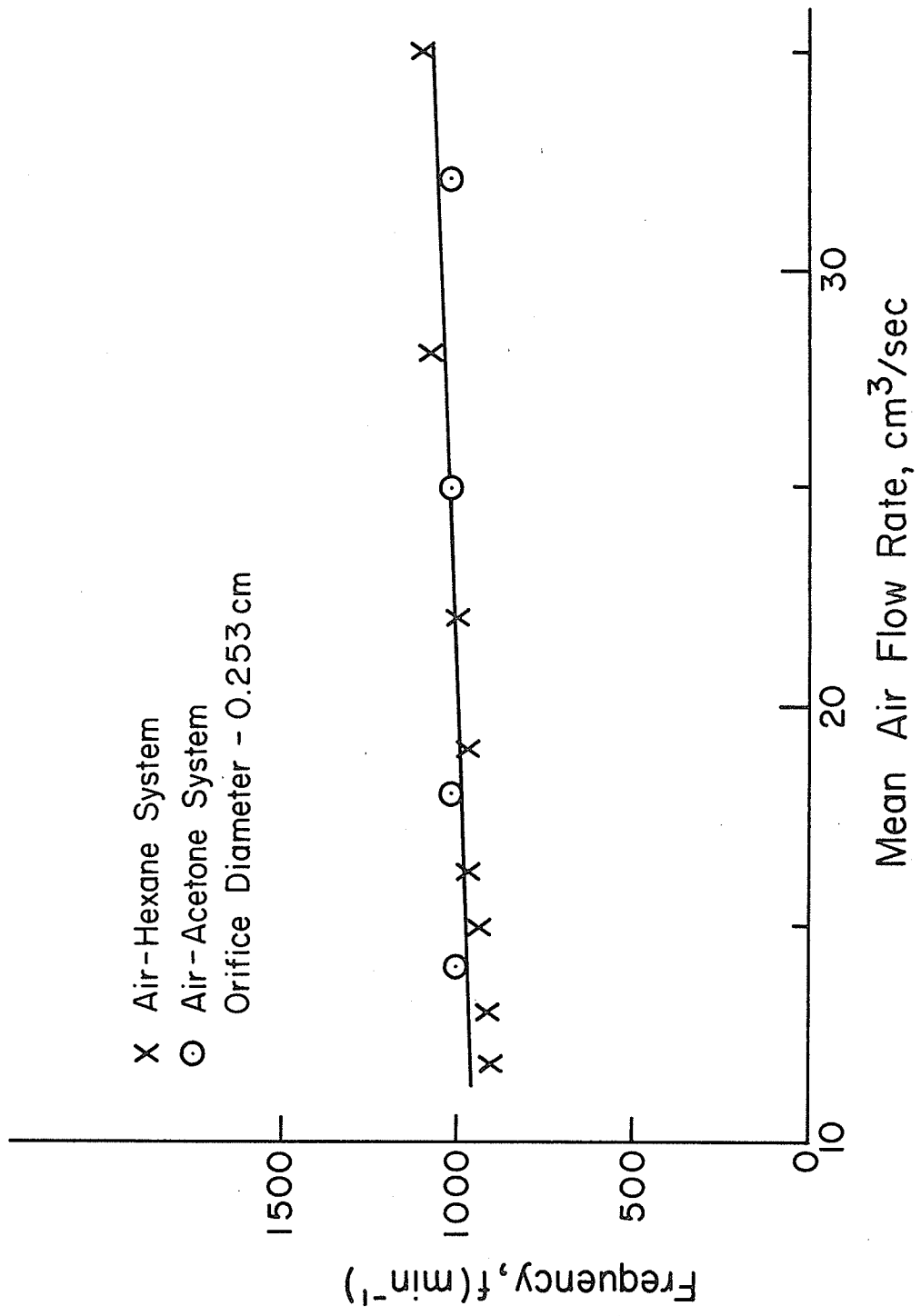


Fig. 3.7 Frequency data for air-acetone and air-hexane systems

Table 3.2. Bubble volume and frequency data for air-water system.

Flow Rate Indicated by Flow Meter @ 70°F, 14.7 psi cm ³ /min	Flow Rate Corrected for Vapour Content cm ³ /min	Frequency $\frac{1}{\text{min}}$	Bubble Departure Volume [†] cm
1580	1621	820	1.98
1720	1765	860	2.05
2020	2073	900	2.30
2340	2401	900	2.67
2940	3017	980	3.08
3540	3633	1020	3.56
4180	4290	1140	3.76

[†] From Eqn. 3.2.

Table 3.3. Bubble volume and frequency data for air-acetone system.

Flow Rate Indicated by Flow Meter @ 70°F, 14.7 psi cm ³ /min	Flow Rate Corrected for Vapour Content cm ³ /min	Frequency $\frac{1}{\text{min}}$	Bubble Departure Volume [†] cm ³
622.5	852.5	1000	0.852
792.5	1082.5	1020	1.060
1120	1530	1020	1.500
1420	1937	1020	1.900
1740	2376	1020	2.375

[†] From Eqn. 3.2.

Table 3.4. Bubble volume and frequency data for air-hexane system.

Flow Rate Indicated by Flow Meter @ 70°F, 14.7 psi cm ³ /min	Flow Rate Corrected for Vapour Content cm ³ /min	Frequency $\frac{1}{\text{min}}$	Bubble Departure Volume [†] cm ³
552.5	669.5	900	0.74
642.5	779	920	0.84
742.5	900	940	0.96
800	970	960	1.01
960	1164	960	1.21
1120	1358	1000	1.36
1420	1722	1080	1.60
1720	2085	1110	1.88

[†] From Eqn. 3.2.

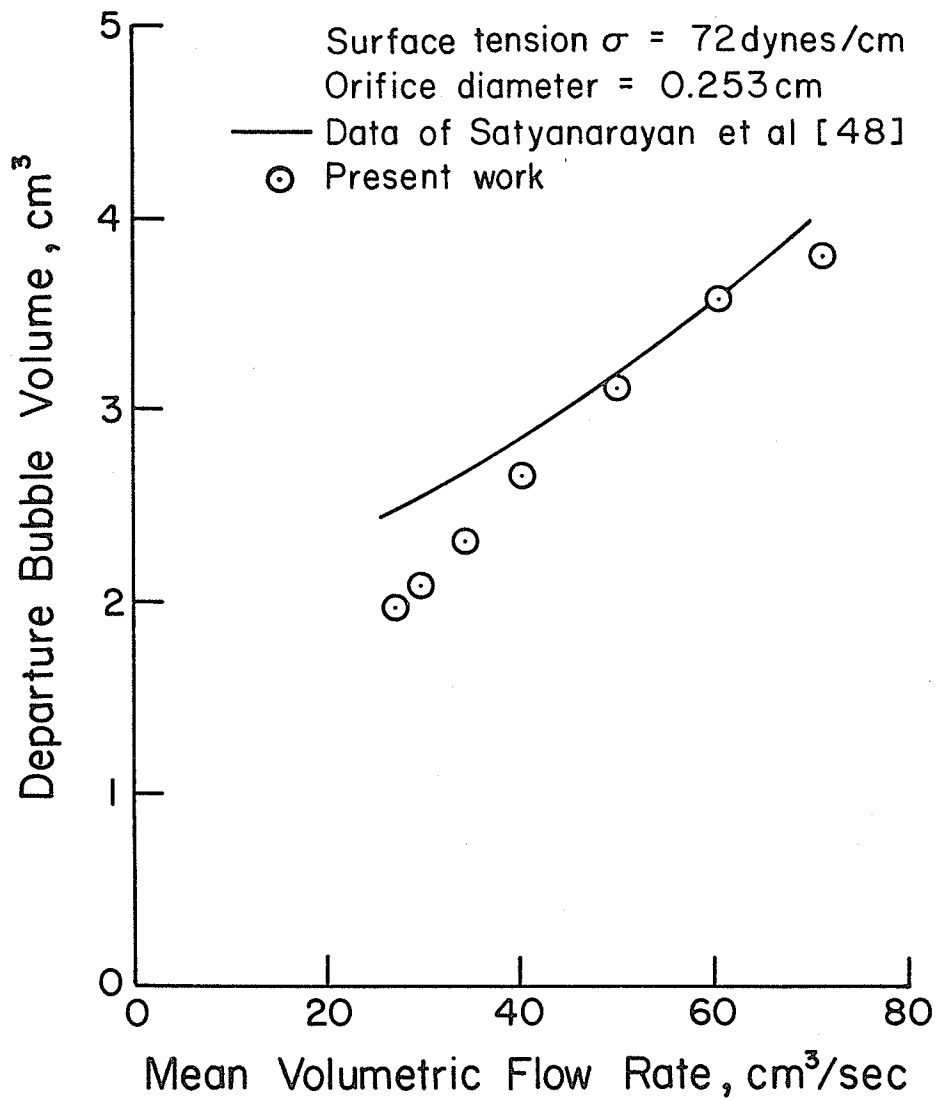


Fig. 3.8 Bubble volume as a function of mean air flow rate for air-water system

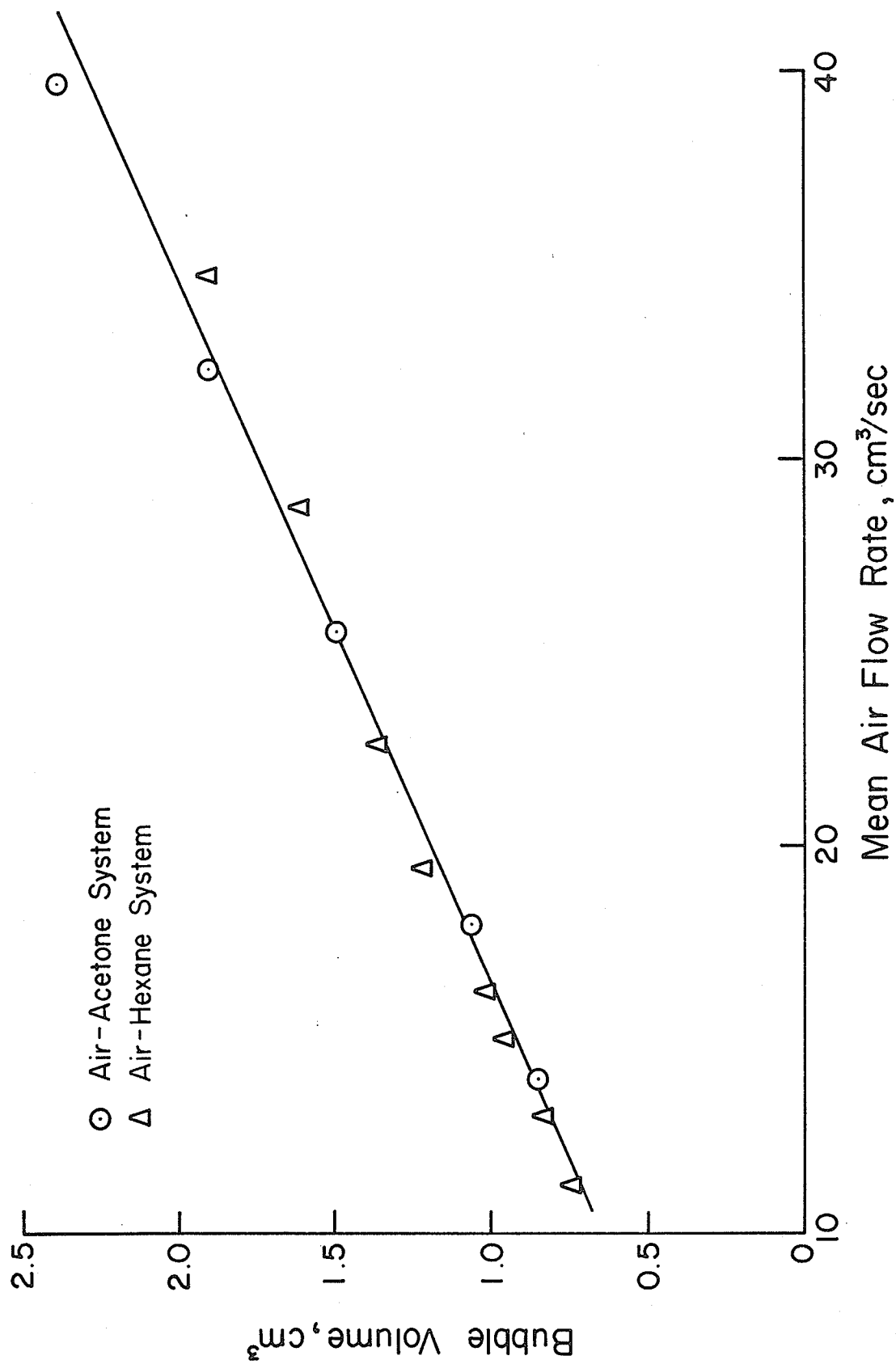


Fig. 3.9 Bubble volume data for air-acetone and air-hexane systems

bubble departure volume with the mean flow rate, as determined by a stroboscope. The departure volumes were calculated from the equation $V_d = Q/f$, where Q refers to the flow rate through the orifice, corrected to include the saturated vapour of the experimental liquid. Tables 3.2 to 3.4 give the tabulated values.

The figures indicate that the bubble volume in the case of all three liquids increases with increasing flow rates as can be expected. Also shown in Fig. 3.8 is a smooth curve representing the experimental results of Satyanarayan *et al.* [48] for water, for the same orifice diameter. It can be seen that the agreement between the present work and that of Satyanarayan is satisfactory, especially at the higher flow rates. In the case of acetone and hexane, no other experimental results were available in literature to make a comparison. Limited data on bubble departure volumes (same bubbles as in Figs. 3.10 through 3.18) available from motion picture films differ from the smooth curves drawn (by eye) through the stroboscopic data by -3.3 per cent to +50 per cent. The resulting rms deviation is about 28 per cent on volume and in terms of equivalent radius about 9 per cent.

3.4.4 Bubble growth data

Bubble growth measurements were made for each liquid at different flow rates by the high-speed photographic technique described earlier. From each film,

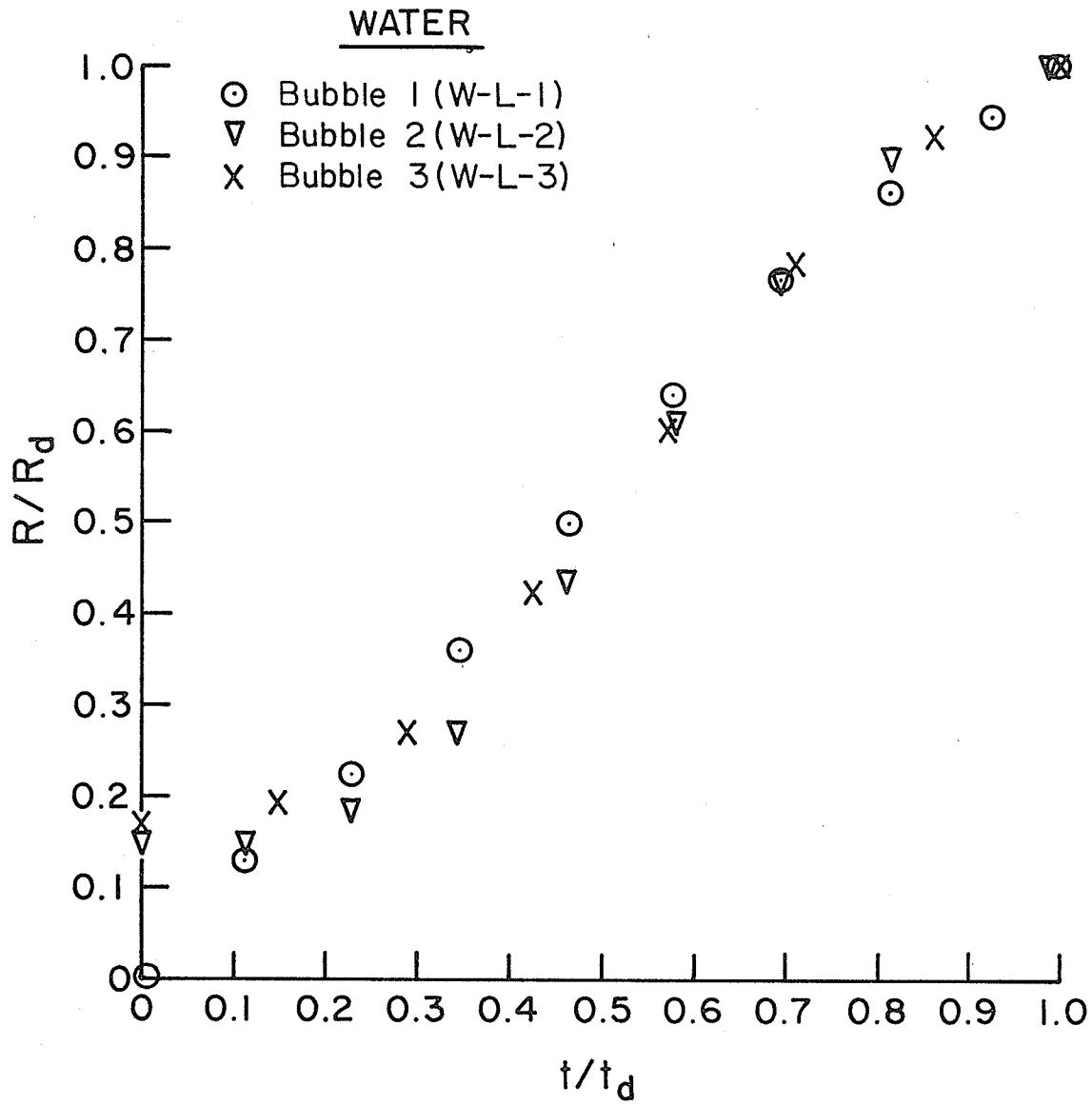


Fig. 3.10 Bubble growth data in water
(air flow rate - $4.07 \text{ cm}^3/\text{sec}$)

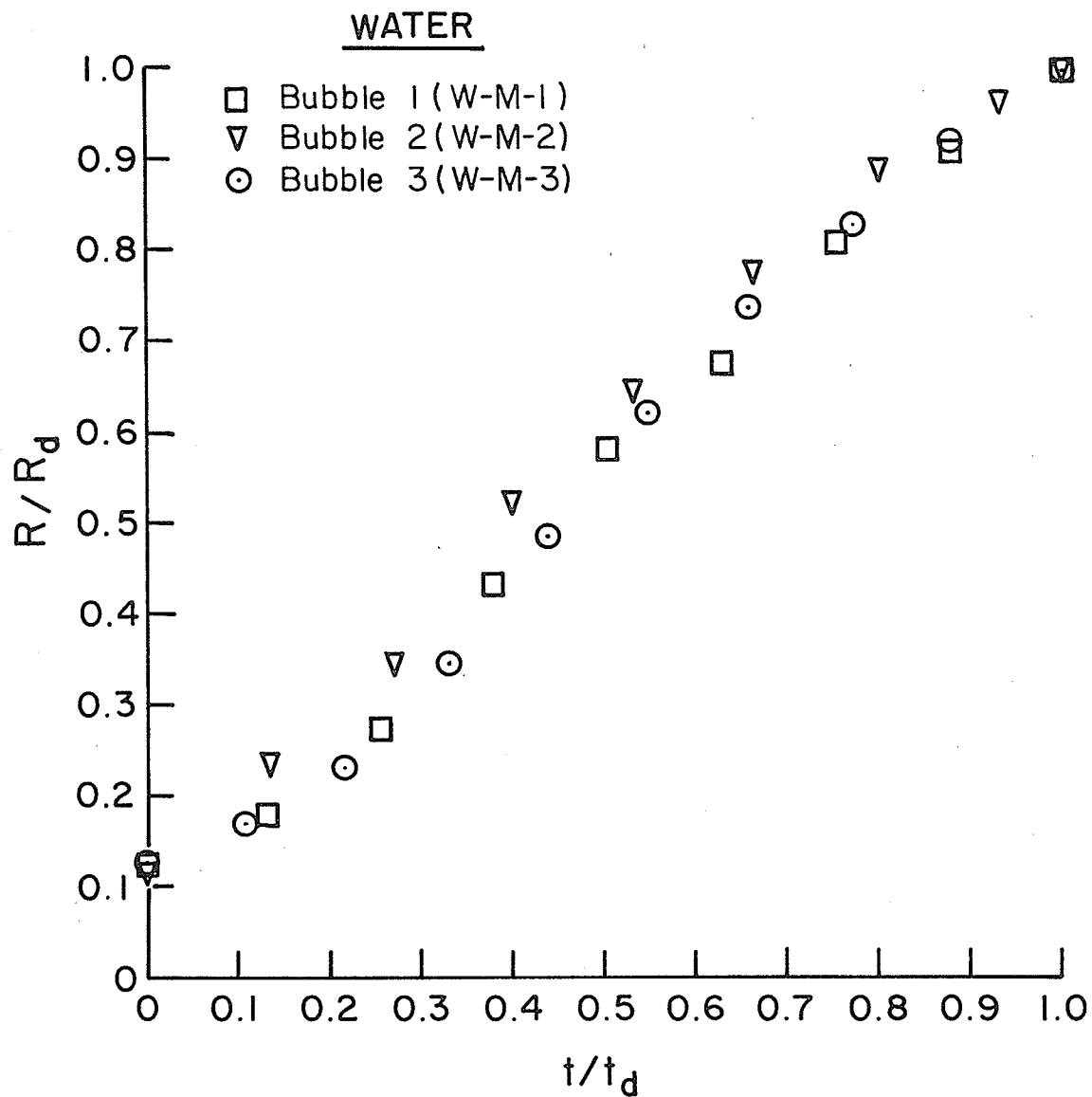


Fig. 3.11 Bubble growth data in water
(air flow rate - $32.5 \text{ cm}^3/\text{sec}$)

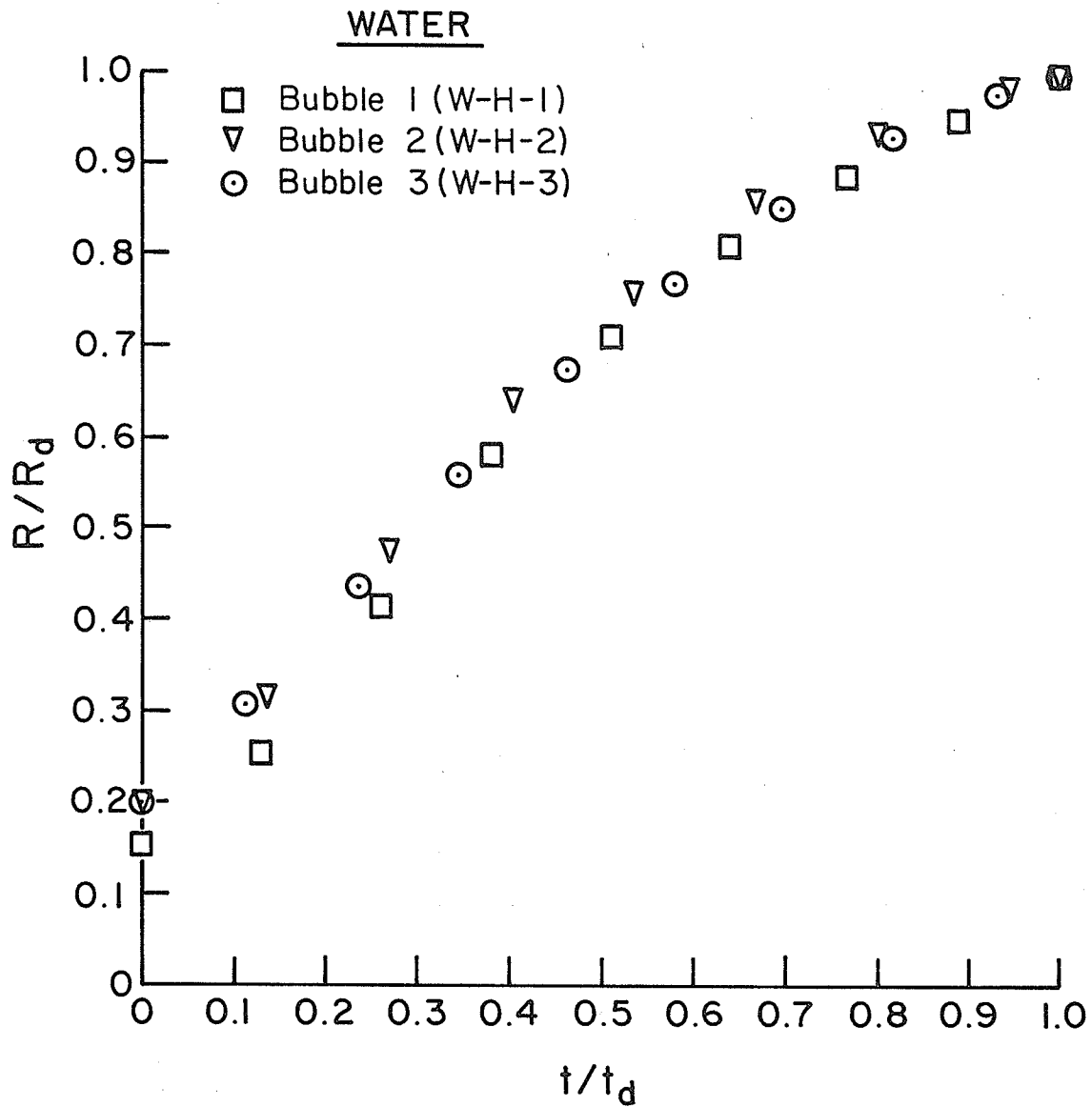


Fig. 3.12 Bubble growth data in water
(air flow rate - $60.5 \text{ cm}^3/\text{sec}$)

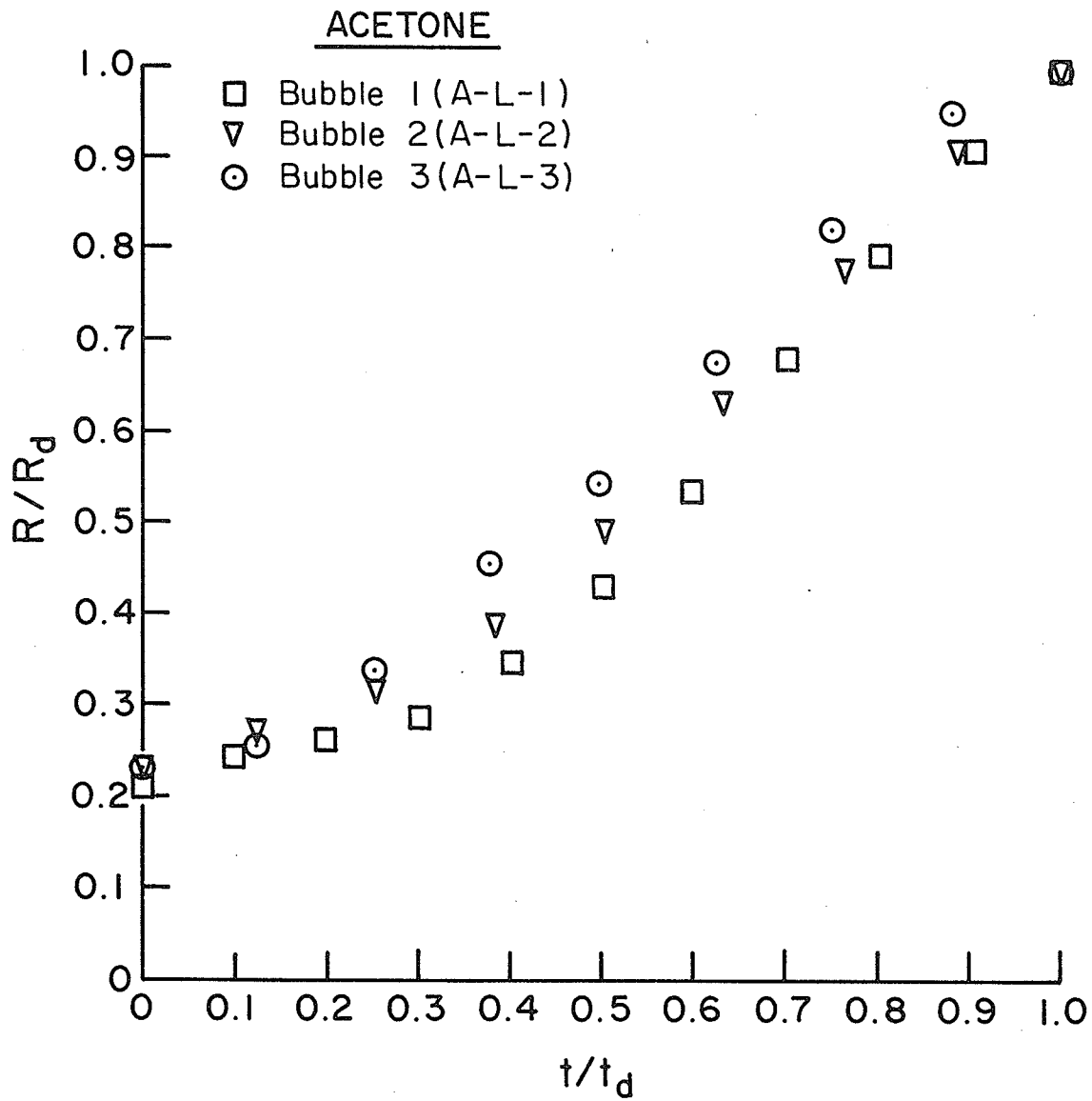


Fig. 3.13 Bubble growth data in acetone
(air flow rate - $8.64 \text{ cm}^3/\text{sec}$)

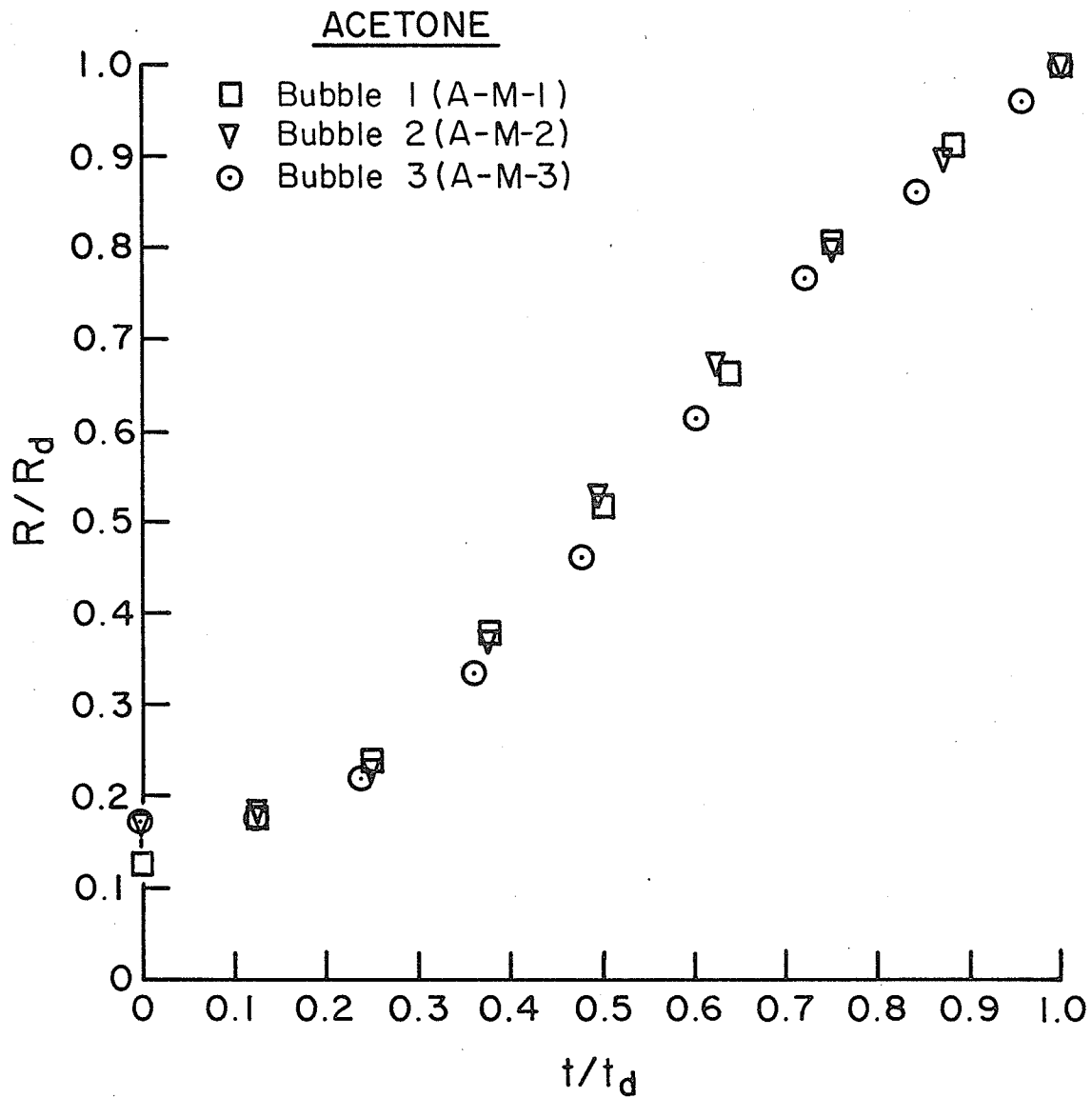


Fig. 3.14 Bubble growth data in acetone
(air flow rate - 19.65 cm³/sec)

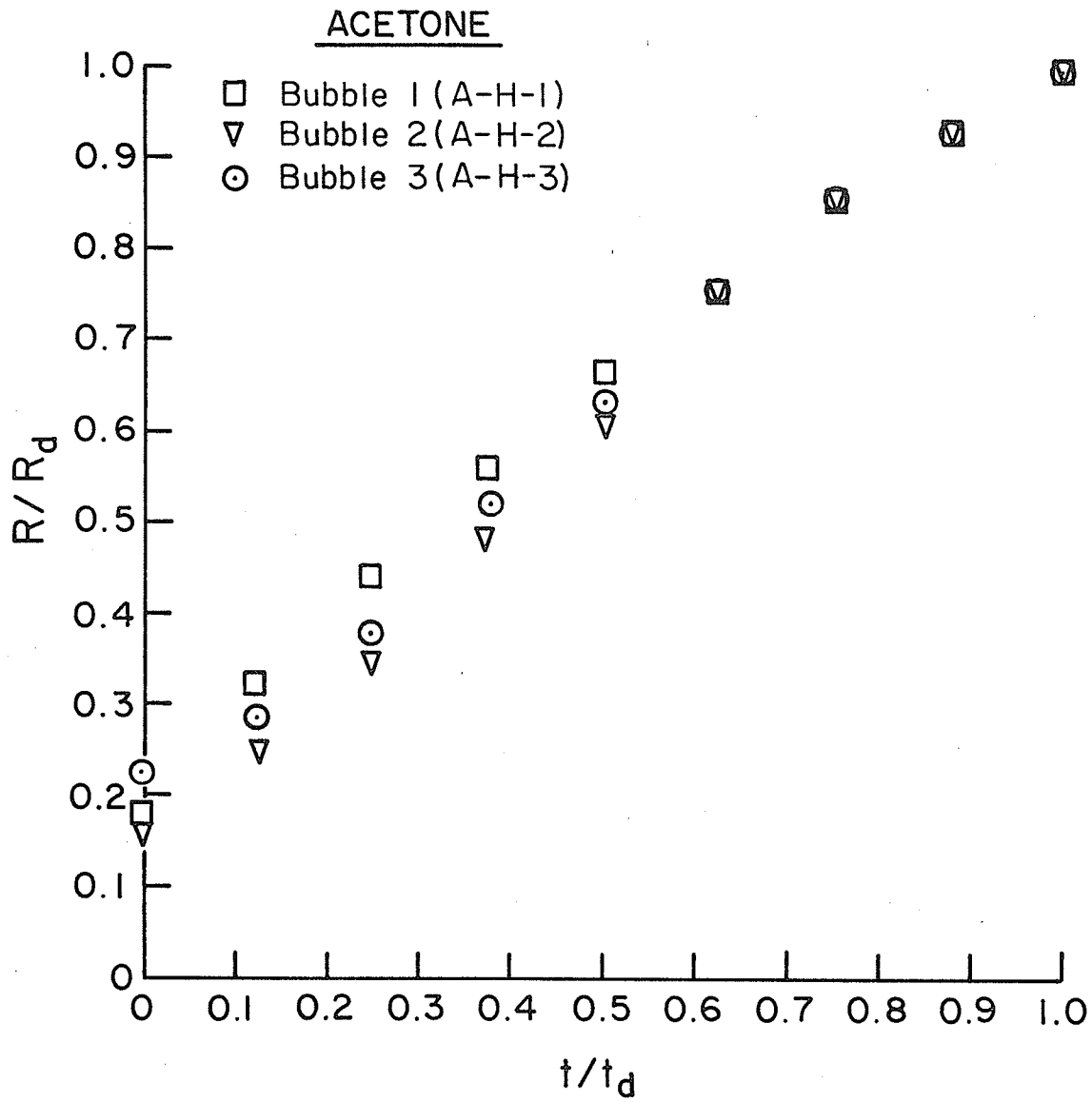


Fig. 3.15 Bubble growth data in acetone
(air flow rate - $32.4 \text{ cm}^3/\text{sec}$)

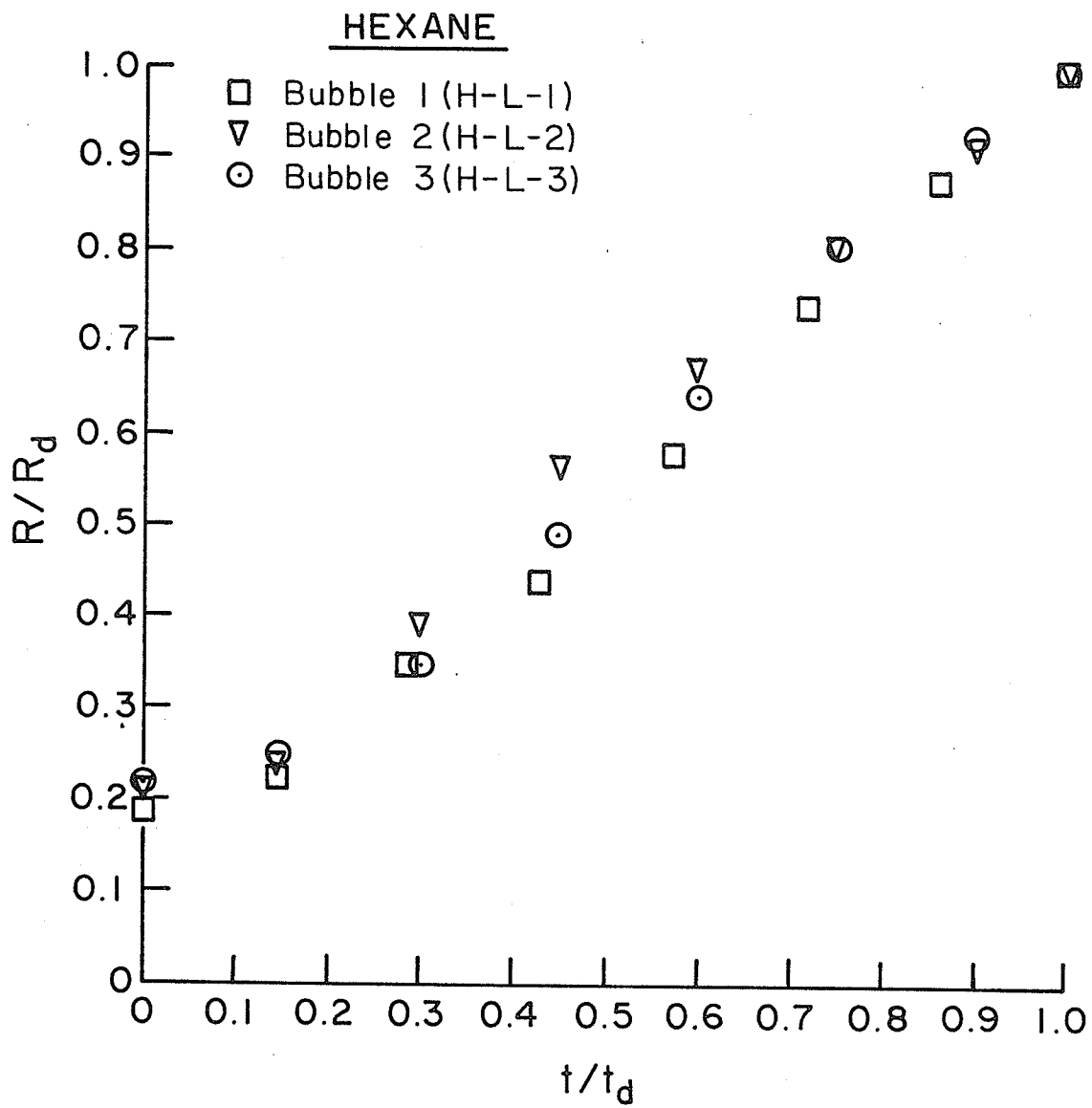


Fig. 3.16 Bubble growth data in hexane
(air flow rate - $8.1 \text{ cm}^3/\text{sec}$)

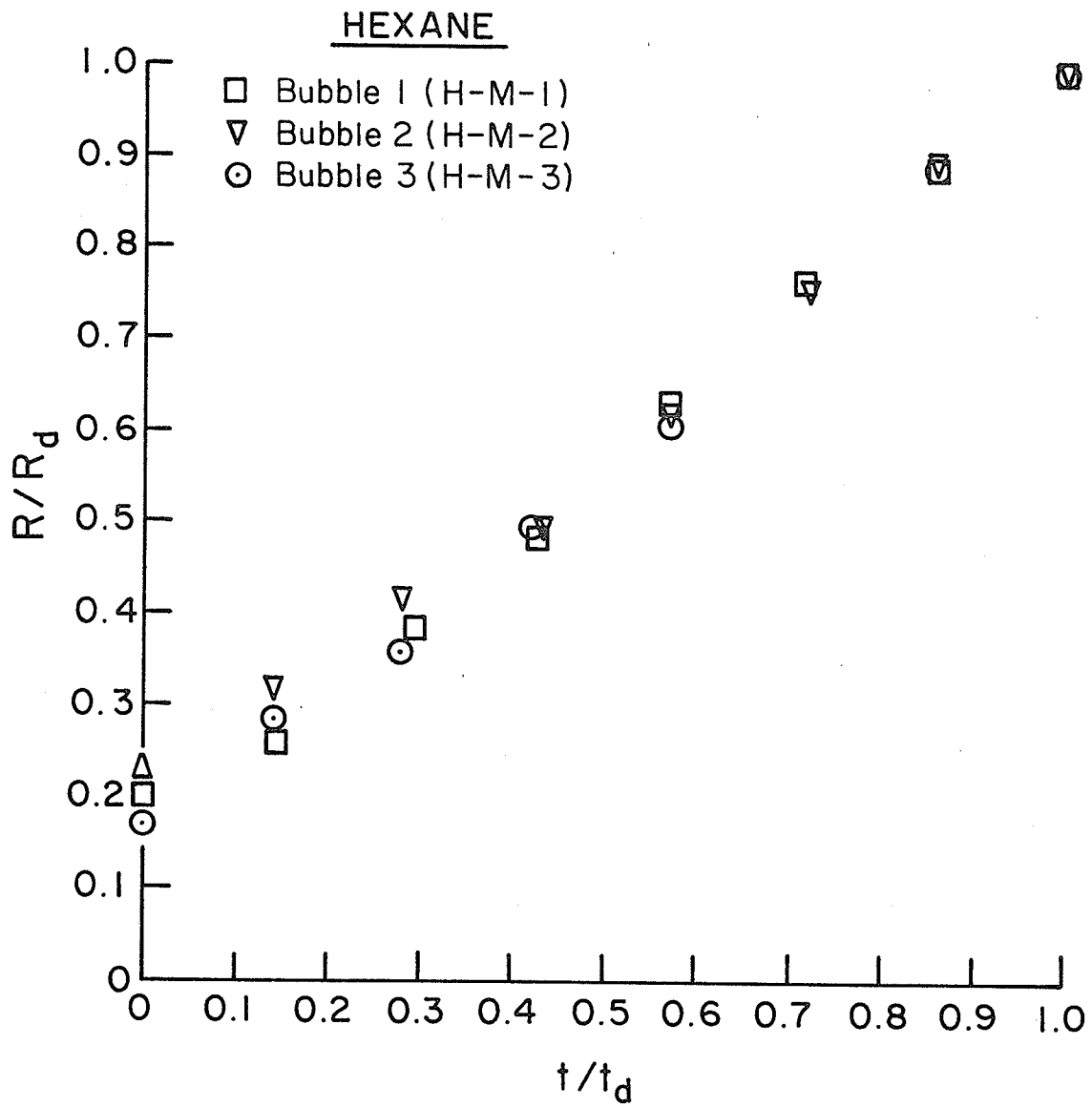


Fig. 3.17 Bubble growth data in hexane
(air flow rate - 15.6 cm³/sec)

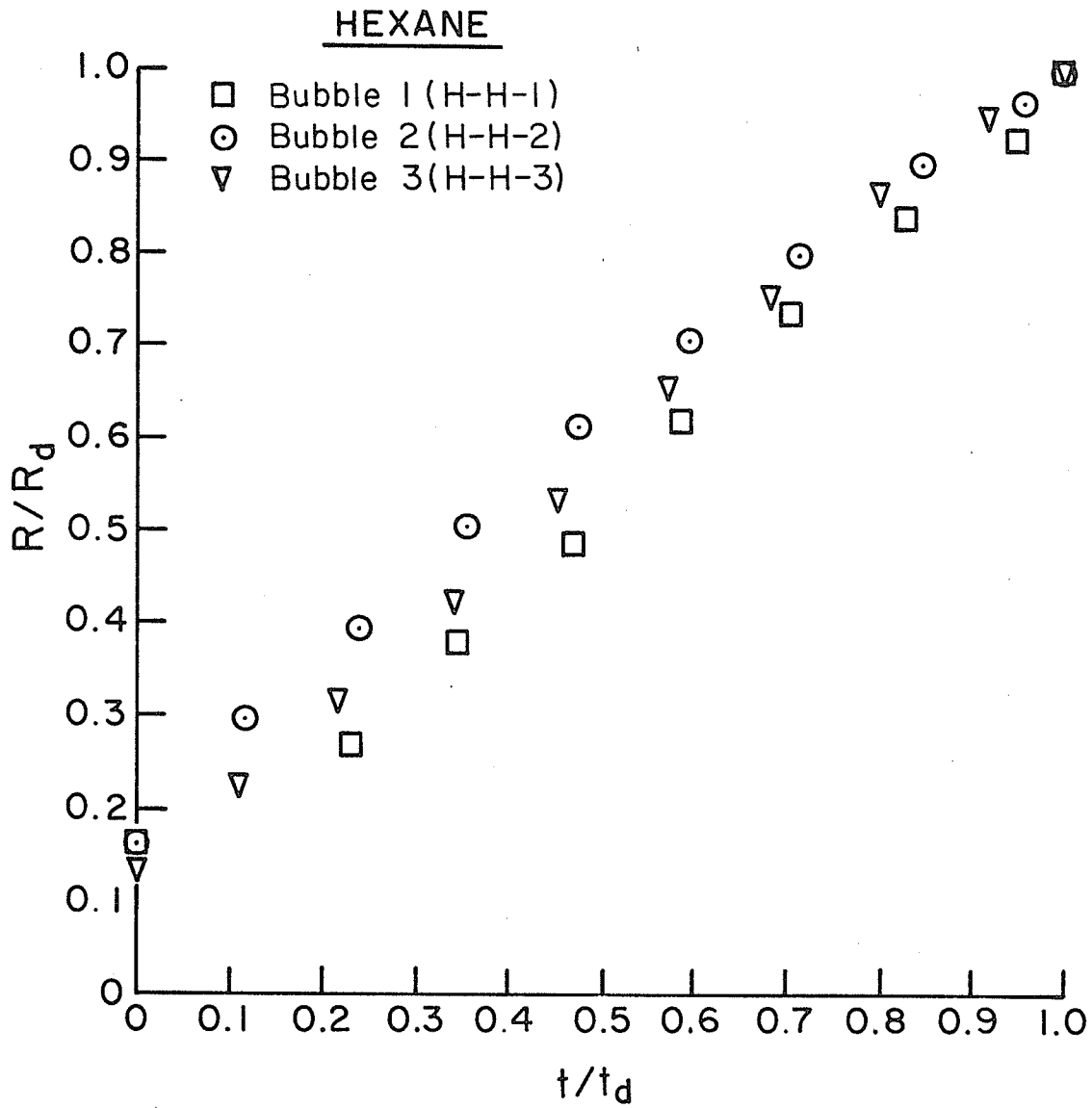


Fig. 3.18 Bubble growth data in hexane
(air flow rate - $30.4 \text{ cm}^3/\text{sec}$)

three typical bubbles were chosen for measuring the growth rate. Since a vast majority of the photographed bubbles belonged to the category starting as a hemisphere at the orifice (Category I), bubbles for growth rate determination were chosen from among these bubbles. However, a few bubbles belonging to Category II (see Sec. 3.4.1) were analysed and compared with the growth curves of the former category. No significant variations were evident in the average slopes of the growth curves (see Appendix F).

Zero time:

"Zero time" for bubbles under Category I was taken to correspond to the frame when a departing bubble just severs its connection with the orifice, leaving an (approximately) hemispherical interface at the orifice. For Category II, the origin of time was taken to correspond to the frame prior to the one where the bubble first appears as a meniscus. Thus, there is an uncertainty in time, in this case, equal to the time between two successive pictures. The error introduced by the above assumption is less than 2 ms, in a total growth time of about 55 ms.

Presentation of bubble growth results:

Figures 3.10 through 3.18 present the variation of the dimensionless radius R/R_d with the dimensionless time t/t_d where R_d and t_d refer to the equivalent radius and time at departure, respectively. Tabulated data are given in Appendix E. The curves correspond to the various conditions

summarised in Table 3.1. The enlarged profiles of typical bubbles for each liquid from which growth data were obtained are illustrated in Figs. E.1 through E.9 in Appendix E.

R_d and t_d for the above graphs

An assumption was made in determining R_d and t_d for the above graphs. As described under Sec. 3.4.1, photographic observations indicated that the bubbles formed in pairs i.e. a bigger 'primary' bubble whose formation ended with a short neck connecting the bubble to the orifice. Next, a 'secondary' bubble started forming as an extension of the neck and subsequently became enveloped by the primary bubble and both rose together as a single unit. For presentation of the results in Figs. 3.10 to 3.18, R_d and t_d were chosen to be the values obtaining at the end of the formation of the primary bubble. A justification for this choice lies in the fact that some of the motion picture runs indicated a slight break between the primary and the secondary bubbles confirming the separate identities of the two bubbles.

In order to check the effect of the choice on the shape of the R_d vs t_d curves, growth rate curves were drawn for a few bubbles taking R_d and t_d at the time of the detachment of the primary-secondary bubble combination. The comparison is performed in Appendix F. It is seen that there is no significant difference in the growth curves

between the two cases.

Discussion:

A simple theory has been proposed in Chapter 5 to predict the above variation of the bubble radius with time by solving the well-known Rayleigh equation for bubble growth. Inasmuch as one of the goals of the present investigation is to make a quantitative comparison of the growth rates in barbotage and boiling, it was decided to recast the above growth rate data in a simpler fashion by assuming a growth equation of the following form to describe the data (see Appendix G):

$$R = at^n$$

where a is a growth constant. In dimensionless form this would be

$$R^* = \theta^n$$

where $R^* = R/R_d$ and $\theta = t/t_d$. The growth exponent, n , was calculated from the above equation by a least-squares fit for each set of data, and was found to vary from 0.56 to 1.1, the lower values of n being associated with high flow rates and the higher values being associated with low flow rates. The values of n are presented in Table 3.5 and are used later in the thesis.

Table 3.5. Growth exponents for barbotage bubbles, obtained in present work.

Liquid	Mean Flow Rate cm ³ /sec	Range of 'n' For 3 Bubbles	'n' (Average for 3 Bubbles)
water	60.50	0.56 - 0.67	0.60
	32.50	0.75 - 0.88	0.83
	4.07	0.97 - 1.20	1.10
acetone	32.40	0.55 - 0.71	0.63
	19.65	0.85 - 0.92	0.89
	8.64	0.66 - 0.67	0.67
hexane	30.40	0.59 - 0.78	0.69
	15.60	0.59 - 0.72	0.66
	8.10	0.76 - 0.77	0.77

CHAPTER 4

COMPARISON OF BARBOTAGE AND NUCLEATE BOILING BUBBLE DYNAMICS

It was pointed out in the Introduction that barbotage systems are indeed attractive for the study of bubble-stirred boundary layers and as analogs of boiling systems. It was further noted that because of the mounting interest in using barbotage systems to study boiling, the time is opportune to examine and compare in more detail the hydrodynamics of these two phenomena. This chapter provides such a comparison.

4.1 Comparison of Bubble Growth Rates

It was pointed out in Sec. 2.3 that Wallis [41] compared the bubble growth rate data of Siemes and Kauffmann [36] for the constant-flow-rate case in barbotage to Stanizewski's [39] boiling growth rate results for water at atmospheric pressure; Wallis concluded that the (volumetric) growth process in both cases was linear in nature during the bulk of a bubble's life time. Recently, however, Bard [2] has argued that boiling bubbles are best simulated by having a large ante-chamber communicate directly with the orifice in barbotage. Moreover, as indicated in Chapter 2

the majority of growth rate theories in boiling predict that the bubble radius should increase as the square root of time and not as the cube root as taken by Wallis. Westwater [44], however, reports a wide variation in the time exponent (0.312 - 0.512) from an experimental investigation of boiling bubbles in pentane and ether.

It is apparent from the above discussion that further quantitative studies comparing bubble growth rates in barbotage and boiling are warranted before any reliable conclusions can be drawn. In an attempt in this direction, the experimental results of the present work were compared with boiling data in the following manner. (Attention was confined to boiling water for reasons mentioned in Sec. 3.2.2.) Inasmuch as experimental boiling growth rate results show a wide variation in the time exponent as compared to most theories which give a single value (0.5) for the same, it was thought that it would be more realistic to show the boiling data as a band for comparison with barbotage results. The same applied to barbotage results of the present work. Accordingly, experimental growth data published by various authors[†] [17,39,19,25,15,46] for saturated nucleate boiling of water at atmospheric pressure were collected and the growth results of individual bubbles of each author were made to fit a simple growth equation of the form,

[†] The survey was confined mostly to western literature which provides sufficient data for boiling water at atmospheric pressure.

$$R^* = \theta^n$$

It may be recalled that this was done in the case of barbotage results of the present work. R^* , θ , and n have again the same meaning ($R^* = \frac{R}{R_d}$, $\theta = \frac{t}{t_d}$). The growth exponent n in each case was obtained, as before, by a least-squares analysis and are given in Table 4.1. The results are also plotted on logarithmic co-ordinates and are presented as a band in Fig. 4.1. It is apparent that all individual curves enclosed by the band must of necessity pass through the point (1,1) in the graph due to the nature of the dimensionless form of the co-ordinates.

Fig. 4.1 also shows the band representing the bubble growth rate results obtained in the present work for the constant-pressure-supply case in barbotage (see Table 3.5). For the constant-flow-rate case in barbotage, the volume of a bubble should increase linearly with time, i.e. $V \propto t$ or $R \propto t^{\frac{1}{3}}$. This was verified by Siemes and Kauffmann [36]. A straight line with a slope of 1/3 and passing through co-ordinates (1,1), therefore, represents the constant-flow rate case in the figure.

A study of the graph leads to some interesting observations. Firstly, it is evident that the boiling growth rate results are 'sandwiched' between the results for the two extreme cases of barbotage systems, with a small region of overlap on the constant-pressure side. The

Table 4.1. Growth exponents for bubbles in saturated pool boiling of water at atmospheric pressure.

Author	Number of Bubbles Analysed	'n' (Average)
Han and Griffith	2	0.33
Zmola	2	0.35
Hatton and Hall	1	0.47
Staniszewski	3	0.50
Keshok and Siegel	1	0.518
Hospeti and Mesler	2	(bubble 1) 0.52
		(bubble 2) 0.64

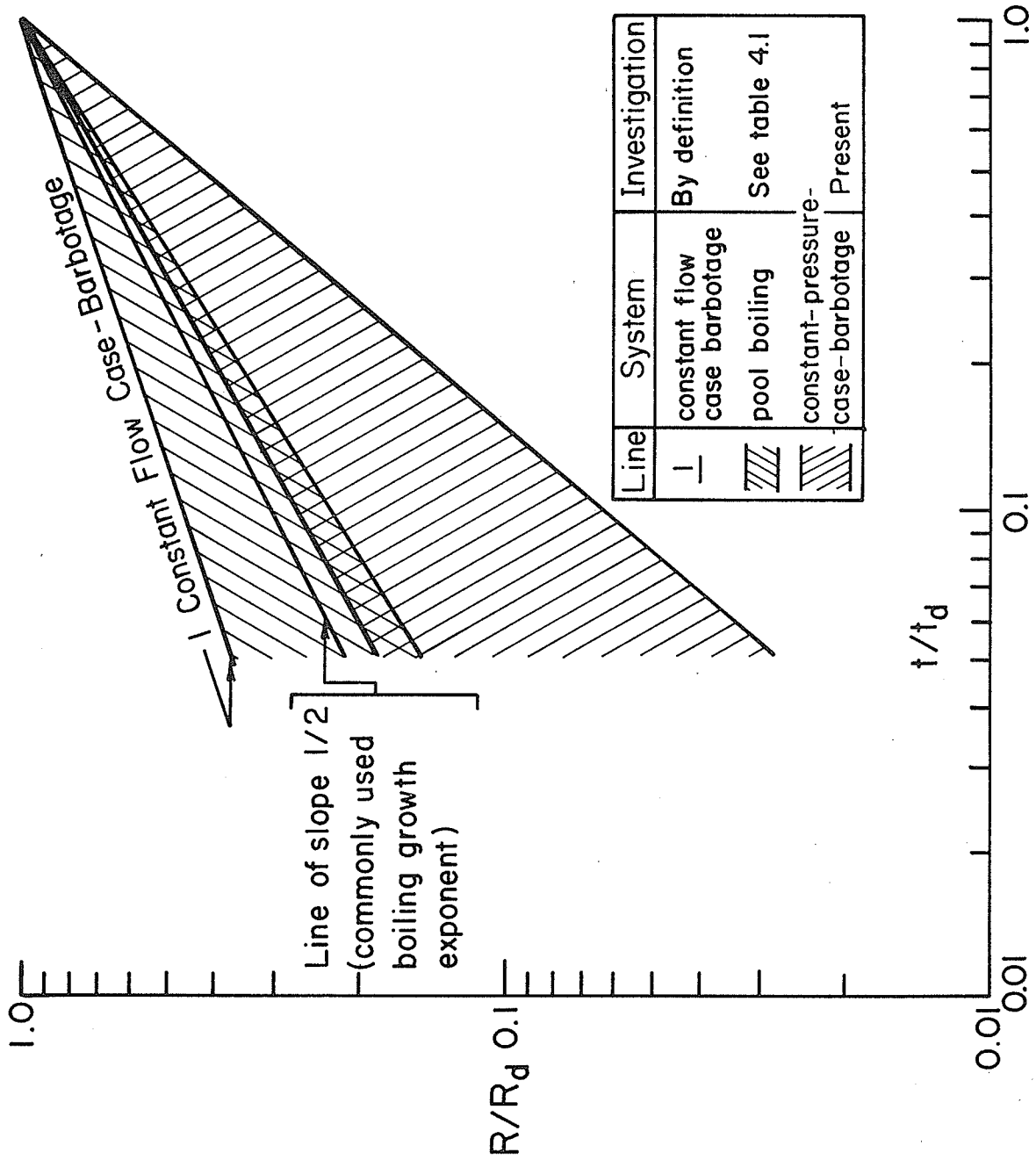


Fig. 4.1 Growth rate results for barbotage and boiling

growth rate results for other barbotage systems so far investigated (including porous surfaces) no doubt lie between the two extreme cases. (Some of the studies using barbotage as an analog of boiling are mentioned in Sec. 2.3). Secondly, it was observed in Sec. 2.1.2 that the fluid dynamic characteristics of the gas supply system in pool barbotage can have a considerable influence on the formation mechanism of a bubble and that such parameters include the L/D ratio of the orifice channel and the volume of the ante-chamber supplying gas to the orifice. It is, therefore, reasonable to conclude that by suitably altering the ante-chamber volume and the L/D ratio of the orifice, it may be possible to control the bubble formation mechanism in such a way as to obtain growth curves of any desired exponent 'n' to match those of boiling bubbles.

4.2 Bubble Departure Size

It was pointed out in Sec. 2.2.3 that the phenomenon of bubble departure in nucleate boiling is characterised by the interaction of the various forces acting on the bubble at the time of its departure. It was also stated that the same type of forces act on a barbotage bubble at departure. It was further noted that the simplest equation for predicting departure diameter in barbotage in the static regime, which takes into account the influence of the orifice diameter, is by Zuber (Eqn. 2.8) which is again given below

for immediate reference:

$$D_d = \left[\frac{12 R_o \sigma}{g(\rho_L - \rho_V)} \right]^{\frac{1}{3}} \quad (4.1)$$

The applicability of the above equation for boiling bubbles was also demonstrated in Sec. 2.2.3. In the present section, a comparison of the bubble departure sizes obtained in the static regime in barbotage and boiling will be performed and it will be clearly demonstrated that in this regime, there is a clear correspondence between the departure sizes in the two systems.

Benzing and Myers [3] have shown that the data for low frequency bubble formation in barbotage (i.e. static regime) may be satisfactorily correlated in terms of bubble diameter, orifice diameter and the physical properties of the liquid by means of the following equation

$$\frac{D_d}{D_o} = 1.82 \left(\frac{\sigma}{g D_o^2 \rho_L} \right)^{0.25} \quad (4.2)$$

where

D_d = bubble departure diameter

D_o = orifice or cavity diameter

We shall now proceed to show the applicability of this equation to the case of saturated pool boiling of liquids. Recourse is again made to Howell and Siegel's results in

boiling since their experiments were performed at a very low heat flux (static regime in boiling) and involved different cavity diameters. By substituting appropriate values for the variables appearing on the right hand side of Eqn. 4.2, values of D_d/D_o can be calculated. These results are shown in Fig. 4.2, where experimental values of D_d/D_o are plotted against the values calculated from Eqn. 4.2. It is evident from the figure that the agreement is reasonably good, with the worst case ($D_o = 0.0097$ cm; $D_d/D_o = 12.9$) giving a deviation of about 30 per cent based on the measured value. It may thus be concluded that the bubble departure sizes in the static regime in barbotage and boiling are indeed comparable in magnitude.

A quantitative comparison of the bubble departure sizes in the dynamic regime does not appear to be possible at the present time due to lack of availability of experimental results in saturated pool boiling for the case of bubbling at high heat-transfer rates from a nucleating cavity of known size, D_o . As indicated in Sec. 2.2.3, D_o appears to be an important factor influencing the size of a departing bubble in both boiling and barbotage; hence, the limitation of the present comparative study to the static regime. It is, however, shown in Chapter 6 that a bubble departure theory, applicable in the dynamic regime in barbotage, can be modified, using an appropriate

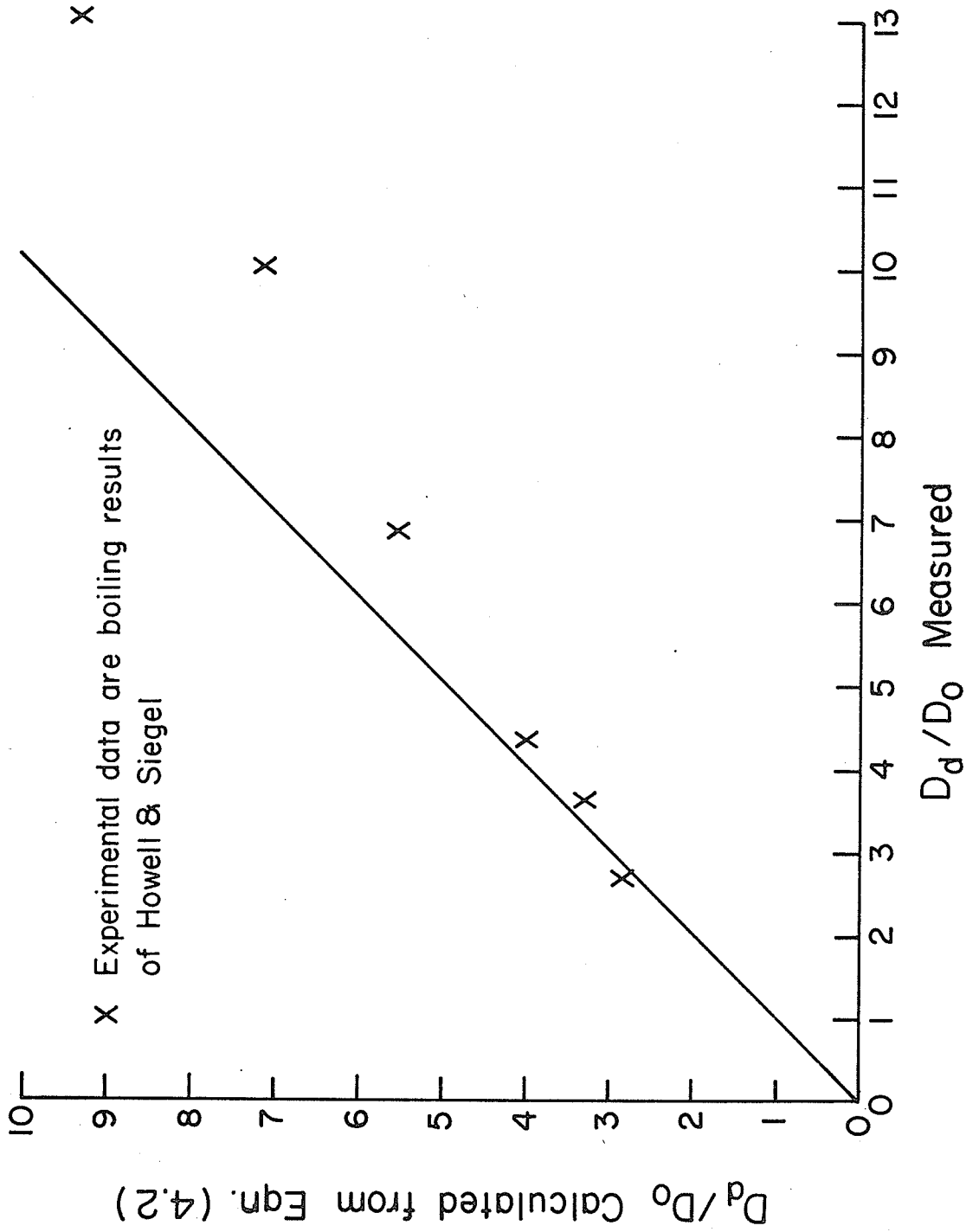


Fig. 4.2 Comparison of measured and calculated values of D_d/D_0

expression for the boiling bubble growth constant, β , to predict bubble departure diameters in boiling where the relevant data exist.

4.3 Bubble Frequency

In order to make a quantitative comparison of the bubble frequencies in barbotage and boiling, recourse was made to Ivey's recent review [20]. Figure 2.2, which was extracted from his work and which gives the data points collected from literature for the f vs D_d relationship in boiling, is reproduced as Fig. 4.3. Because of the large amount of scatter seen in the data in Fig. 2.2 it was decided to present these data as a closed region in Fig. 4.3 for purposes of comparison with barbotage data. Superimposed on this figure are experimental barbotage data collected from the present work and the literature. A comparison of the boiling and barbotage data leads to the following observations:

- (i) It can be seen that the barbotage data generally either straddle or overlap with the boiling data.
- (ii) On the figure, orifice diameters associated with particular barbotage results are indicated; apparently the effect of increasing D_o is to increase D_d and reduce f . This same trend is especially apparent in the boiling results of Hatton and Hall (see Fig. 2.2).

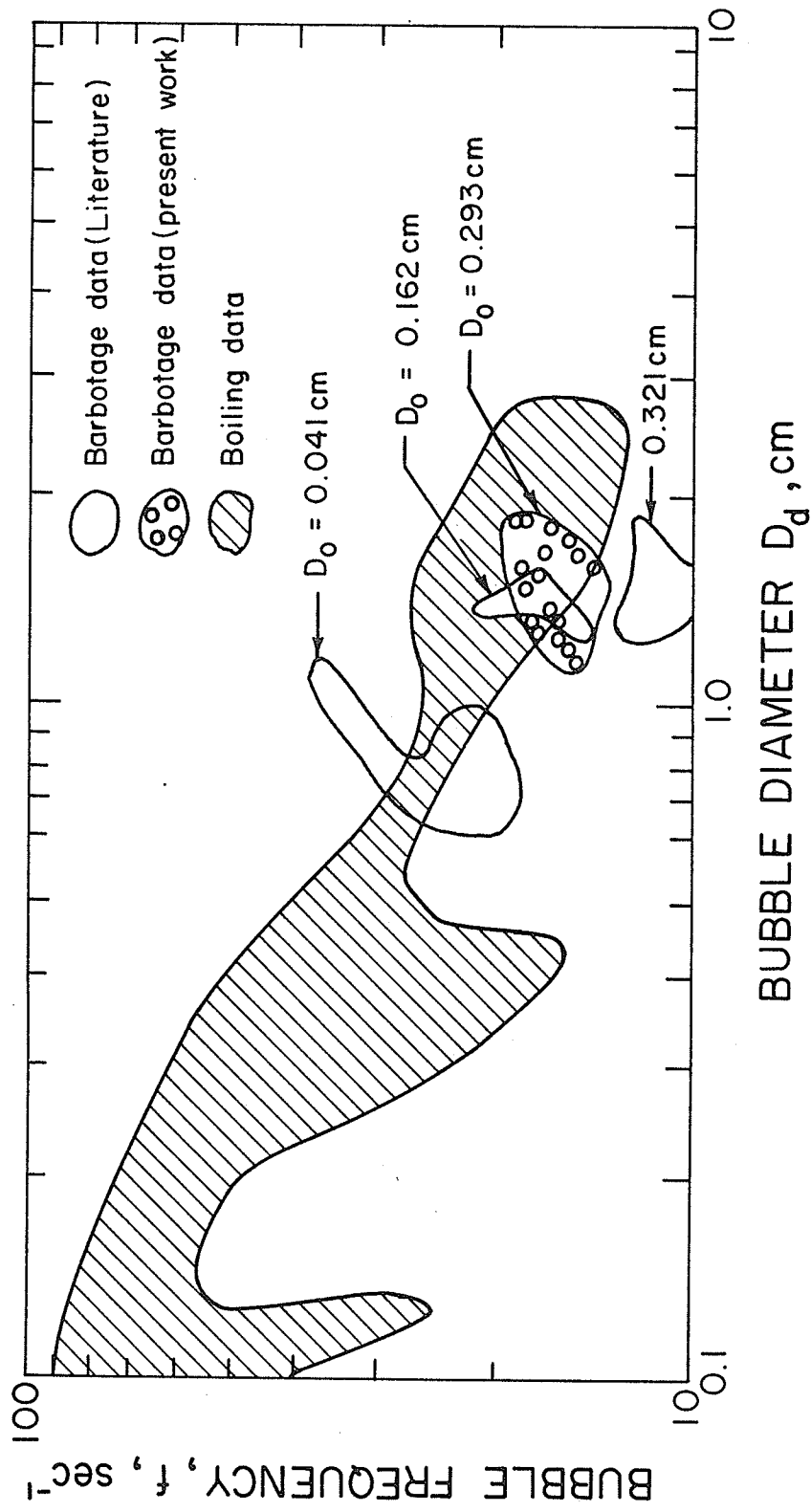


Fig. 4.3 Comparison of frequencies in barbotage and boiling

CHAPTER 5

THEORETICAL ANALYSIS OF THE PROBLEM OF BUBBLE GROWTH UNDER CONSTANT-PRESSURE-SUPPLY CONDITIONS FROM A SUBMERGED ORIFICE

The objective of the present chapter is to perform a theoretical analysis of the problem of bubble growth from a submerged orifice when a gas from a constant-pressure reservoir is injected through the orifice. The liquid and gas properties are assumed to be available.

5.1 Theoretical Formulation of the Problem

Frequent reference is made in the literature on cavitation to Rayleigh's solution for the problem of the collapse of a spherical cavity in a liquid [47]. For the present problem of the growth of a bubble, the extension of the Rayleigh theory, as carried out by Plesset [30], can be used to obtain the equation of motion. The equation is

$$R\ddot{R} + \frac{3}{2} \dot{R}^2 + \frac{2\sigma}{\rho_L R} = \frac{P_b - P_\infty}{\rho_L} \quad (5.1)$$

where

R = radius of the bubble,

\dot{R} = first derivative of the radius with respect

to time,

\ddot{R} = second derivative of the radius with respect
to time,

σ = surface tension of the liquid,

ρ_L = the liquid density,

p_b = pressure in the bubble, and

p_∞ = pressure at a large distance from the bubble
at the level of the orifice.

A complete derivation of the above equation is given in Appendix H. The assumptions made in the formulation and use of the above equation are as follows:

- (i) The gas-liquid interface is spherical at all times during growth.
- (ii) The medium surrounding the interface is quiescent and incompressible and of infinite extent.
- (iii) The pressure inside the bubble is uniform and constant at any instant.
- (iv) Liquid flow is irrotational.
- (v) There is no transfer of liquid vapour into the bubble.

The assumption of a spherical shape for the bubble throughout the period of growth simplifies the geometrical specification of the bubble surface and enables the determination of the inviscid flow field in the liquid by means of potential theory.

Assumption (ii) neglects all effects due to

preceding bubbles. In the real case of a bubble forming at an orifice, however, some circulation does exist as the bubble moves upward at detachment. The effect of that circulation upon the formation of the succeeding bubble is difficult to take into account theoretically. However, it has been found that the effect of liquid circulation on bubble formation is minimized when the liquid is prevented from circulating up along the base of the bubble. That is ensured, to an extent, for example, in the case of a bubble formed above a flat plate orifice.

Assumptions (iii) and (iv) need no comment.

Regarding Assumption (v), in the present experiment care was taken to saturate the air with the appropriate experimental liquid before injection through the orifice. This minimizes any transfer of liquid vapour into the bubble during formation.

Orifice equation:

An examination of Eqn. 5.1 reveals that it consists of two unknown variables, R and p_b , the bubble pressure which varies with R . Another equation involving these quantities is therefore essential for a solution. A simple orifice equation describing the flow rate of gas into the bubble is used for this purpose and is given below. The fluid here (air) is assumed to be incompressible.

$$Q = \frac{dV}{dt} = CM'A_0 \left[\frac{2(p_1 - p_b)}{\rho_g} \right]^{1/2} \quad (5.2)$$

where

Q = gas flow rate,

C = coefficient of discharge,

$$M' = \frac{1}{(1 - (A_0/A_1)^2)^{1/2}},$$

A_1 = cross-sectional area of chamber upstream of the orifice,

A_0 = cross-sectional area of orifice,

ρ_g = gas density,

p_1 = pressure in the ante-chamber, and

p_b = pressure in the bubble.

5.2 Method of Solution

Equation 5.1 can be solved explicitly for R as a function of t by substituting for p_b from Eqn. 5.2.

Assuming the volume of the bubble to be given by $\frac{4}{3} \pi R^3$ and the area of the orifice to be πR_0^2 , the equation (after the above substitution for p_b) can be further manipulated into a dimensionless form and the result is as follows:

$$R^* \ddot{R}^* + 1.5 \dot{R}^{*2} + 8ER^{*4} \dot{R}^{*2} + \frac{2}{R^*} = 2\Delta P^* \quad (5.3)$$

where

$$\begin{aligned} R^* &\equiv \frac{R}{R_0}, \\ \dot{R}^* &\equiv \frac{dR^*}{dt^*}, \\ \ddot{R}^* &\equiv \frac{d}{dt^*} \left(\frac{dR^*}{dt^*} \right), \\ t^* &\equiv t \left[\frac{\sigma}{\rho_L R_0^3} \right]^{1/2}, \end{aligned}$$

$$\Delta P^* \equiv \frac{\Delta P}{\Delta P_{\text{crit}}} \equiv \left[\frac{P_1 - P_\infty}{\frac{2\sigma}{R_0}} \right]$$

K = the product CM' (see Eqn. 5.2)

$$E = \frac{1}{(K)^2} \frac{\rho_g}{\rho_L}$$

The initial conditions for solving Eqn. 5.3 are:

at time $t=0$

$$R^*(0) = 1$$

$$\dot{R}^*(0) = 0$$

The solution of Eqn. 5.3 was carried out by numerical integration, using a fourth order Runge-Kutta formula. The integration can be performed for any desired length of time up to break-off (departure).

5.3 Results and Discussion

An examination of Eqn. 5.3 reveals that there are two dimensionless parameters, namely $E (= \frac{1}{K^2} \frac{\rho_g}{\rho_L})$ and ΔP^* whose values can be varied to obtain sets of curves for R^* vs t^* . In the present work, the value of ΔP^* was increased from 1.0 to 3.0 for fixed values of E (0 to 0.01) and the resulting curves are presented in Figs. 5.1 through 5.5. Such a presentation allows one to determine quickly the appropriate growth curve, once the fluid properties, the pressure drop ΔP and the factor K are established for any given system. The range of values of ΔP^* and E

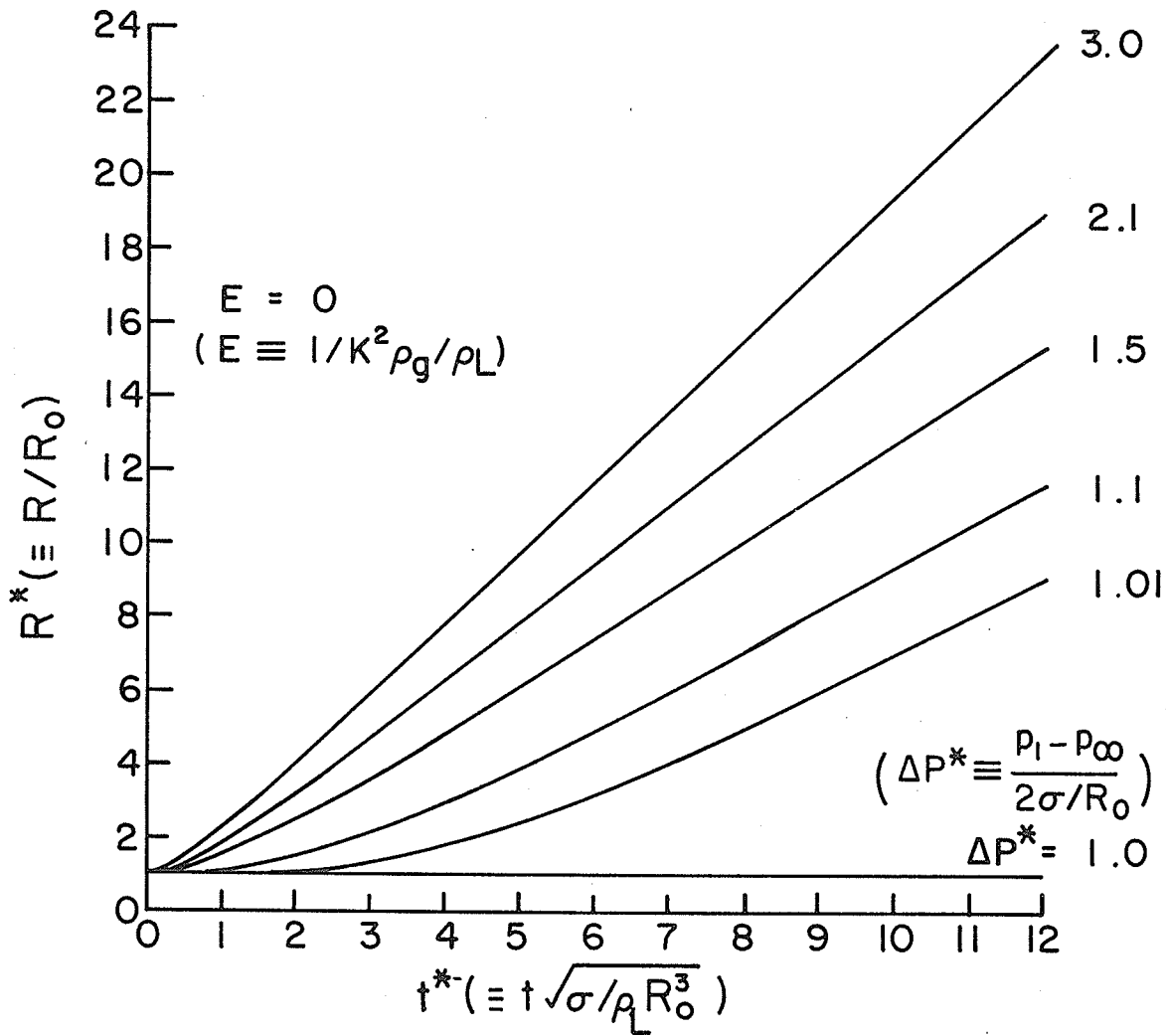


Fig. 5.1 Theoretical bubble growth curve for $E = 0.0$

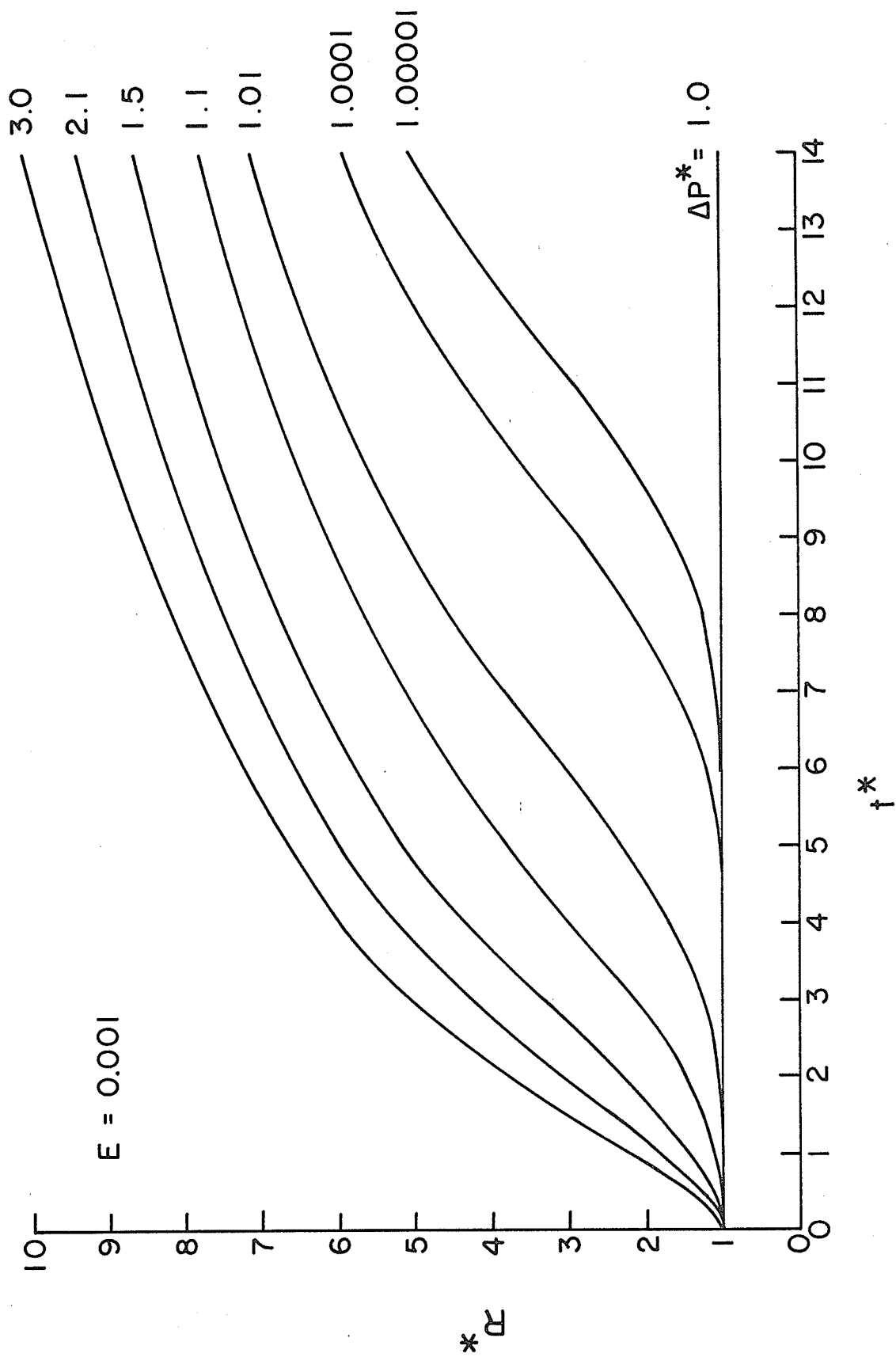


Fig. 5.2 Theoretical bubble growth curve for $E = 0.001$

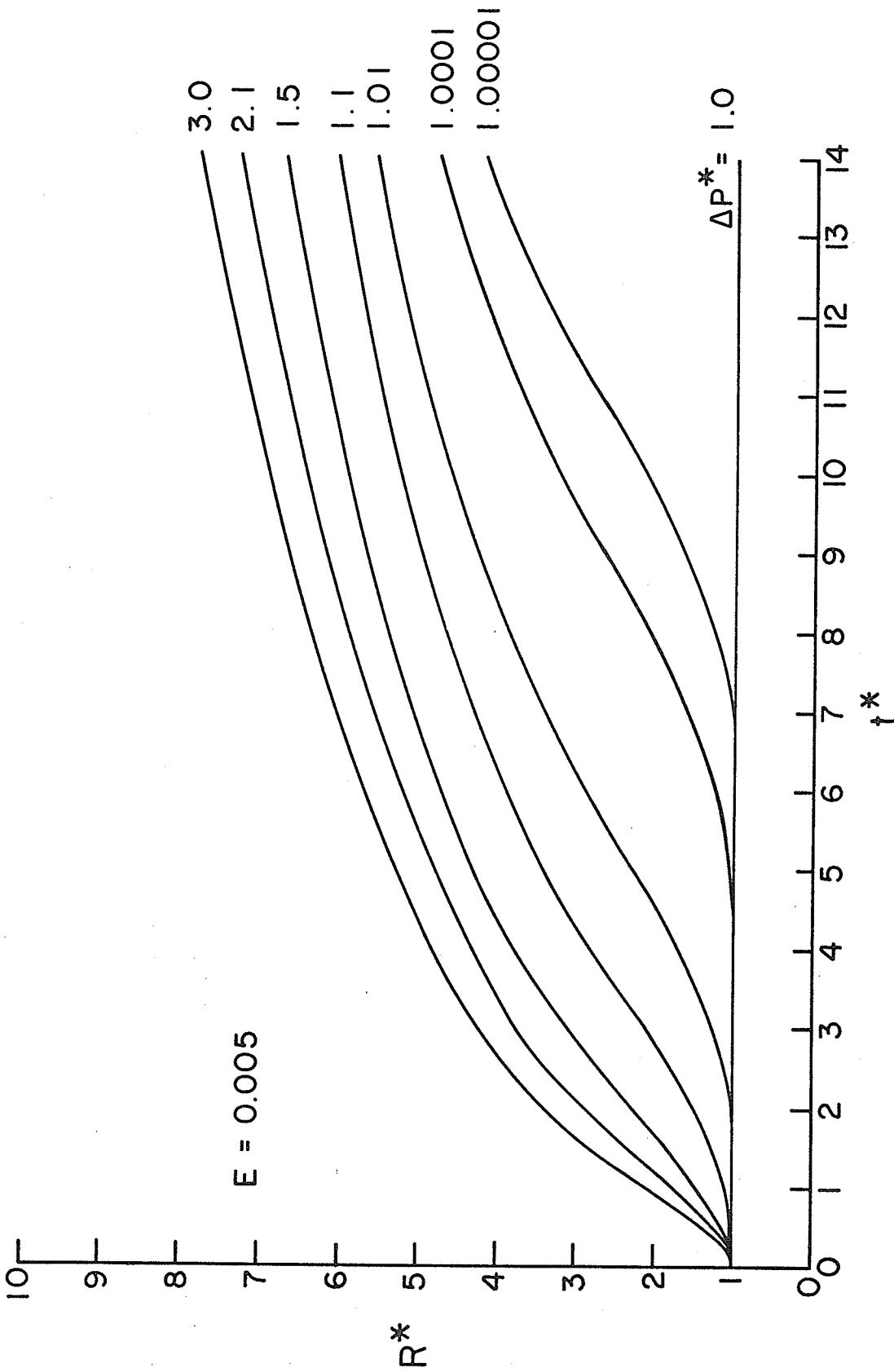


Fig. 5.3 Theoretical bubble growth curve for $E = 0.005$

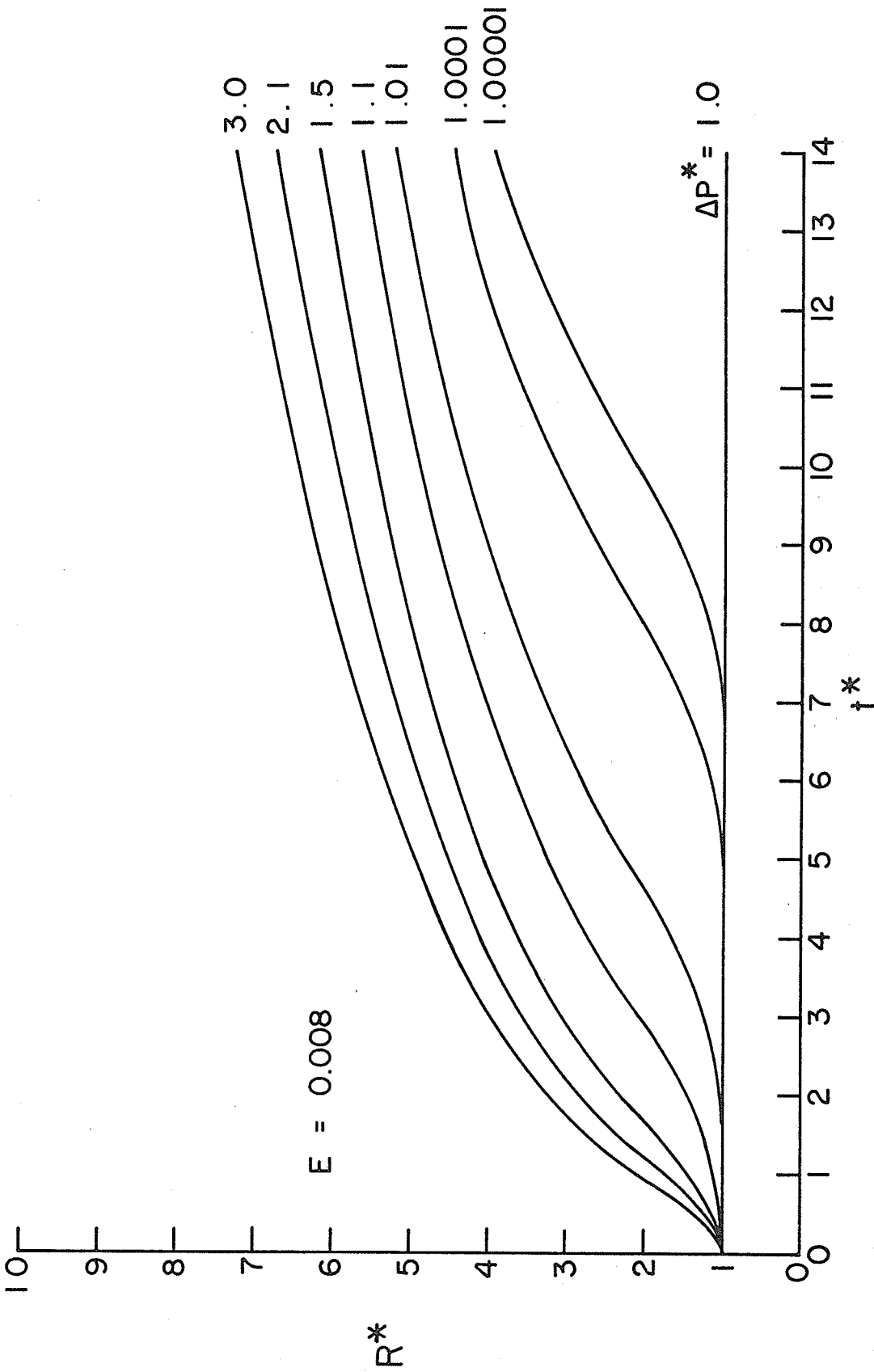


Fig. 5.4 Theoretical bubble growth curve for $E = 0.008$

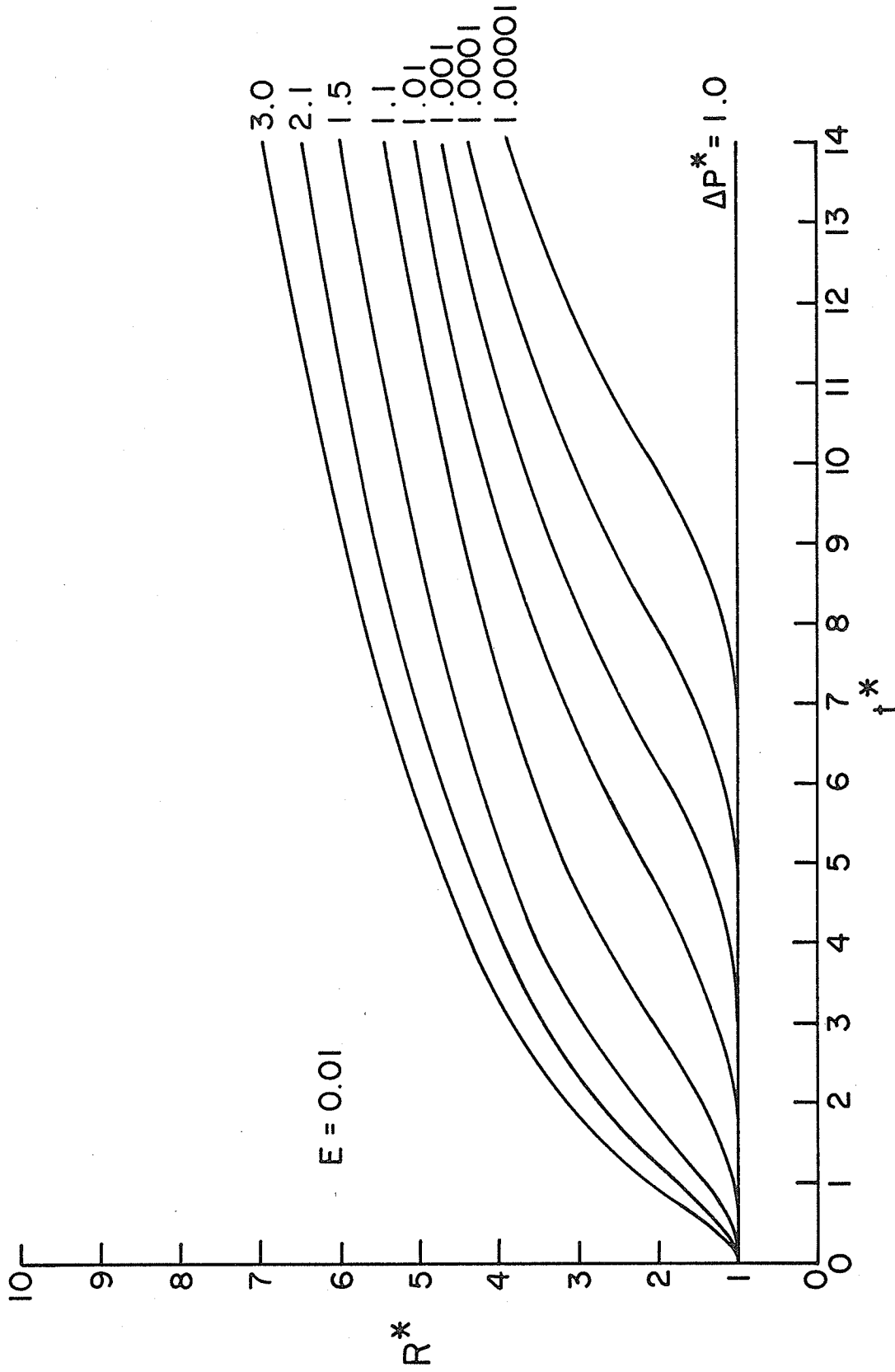


Fig. 5.5 Theoretical bubble growth curve for $E = 0.01$

obtained in the present experimental work were 1.1 to 2.9 and 0.00284 to 0.00428, respectively.

Figures 5.6 through 5.14 present experimental growth rate curves obtained in the present work, along with the corresponding theoretical curves obtained by solving Eqn. 5.3. The experimental curves are the curves of bubbles shown in Figs. 3.10 to 3.18 and belong, in each case, to the bubble whose growth curve lies (in these figures) between those of the other two bubbles analysed for the same conditions. For the present comparison and for any one particular condition, the time and radius of the bubble have been recalculated in non-dimensional quantities (see tabulated data in Tables E.1, E.2 and E.3); also, the end of the formation time for the experimental curves has been taken to correspond to the time at which the actual detachment of primary-secondary bubble combination from the orifice occurs. The relevant dimensionless parameters are indicated on the figures. The value of K to be used in the parameter E was determined in the following manner. Experimental values of K determined accurately by several investigators [7,8,23] for a range of orifice diameters were plotted against the corresponding orifice diameter and a smooth curve drawn through the points. The values of K were found to vary from a value of 0.58 for a 0.05 cm diameter orifice to a value of 0.67 for a 0.4 cm diameter orifice. From the curve the value of K corresponding to the diameter of the orifice

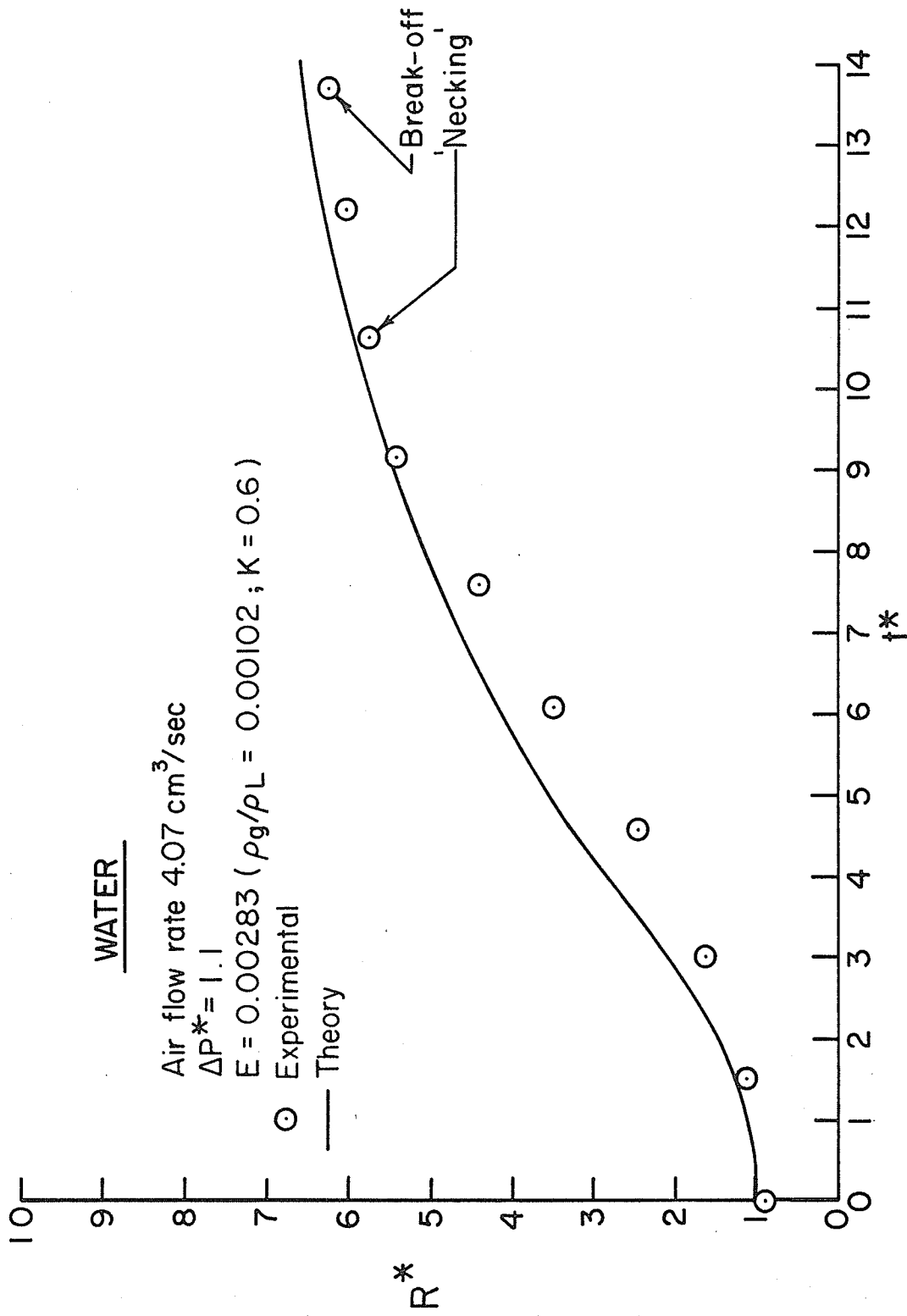


Fig. 5.6 Comparison of experimental and theoretical bubble growth rates for water - air flow rate 4.07 cm³/sec

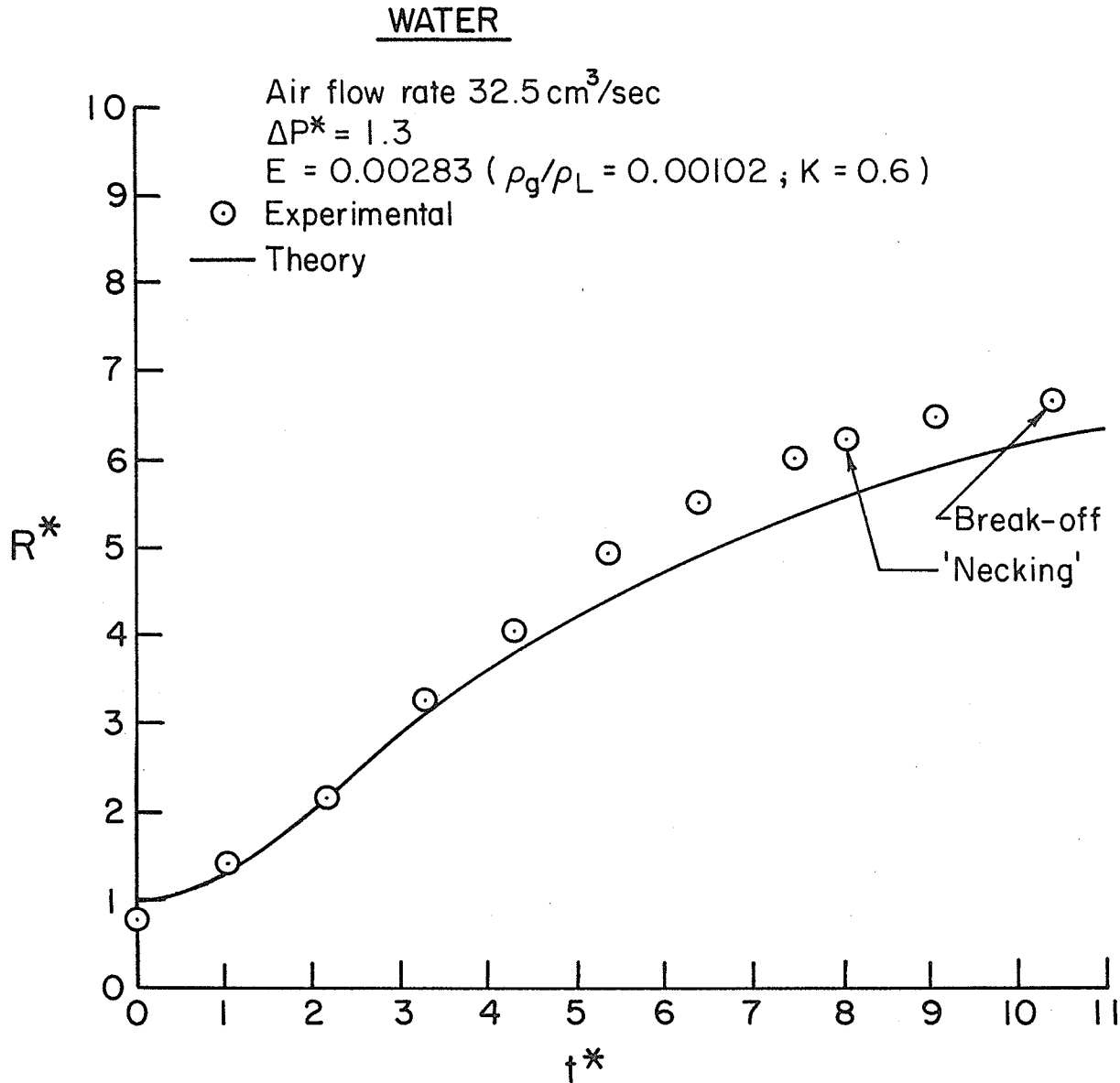


Fig. 5.7 Comparison of experimental and theoretical bubble growth rates for water
 - air flow rate $32.5 \text{ cm}^3/\text{sec}$

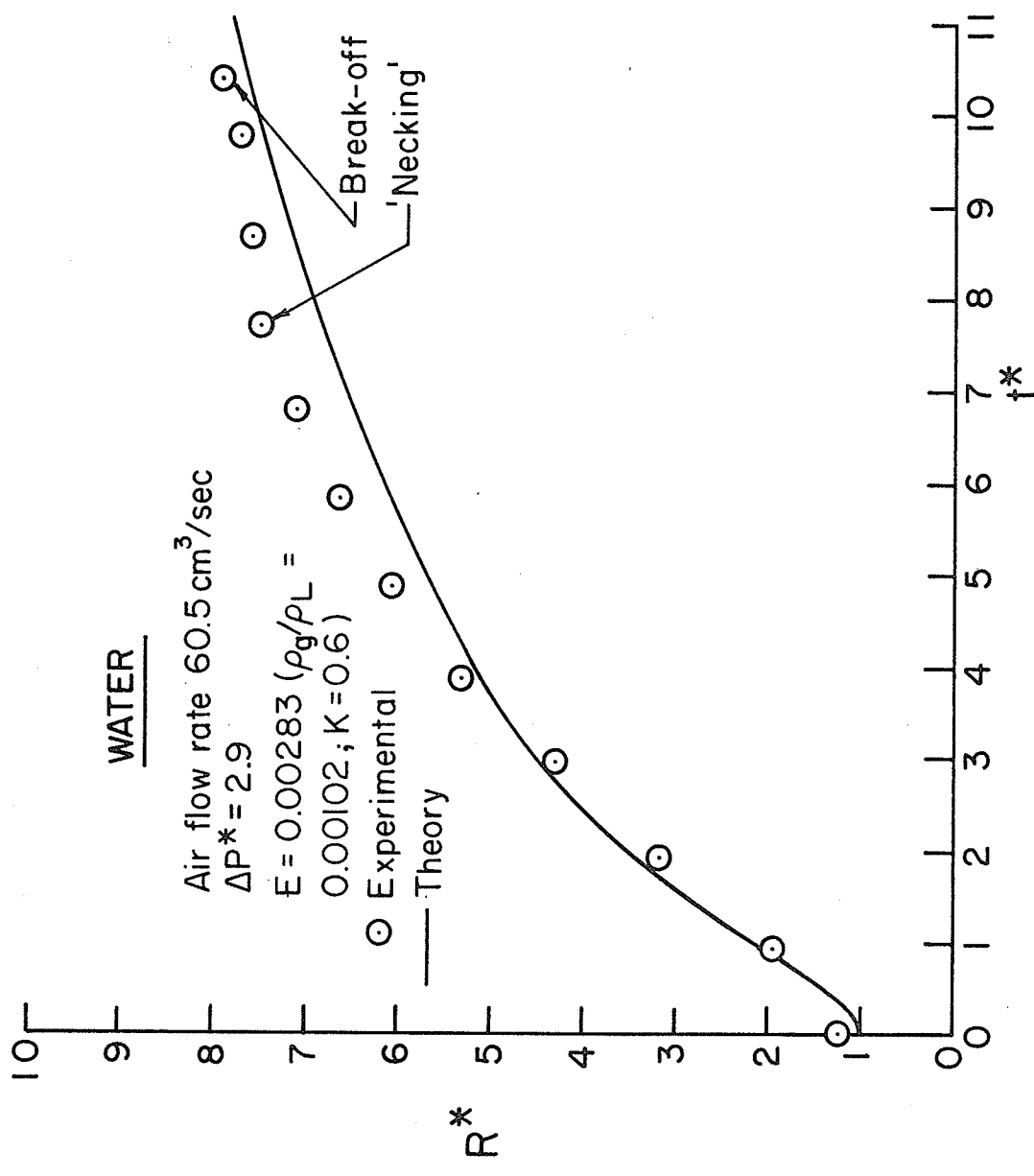


Fig. 5.8 Comparison of experimental and theoretical bubble growth rates for water - air flow rate 60.5 cm³/sec

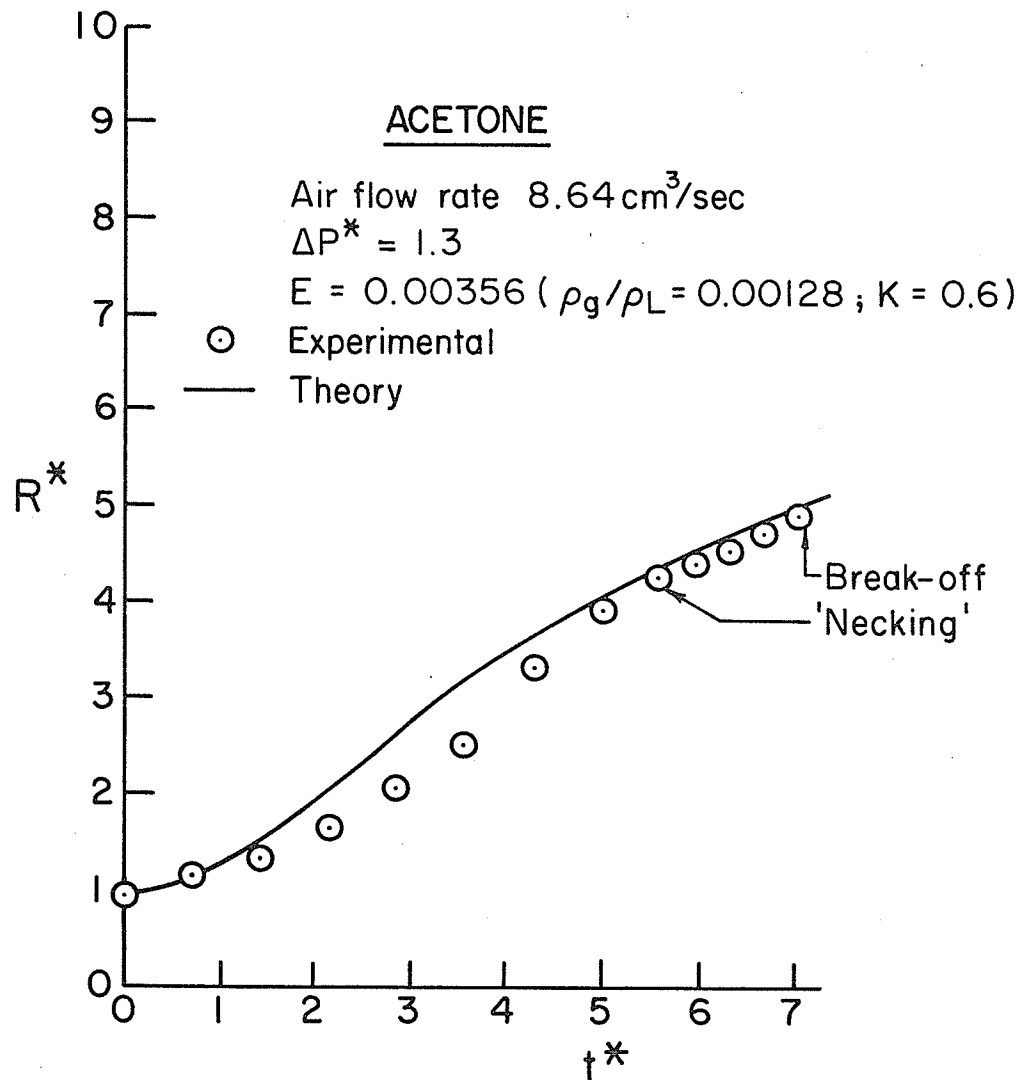


Fig. 5.9 Comparison of experimental and theoretical bubble growth rates for acetone - air flow rate $8.64 \text{ cm}^3/\text{sec}$

ACETONE

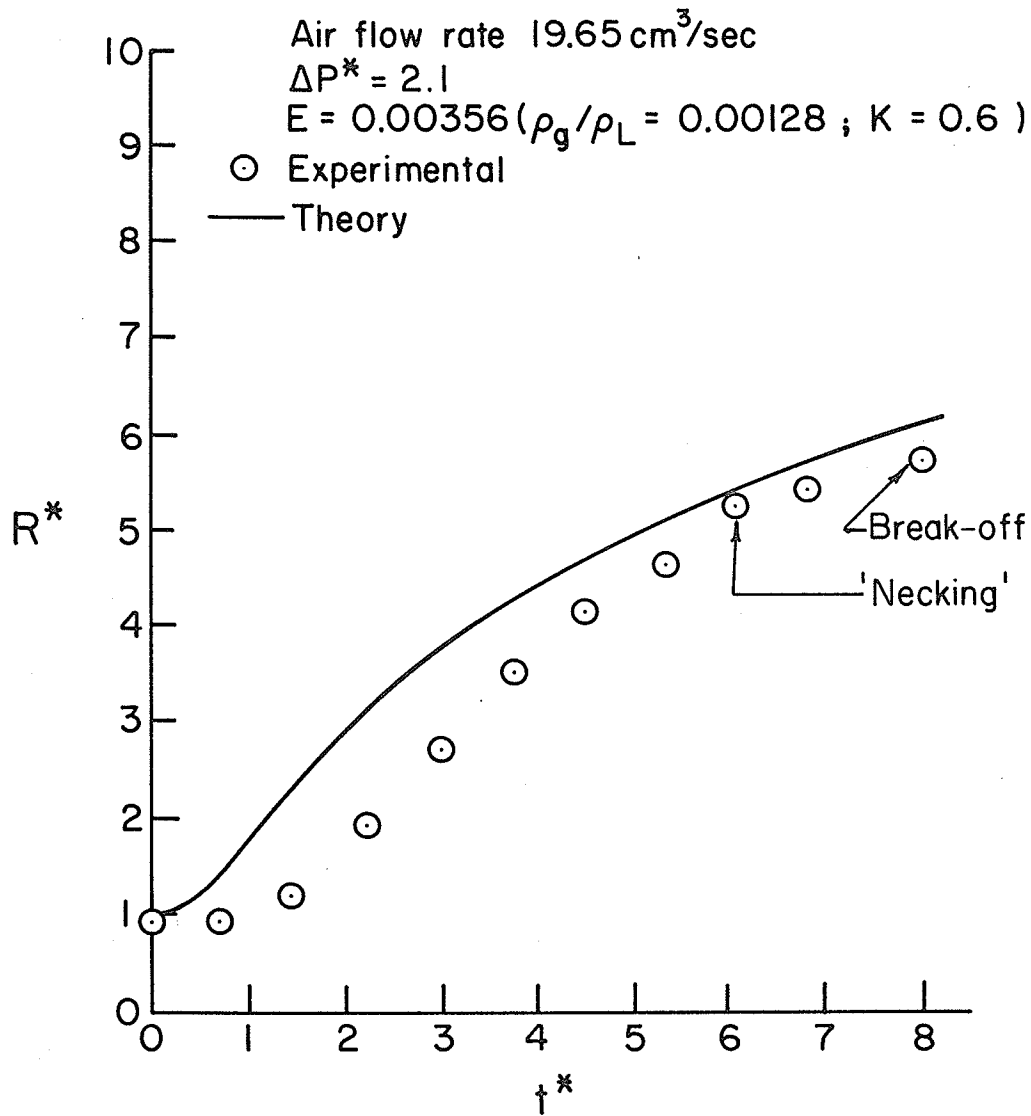


Fig. 5.10 Comparison of experimental and theoretical bubble growth rates for acetone
 - air flow rate $19.65 \text{ cm}^3/\text{sec}$

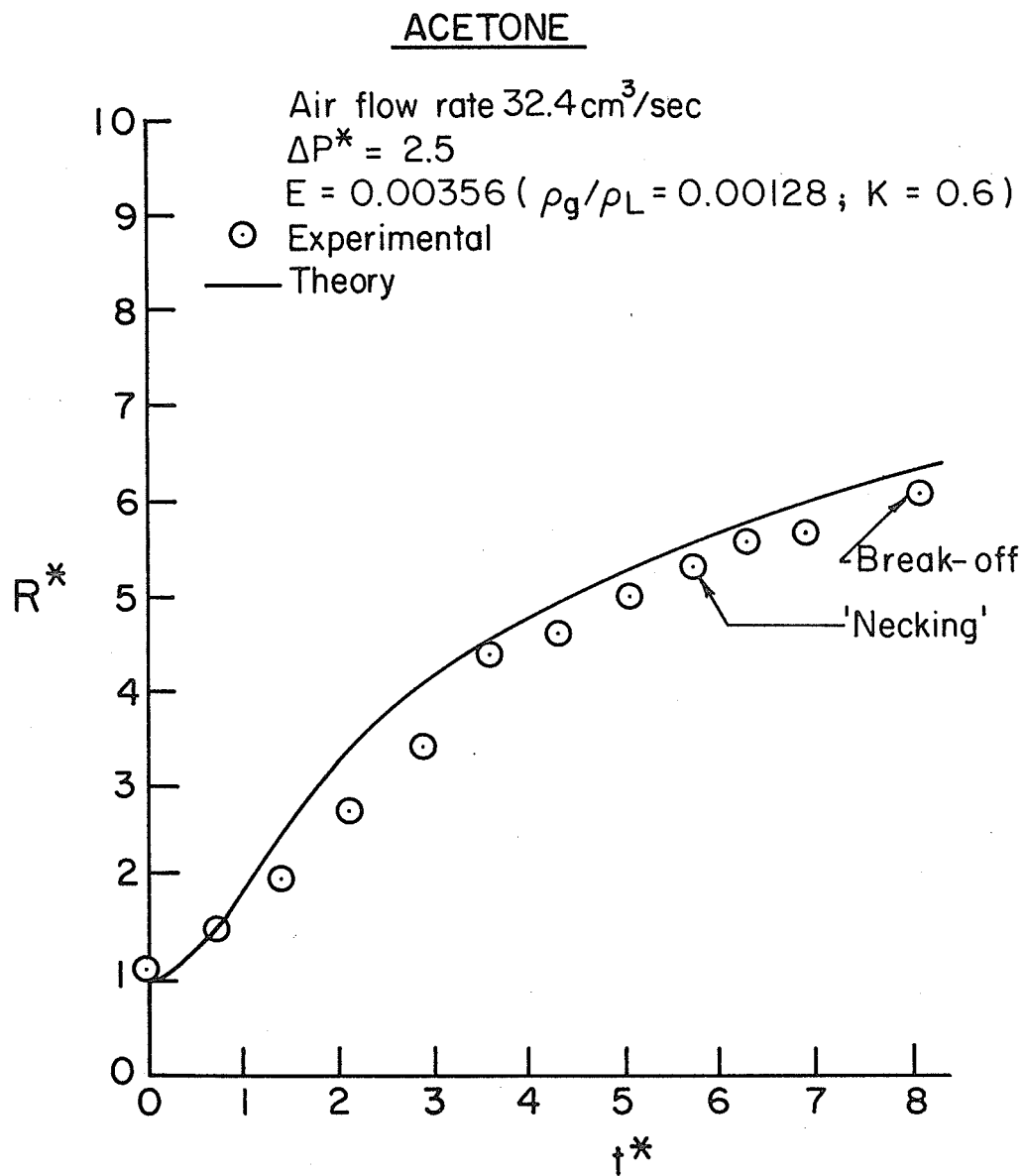


Fig. 5.11 Comparison of experimental and theoretical bubble growth rates for acetone
 - air flow rate $32.4 \text{ cm}^3/\text{sec}$

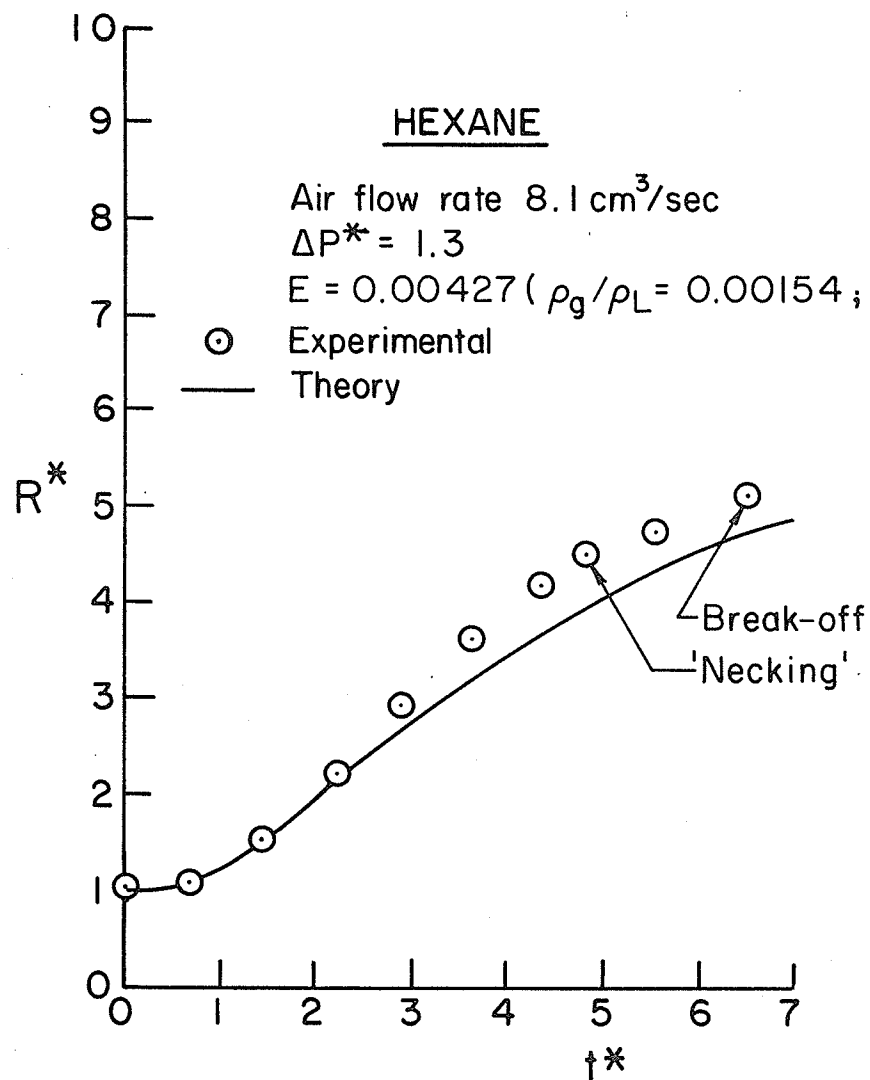


Fig. 5.12 Comparison of experimental and theoretical bubble growth rates for hexane
 - air flow rate $30.4 \text{ cm}^3/\text{sec}$

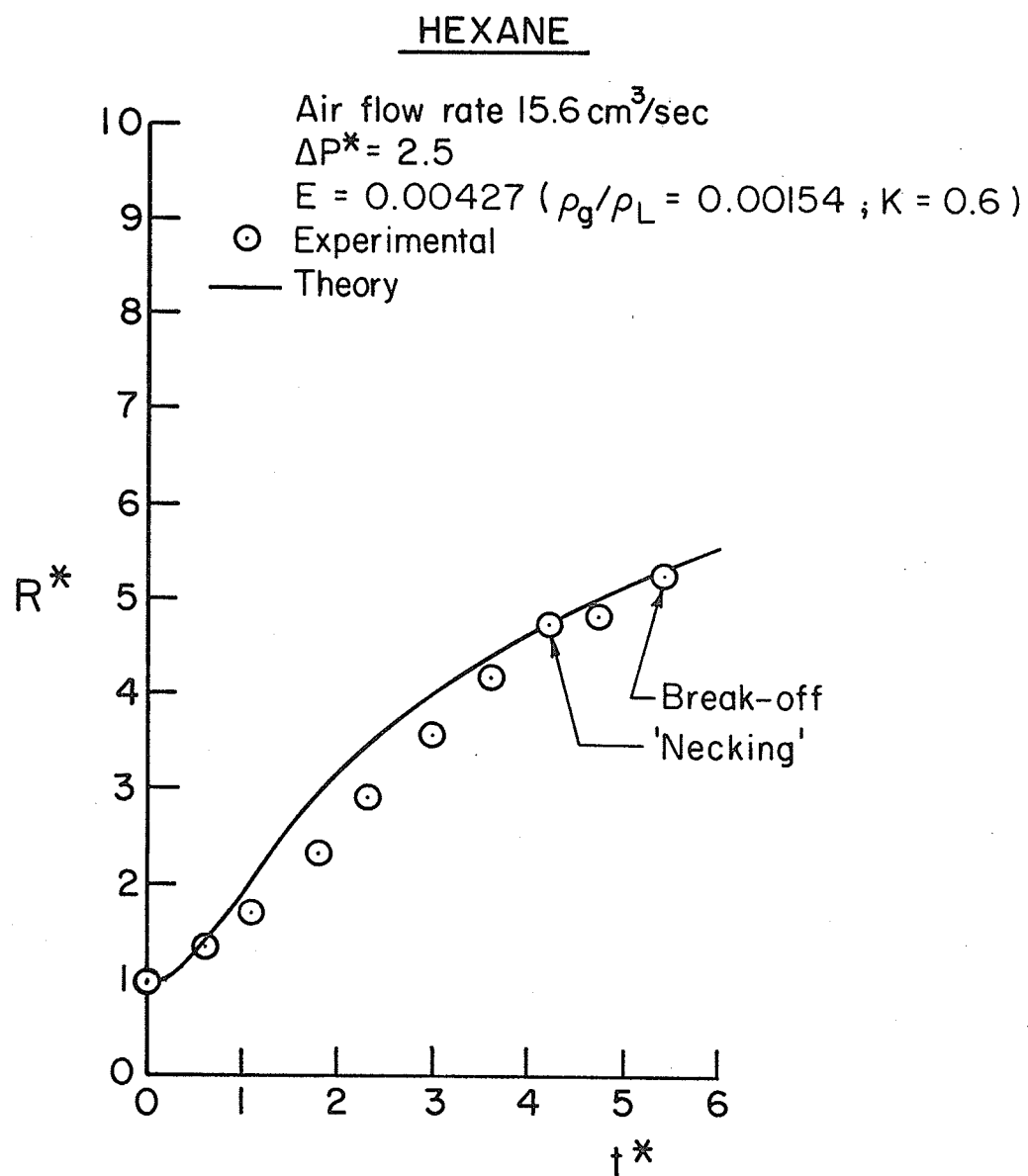


Fig. 5.13 Comparison of experimental and theoretical bubble growth rates for hexane
 - air flow rate $15.6 \text{ cm}^3/\text{sec}$

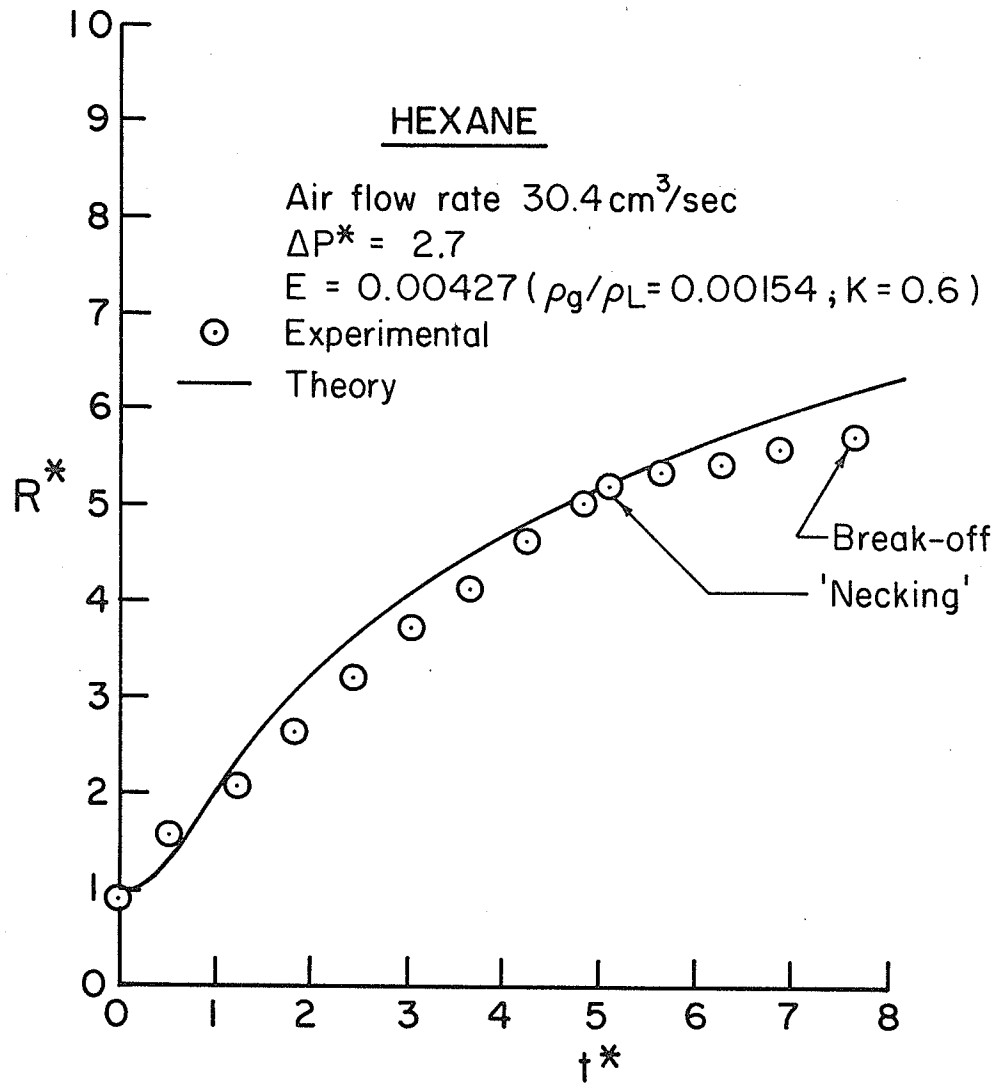


Fig. 5.14 Comparison of experimental and theoretical bubble growth rates for hexane
 - air flow rate $30.4 \text{ cm}^3/\text{sec}$

used in the present work was obtained as 0.6. This is as one would expect since $K = CM'$, where C is the coefficient of discharge, whose value is expected to be approximately 0.6 while M' , the velocity of approach factor is essentially equal to one. The growth rate solution was, in any case, found to be quite insensitive to small changes in K . This was verified by varying the value of K in the parameter E from 0.5 to 0.7. The resulting deviation in the dimensionless radius of the bubble was found to vary from zero per cent at zero time to about 10 per cent at the time of departure.

It can be seen from the figures that the agreement between the theoretical and experimental curves are surprisingly good for all test liquids, when one considers the various simplifying assumptions made in the theoretical analysis. Further, this is the first time the problem of bubble growth under constant-pressure-supply conditions has been analysed by combining Rayleigh's equation with an orifice equation and a set of general solutions obtained. It should, however, be emphasized here that although the present analysis seems adequate for the case of inviscid liquids, further theoretical and experimental investigations are necessary to deal with the case of viscous fluids where the drag forces will be influential in determining the growth rate.

CHAPTER 6

APPLICATION OF BARBOTAGE THEORY TO BOILING FOR THE PREDICTION OF DEPARTURE DIAMETERS

6.1 Background

The prediction of the bubbling frequency and bubble departure diameter is of central importance in the theoretical study of nucleate boiling. Several investigators [13,30,15,10,9,4] have attacked the problem of bubble growth and departure in both uniformly-superheated liquids and in saturated pool boiling characterised by a non-uniform temperature field. Most of the expressions proposed for bubble departure from a nucleation site assume, for the sake of simplicity, a spherical shape for the bubble at departure and result from equating the downward forces acting on the bubble to upward forces at the moment of departure. Some experimenters, e.g., [17,23], have mentioned that a small neck is formed prior to the departure of the bubble connecting the bubble to the heated wall or the cavity. Saddy and Jameson [35] used this fact in their theory for prediction of bubble departure diameter in uniformly-superheated liquids from a nucleation site of known geometry. To determine the criterion for

detachment of the bubbles, resort was made to experiment. It was observed that detachment occurred when the distance travelled by the centre of the bubble equalled 1.5 times the radius of the bubble.

Kumar *et al.* [23] have proposed a two-stage theory for barbotage bubble formation from submerged orifices and found excellent agreement between their theory and experimental results. Inasmuch as this dissertation deals with the comparison of the bubble dynamics in barbotage and boiling, it is proposed to show in this chapter that the theory of Kumar *et al.* for barbotage can be used with appropriate modifications for successfully predicting bubble departure diameters in nucleate boiling. Such a prediction is, however, subject to availability of reliable information regarding two important parameters, viz, the boiling bubble growth constant β and the cavity diameter D_0 ; this will be apparent from the equations derived below. A survey of boiling literature to find experimental data for purposes of comparison with theory indicated only one source which offers a combination of D_0 and experimental conditions which strictly satisfy the requirements of a well-known theoretical expression (viz, Scriven's [37]) for the growth constant β . These are the results of Saddy and Jameson [35], who performed experiments in uniformly-superheated liquids. (As indicated earlier, the phenomenon of 'neck' was observed in their experiments.)

In view of the above, the barbotage theory to be described below has been modified to incorporate the aforesaid expression of Scriven for the constant β , and compares the predicted values with the experimental results of Saddy and Jameson.

6.2 Development of the Model

Consider a spherical vapour bubble growing at a nucleation site on a solid surface. The present model assumes bubble formation to take place in two stages, namely the 'expansion' stage and the 'detachment' stage. During the first stage, the bubble expands while its base remains attached to the nucleation site, whereas, in the detachment stage, the bubble base moves away from the site, the bubble itself being in contact with the site through a neck. The two stages of bubble formation are shown in Fig. 6.1. The final volume of the bubble V_{FIN} is the sum of the individual volumes developed during the two stages. Thus,

$$V_{FIN} = V_{EXP} + V_{TRANS}$$

where

V_{EXP} = volume of the bubble at the end of the first stage, and

V_{TRANS} = volume added to the bubble during the second stage.

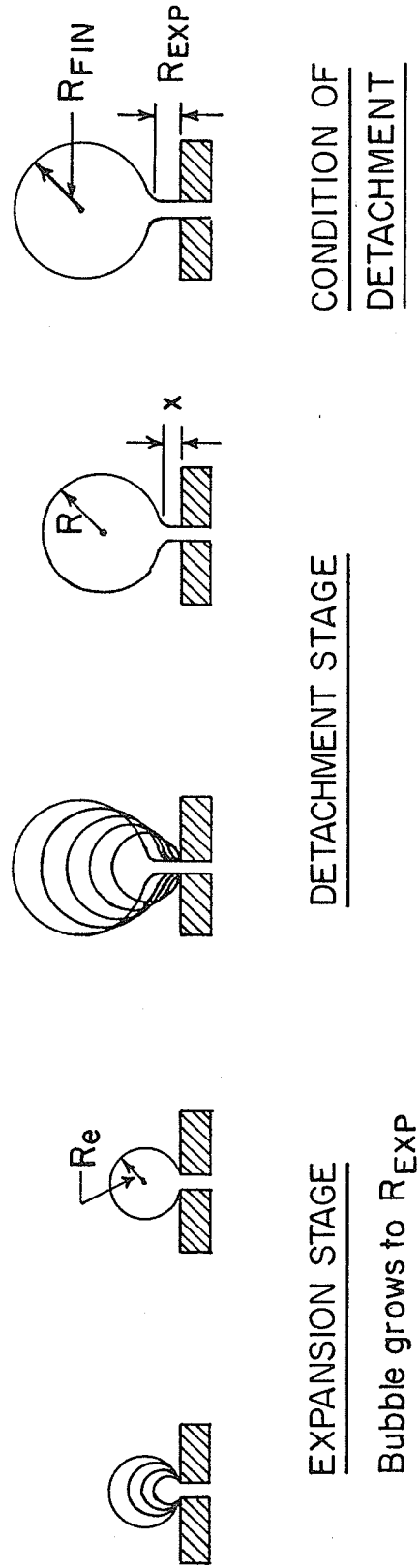


Fig. 6.1 Mechanism of bubble formation

The evaluation of V_{EXP} and V_{FIN} is discussed below. Knowing V_{FIN} , the 'equivalent' bubble departure diameter can be evaluated from the following equation relating D_d (departure diameter) and V_{FIN}

$$D_d = \frac{6 V_{FIN}^{1/3}}{\pi}$$

6.3 Evaluation of V_{EXP}

In setting up a mathematical description of the process, the following assumptions are made:

(i) Single spherical bubbles are formed and released one at a time and there is no interaction between successive bubbles.

(ii) Viscous effects are neglected.

(iii) Density of the vapour in the bubble is neglected since it is very small when compared with liquid density and it is also assumed that there are no pressure variations inside the bubble.

Expansion stage:

During the first stage of formation of the bubble the forces acting on the bubble are as follows. The first stage ends when the downward forces equal the upward forces.

(a) Buoyancy force = $V(\rho_L - \rho_V)g$, acting upwards on the bubble. Here,

V = volume of the bubble,
 ρ_L = liquid density,
 ρ_v = vapour density, and
 g = acceleration due to gravity.

(b) Surface tension force = $\pi D_o \sigma \sin \theta$, acting to restrain the bubble at the orifice. Here,

D_o = orifice diameter,
 σ = surface tension of liquid, and
 θ = the contact angle between the bubble and the heated surface.

(c) Liquid inertial force = $\frac{d}{dt_e} (Mv_e)$. This dynamic force is set up due to the expansion velocity of the bubble and acts to restrain the bubble at the orifice. In the above equation

M = virtual mass [7,23] of the bubble, which is the sum of the mass of vapour and that of 11/16 times the mass of liquid displaced by the bubble. Since $\rho_v \ll \rho_L$, $M \approx \frac{11}{16} V \rho_L$,

v_e = velocity of expansion during the first stage, and

t_e = any time during expansion stage.

Now, the base of the bubble remains stationary while the uppermost point of it moves with a velocity equal to the rate of change of the bubble diameter. Hence, the average bubble velocity is the velocity of its centre and is equal to the rate of change of bubble radius. Therefore,

$$v_e = \frac{dR_e}{dt_e} \quad (6.1)$$

Equating the upward and downward forces at the end of the first stage, and discarding ρ_v as negligible when compared with ρ_L , we have

$$V_{EXP} \rho_L g = \pi D_o \sigma + \frac{d}{dt_e} (Mv_e) \quad (6.2)$$

Here, $\sin \theta$ is assumed to be unity, since at the end of the first stage a short neck develops at the site which makes an angle of approximately 90° with the surface. In order to evaluate the growth velocity and acceleration during the expansion stage, for substitution in the third term above, we need to know R_e as a function of time. There is general agreement among most investigators that the radius-time relationship in nucleate boiling bubble growth is approximated by the following equation:

$$R = \beta t^{\frac{1}{2}} \quad (6.3)$$

or

$$V = \frac{4}{3} \pi \beta^3 t^{3/2} \quad (6.4)$$

where β is the growth constant, which will be treated in more detail below. Various expressions have been proposed with limited success for the growth constant β which is a function of the thermo-physical properties of the liquid and the superheat. Making use of the above equation, the

growth velocity and acceleration during the expansion stage of the bubble can be derived:

$$v_e = \frac{dR_e}{dt_e} = \frac{1}{2}\beta t_e^{-1/2} \quad (6.5)$$

and

$$\frac{dv_e}{dt_e} = \frac{d^2R_e}{dt_e^2} = -\frac{1}{4}\beta t_e^{-3/2} \quad (6.6)$$

Consider now the second term on the right-hand side of Eqn. 6.2 which can be expanded as follows:

$$\frac{d}{dt_e}(Mv_e) = M\frac{dv_e}{dt_e} + v_e\frac{dM}{dt_e} \quad (6.7)$$

Using $M = \frac{11}{16}V\rho_L$ and $V = \frac{4}{3}\pi R^3$, performing the differentiation and substituting from Eqns. 6.3 to 6.6, the right-hand side of the above equation can be simplified. The result is

$$\frac{d}{dt_e}(Mv_e) = \frac{11}{24}\pi\rho_L\beta^4 \quad (6.8)$$

This equation can now be combined with Eqn. 6.2 to give

$$V_{EXP}\rho_L g = \pi D_o \sigma + \frac{11}{24}\pi\rho_L\beta^4 \quad (6.9)$$

Knowing β , D_o and the properties of the liquid, the above equation can be solved to obtain V_{EXP} , the volume at the end of the expansion stage. The radius at the end of the expansion stage R_{EXP} can then be quickly obtained from

$$R_{EXP} = \left(\frac{3V_{EXP}}{4\pi} \right)^{1/3} .$$

6.4 Evaluation of V_{FIN}

6.4.1 Detachment stage

During the second stage, the upward forces are larger than the downward forces and the bubble base starts moving away from the orifice. It is to be noted that the bubble continues to grow during the detachment stage, according to Eqn. 6.3. The bubble is assumed to detach when its base has covered a distance equal to the radius R_{EXP} of the force-balance bubble (i.e., the bubble radius at the end of the first stage). This departure criterion is based on the observation of a number of barbotage systems by Kumar *et al.* Expressing the bubble movement by Newton's second law of motion, we obtain,

$$\frac{d}{dt}(Mv') = V\rho_L g - \pi D_o \sigma \quad (6.10)$$

where the velocity v' pertains to the centre of the bubble and is made up of the velocity of the centre due to expansion $\frac{dR}{dt}$, and the velocity v_b with which the bubble base is moving. Therefore,

$$v' = v_b + \frac{dR}{dt} \quad (6.11)$$

Expanding Eqn. 6.10 and introducing Eqn. 6.11 in Eqn. 6.10

and simplifying, we get,

$$M \frac{dv_b}{dt} + v_b \frac{dM}{dt} = V \rho_L g - \pi D_o \sigma - \frac{11}{24} \pi \rho_L \beta^4 \quad (6.12)$$

Consider now the left-hand side of Eqn. 6.12. Once again using M , the virtual mass as $\frac{11}{16} V \rho_L$, V as $\frac{4}{3} \pi R^3$ and Eqns. 6.3 and 6.5 without subscripts, the left-hand side of Eqn. 6.12 becomes,

$$M \frac{dv_b}{dt} + v_b \frac{dM}{dt} = \frac{11}{16} \rho_L V \frac{dv_b}{dt} + \frac{11}{8} \pi \rho_L \beta^3 v_b t^{\frac{1}{2}} \quad (6.13)$$

Combining the above equation with Eqn. 6.12, we get,

$$\frac{11}{16} \rho_L V \frac{dv_b}{dt} + \frac{11}{8} \pi \rho_L \beta^3 v_b t^{\frac{1}{2}} = V \rho_L g - \pi D_o \sigma - \frac{11}{24} \pi \rho_L \beta^4 \quad (6.14)$$

Dividing by $\frac{11}{16} \rho_L$ throughout and eliminating V by means of Eqn. 6.4 and simplifying, we obtain,

$$\frac{dv_b}{dt} = \frac{16}{11} g - \frac{3}{2} \frac{v_b}{t} - \frac{1}{t^{3/2}} \left(\frac{12}{11} \frac{D_o \sigma}{\rho_L \beta^3} + \frac{\beta}{2} \right) \quad (6.15)$$

Setting $v_b = \frac{dx}{dt}$, where x is the distance moved by the bubble base from the orifice, Eqn. 6.15 becomes

$$\frac{d^2x}{dt^2} = \frac{16}{11} g - \frac{3}{2t} \frac{dx}{dt} - \frac{1}{t^{3/2}} \left(\frac{12}{11} \frac{D_o \sigma}{\rho_L \beta^3} + \frac{\beta}{2} \right) \quad (6.16)$$

Eqn. 6.16 is the equation for the translational motion of

the base of the bubble during the second stage.

6.4.2 Solution of equation of motion

The above equation of motion (6.16) was integrated numerically using a fourth order Runge-Kutta formula with a time interval of 0.001 sec. This is a straight-forward calculation which gives x as a function of t until the breakoff criterion, namely $x = R_{EXP}$ is satisfied and the bubble detaches at t_{FIN} . The initial conditions for this integration are:

at $t=t_{EXP}$

$$x = 0$$

and

$$\frac{dx}{dt} = 0$$

The final volume V_{FIN} can then be obtained directly from Eqn. 6.4. It may be noted that the above analysis neglects the volume of vapour contained in the neck.

6.4.3 Growth constant

For the growth constant to be used in Eqn. 6.3 resort was made to Scriven's work [37]:

$$R = 2\delta(\alpha t)^{\frac{1}{2}} = \beta t^{\frac{1}{2}}$$

where

$$\beta = 2 \left(\frac{3}{\pi}\right)^{\frac{1}{2}} \alpha^{\frac{1}{2}} \Delta T \left[\frac{\rho_g}{\rho_L} \left\{ \frac{h_{fg}}{C_L} + \left(\frac{C_L - C_g}{C_L} \right) \Delta T \right\} \right]^{-1} \quad (6.17)$$

where

ΔT = superheat,

h_{fg} = latent heat of vaporisation,

C_g = specific heat of gas,

C_L = specific heat of liquid, and

α = thermal diffusivity.

As indicated earlier, this expression is valid for large values of β and the dimensionless superheat $\frac{C_L \Delta T}{h_{fg}}$. Saddy and Jameson's experiments satisfy these conditions.

6.5 Results and Discussion

The recent experimental work by Saddy and Jameson [35] is used here for comparison with predicted values of bubble departure diameters and times. Saddy and Jameson measured these quantities for bubbles growing in uniformly-superheated acetic acid and water from a nucleation cavity of radius 0.022 cm. The properties of acetic acid and water at various superheats are reproduced from their work in Tables 6.1 and 6.2. Tables 6.3 and 6.4 give the value of β for these liquids as evaluated from Eqn. 6.17. Table 6.5 compares the experimental departure radii and times as reported by Saddy and Jameson with the predictions from the present work. It is seen that the agreement is very good for both liquids.

In the theoretical development, viscous effects were entirely neglected. Justification of this is given by Saddy

Table 6.1. Properties of water and water vapour.

T (°C)	ρ_L (gm/cm ³)	$\rho_g \times 10^4$ (gm/cm ³)	h_{fg} cal/gm	$k \times 10^3$ (cal/cm ² °C)	C_L (cal/gm °C)	σ ($\frac{\text{dyne}}{\text{cm}}$)	$\alpha \times 10^3$ cm ² /sec
100	0.958	5.975	539.1	1.598	1.0076	58.85	1.655
102	0.957	6.390	537.9	1.599	1.0082	58.47	1.657
103	0.956	6.60	537.2	1.600	1.0085	58.29	1.659
104	0.955	6.82	536.6	1.601	1.0088	58.10	1.661

Table 6.2. Properties of acetic acid.

T (°C)	ρ_L (gm/cm ³)	$\rho_g \times 10^3$ (gm/cm ³)	h_{fg} cal/gm	$k \times 10^4$ (cal/cm ² °C)	C_L (cal/gm °C)	σ ($\frac{\text{dyne}}{\text{cm}}$)	$\alpha \times 10^3$ cm ² /sec
118	0.9368	3.15	96.89	3.627	0.5787	18.10	0.6677
120	0.9386	3.30	96.67	3.617	0.5806	17.91	0.6654
121	0.9348	3.41	96.56	3.612	0.5815	17.81	0.6645
122	0.9335	3.52	96.45	3.607	0.5824	17.71	0.6635
123	0.9321	3.63	96.35	3.602	0.5834	17.62	0.6624
124	0.9308	3.74	96.24	3.598	0.5843	17.52	0.6616

Table 6.3. Theoretical growth parameters for acetic acid (Scriven).

T (°C)	β (cm/sec ^{1/2})
120	0.178
121	0.265
122	0.352
123	0.438
124	0.522

Table 6.4. Theoretical growth parameters for water (Scriven).

T (°C)	β (cm/sec ^{1/2})
102	0.476
103	0.713
104	0.950

Table 6.5. Bubble properties at break-off in uniformly-superheated liquids.

System	T (°C)	Departure Radius R_d (cm)		Departure Time t_d (sec)	
		Theory (Present)	Experiment (Saddy and Jameson)	Theory (Present)	Experiment (Saddy and Jameson)
acetic acid	121	0.1005	0.1041	0.143	0.127
	122	0.1070	0.1026	0.093	0.082
	123	0.1124	0.1050	0.068	0.062
	124	0.1220	0.1126	0.055	0.050
water	102	0.158	0.1489	0.111	0.124
	103	0.183	0.1654	0.066	0.067
	104	0.211	0.1980	0.050	0.046

and Jameson, who showed that when the translational Reynolds number

$$\frac{2R \frac{dx}{dt}}{v_L} \gg 1$$

the viscous forces are negligible when compared with inertial forces and may therefore be neglected.

CHAPTER 7

SUMMARY AND CONCLUSIONS

The work reported here and the conclusions drawn may be summarised as follows:

- (i) For the first time, bubble growth rates, under constant-pressure-supply conditions in pool barbotage and determined using high-speed cine photography, were reported. Distilled water, acetone and hexane were used as the test liquids and air as the injected gas.
- (ii) A theoretical analysis of the problem of bubble growth under constant-pressure-supply conditions was performed. The theoretically predicted growth rates were found to be in good agreement with the experimental data.
- (iii) Bubble departure volumes and frequencies, determined by the stroboscopic method, were reported for a wide range of air flow rates for the three test liquids. The data for water agree well with data available in the literature. For acetone and hexane, no other data source is known to the author.

- (iv) A quantitative comparison of the bubble growth rates, departure sizes and frequencies in pool barbotage and saturated pool boiling was presented. The conclusions drawn are:
- (a) The experimental bubble growth rate results in saturated pool boiling lie between the growth rate results determined for the two extreme cases in barbotage, viz, the constant-volume case and the constant-pressure-supply case.
 - (b) The bubble departure sizes in pool barbotage and pool boiling are comparable in magnitude in the static regime (i.e. at very low gas flow rates in barbotage and very low heat fluxes in boiling).
 - (c) Barbotage frequency data obtained from the present work and from literature and boiling frequency data overlap over a wide range of bubble departure diameters. For larger diameters beyond this range, the barbotage data fall completely outside the boiling results (see Fig. 4.3).
 - (d) Both the barbotage data and the available boiling data indicate that in general, bubbling frequencies decrease with increasing orifice (or cavity) sizes.

- (v) The above comparison of pool boiling and pool barbotage data indicates that barbotage can serve as a good analog for boiling.
- (vi) It was shown that the two-stage model developed by Kumar *et al.* to predict bubble departure diameters in barbotage, can be successfully applied with suitable modifications for the prediction of departure radii and times in nucleate boiling in uniformly-superheated liquids.

REFERENCES

1. Akturk, N.U., Heat transfer from a heated porous surface to a pool of liquid with gas injection at the interface, Proceedings of the Symposium on Two-phase Flow, Vol II, Exeter, pp. D501-520 (1965).
2. Bard, Y., Heat transfer in simulated boiling, Ph.D. Dissertation, Columbia University (1966).
3. Benzing, R.J. and J.E. Myers, Low frequency bubble formation at horizontal circular orifices, *Ind. Eng. Chem.*, 47, 2087 (1955).
4. Cooper, M.G. and R.M. Vijuk, Bubble growth in nucleate pool boiling, in *Heat Transfer 1970*, Vol. V, Grigull (Ed.), Elsevier Publishing Company, Amsterdam (1970).
5. Davidson, L. and E.H. Amick, Jr., Formation of gas bubbles at horizontal orifices, *A.I.Ch.E.J.*, 2, 336 (1956).
6. Dergerabedian, P., The rate of growth of vapour bubbles in superheated water, *J. Appl. Mechanics*, 20, 537 (1953).
7. Davidson, J.F. and B.O.G. Schüller, Bubble formation at an orifice in a viscous liquid, *Trans. Instn. Chem. Engrs.*, 38, 144-154 (1960).
8. Davidson, J.F. and B.O.G. Schüller, Bubble formation at an orifice in an inviscid liquid, *Trans. Instn. Chem. Engrs.*, 38, 335-341 (1960).
9. Dzakowic, G.S. and W. Frost, Vapour bubble growth in saturated pool boiling by microlayer evaporation of liquid at the heated surface, in *Heat Transfer 1970* (papers presented at the Fourth International Heat Transfer Conference Paris-Versailles, 1970), Vol. 5, Elsevier Publishing Company, Amsterdam (1970).

10. Forster, H.K. and N. Zuber, Growth of a vapour bubble in a superheated liquid, *J. Appl. Physics*, 25, 474-478 (1954).
11. Fritz, W. and W. Ende, The vapourization Process according to cinematographic pictures of vapour bubbles, *Physikalische Zeitschrift*, 37, 391-401 (1936).
12. Fritz, W., Berechnung des maximal volumen von dampflasen, *Phys. Z.*, 36, 379 (1935).
13. Griffith, P., Bubble growth rates in boiling, *Trans. Am. Soc. Mech. Engrs.*, 80, 721 (1958).
14. Hughes, R.R., A.E. Handlos, H.D. Evans and R.L. Maycock, The formation of bubbles at simple orifices, *Chemical Engng. Prog.*, 51, No. 12, 557 (1955).
15. Han, C.Y. and P. Griffith, The mechanism of heat transfer in nucleate boiling - Part I, *Int. J. Heat Mass Transfer*, 8, 887 (1965).
16. Hsu, S.T. and F.W. Schmidt, Measured variations in local surface temperatures in pool boiling of water, *J. Heat Transfer*, 83, 254 (1961).
17. Hatton, A.P. and I.S. Hall, Photographic study of boiling on prepared surfaces, *Proceedings of the Third International Heat Transfer Conference, Chicago IV*, 24 (1966).
18. Howell, J.R. and R. Siegel, Activation, growth, and detachment of boiling bubbles in water from artificial nucleation sites of known geometry and size, *NASA TND-4101* (1967).
19. Hospeti, N.B. and R.B. Mesler, Vaporization at the base of bubbles of different shape during nucleate boiling of water, *A.I.Ch.E.J.*, 15, 214-219 (1969).
20. Ivey, H.J., Relationships between bubble frequency, departure diameter and rise velocity in nucleate boiling, *Int. J. Heat Mass Transfer*, 10, 1023 (1967).
21. Jakob, M., *Heat Transfer*, Vol. I, Wiley, New York (1949).

22. Kudirka, A.A., Two-phase heat transfer with gas injection through a porous boundary surface, U.S. Atomic Energy Commission Report ANL-6862 (1964).
23. Kumar, R. and N.R. Kuloor, The formation of bubbles and drops, in *Advances in Chemical Engineering*, Vol. 8, 255, Academic Press, New York (1970).
24. Kutateladze, S.S. *Heat Transfer in Condensation and Boiling*, Second Edition (1952); translated as U.S. Atomic Energy Commission Report AEC-tr-3770 (1959), p. 99.
25. Keshock, E.G. and R. Siegel, Effects of reduced gravity on nucleate boiling bubble dynamics in saturated water, *A.I.Ch.E.J.*, 10, 509 (1964).
26. L'Ecuyer, M.R. and S.N.B. Murthy, Energy Transfer from a liquid to gas bubbles forming at a submerged orifice, NASA TND-2547 (1965).
27. Lummis, R.C., Ph.D. dissertation, Columbia University (1963).
28. Leibson, I., E.G. Holcomb, A.G. Cacosso and J.J. Jacmic, Rate of flow and mechanics of bubble formation from single submerged orifices, *A.I.Ch.E.J.*, 2, 296-306 (1956).
29. Moore, F.D. and R.B. Mesler, The measurement of rapid surface temperature fluctuations during nucleate boiling of water, *Trans. Am. Inst. Chem. Engrs.*, 10, 620 (1961).
30. Plesset, M.S. and S.A. Zwick, A non-steady heat diffusion problem with spherical symmetry, *J. Appl. Phys.*, 23, 95 (1952).
31. Quigley, C.J., A.I. Johnson and B.L. Harris, Size and mass transfer studies of gas bubbles, *Chem. Eng. Prog. Symp. Series*, 16, 31-45 (1955).
32. Rallis, C.J. and H.H. Jawurek, Latent heat transport in saturated nucleate boiling. *Int. J. Heat Mass Transfer*, 7, 1051-1068 (1964).
33. Sims, G.E., V. Akturk and K.O. Evans-Lutterodt, Simulation of pool boiling heat transfer by gas injection at the interface, *Int. J. Heat Mass Transfer*, 6, 531-535 (1963).

34. Sims, G.E. and P.L. Duffield, Comparison of heat transfer coefficients in pool barbotage and saturated pool boiling, Paper No. 70-CSME-12, (EIC-70-1067), The Engineering Institute of Canada (1970).
35. Saddy, M. and G.J. Jameson, Prediction of departure diameter and bubble frequency in uniformly superheated liquids, *Int. J. Heat Mass Transfer*, 14, 1771-1785 (1971).
36. Siemes, W. and J.F. Kauffmann, *Chem. Eng. Sci.*, 5, 127 (1956).
37. Scriven, On the dynamics of phase growth. *Chem. Eng. Sci.*, 10, 1 (1959).
38. Strenge, P.H., A. Orell and J.W. Westwater, Microscopic study of bubble growth during nucleate boiling, *A.I.Ch.E.J.*, 7, 578-583 (1961).
39. Staniszewski, B.E., Nucleate boiling bubble growth and departure, DSR7-7673, M.I.T. (1959).
40. van Krevelen, D.W. and P.J. Hoftijzer, Studies of gas bubble formation, *Chem. Eng. Prog.*, 46, 29 (1950).
41. Wallis, G.B., The analogy between the bubbling of air into water and nucleate boiling at saturation temperature, U.K. Atomic Energy Authority Report AEEW-R28 (1960).
42. Wallis, G.B., Two-phase flow aspects of pool boiling from a horizontal surface, U.K. Atomic Energy Authority Report AEEW-R103 (1961).
43. Walters, J.K. and J.F. Davidson, The initial motion of a gas bubble formed in an inviscid liquid, *Jour. Fl. Mech.*, 12, 408 (1962).
44. Westwater, J.W., Boiling of liquids, Part I, in *Advances in Chemical Engineering*, Vol. I, T.B. Drew (Ed.), Academic Press, New York (1956).
45. Yamagata, K., F. Hirano, K. Nishikawa and H. Matsuoka, Nucleate boiling of water on the horizontal heating surface, *Mem. Fac. Engng. Kyushu*, 15, No. 1, 97-163 (1955).

46. Zuber, N. Hydrodynamic aspects of boiling heat transfer (thesis), U.S. Atomic Energy Commission Report AECU-4439 (1959).
47. Lord Rayleigh, On the pressure developed in a liquid during the collapse of a spherical cavity, *Phil. Mag.*, 34, 94-98 (1917).
48. Satyanarayan, A., R. Kumar and N.R. Kuloor, Studies in bubble formation. II. Bubble Formation under constant pressure conditions, *Chem. Eng. Sci.*, 24, 749 (1969).
49. Linqvist, R.D., Investigation into the transfer of mass from a liquid to a growing gas bubble during formation, M.Sc. Thesis, August, 1963, Purdue University.

APPENDICES

APPENDIX A

FORCES ACTING ON A BUBBLE FORMING AT AN ORIFICE (OR A NUCLEATING CAVITY)

This appendix presents the general expressions available in the literature (barbotage and boiling) for the various forces acting on a gas or a vapour bubble. Below, where the subscript "g" appears it is understood that this applies to either gas or vapour. A basic assumption involved is that the bubble is spherical at all times till departure.

Static Forces

1. Surface tension force = $\pi D_o \sigma \sin \theta$, where D_o is the diameter of the orifice or a nucleating cavity as the case may be; θ is the contact angle between the bubble and the plate surface.

2. Buoyancy force = $\frac{\pi}{6} D^3 \Delta \rho g$, where D is the 'equivalent' diameter and $\Delta \rho$ is the difference between the densities of liquid and gas or vapour.

3. Excess pressure at bubble base (equivalent to a loss of buoyancy due to the fact that liquid pressure does not act over the bubble base).

$$\text{Excess pressure force} = \frac{\pi D_o^2 (p_g - p_L)}{4} = \frac{\pi D_o^2 \sigma}{D} ,$$

since

$$p_g - p_L = \frac{4\sigma}{D}$$

Dynamic Forces

1. The liquid inertia force: This is a consequence of the force necessary to accelerate the mass of the gas or vapour in the bubble along with some equivalent mass of liquid surrounding it [23].

$$\text{inertia force} = \frac{d}{dt}(Mv)$$

where M is the (virtual) mass [23] of the gas or vapour in the bubble and that of ψ times its volume of liquid surrounding it. The symbol ψ is a constant which is assigned different values (normally 1/2 or 11/16) by different investigators, i.e.,

$$M = V(\rho_g + \psi\rho_L) ,$$

and v is the velocity of the centre of the expanding bubble and is equal to $\frac{dR}{dt}$.

2. Viscous drag force: This force is assumed to depend on the velocity of the rising bubble.

$$\text{viscous force} = \frac{1}{2} C_d \rho_L \pi R^2 \left(\frac{dR}{dt}\right)^2$$

where C_d is the drag coefficient. Another expression

available in barbotage literature alone is as follows:

$$\text{viscous force} = 6\pi\mu_L R \frac{dR}{dt}$$

where μ_L is the liquid viscosity. This assumes that the bubble at any time is moving at its 'Stokes' velocity.

APPENDIX B

PHYSICAL PROPERTIES OF WATER, ACETONE AND HEXANE

<u>Property</u>	<u>Water</u>		<u>Acetone</u>	<u>Hexane</u>
Grade	single	distilled	commercial (purity 99.5% by weight)	commercial
Temperature at which fluid properties are quoted	100°C	20°C	20°C	20°C
Density (gm/cm ³)	0.9584	0.9982	0.7915	0.6600
Dynamic viscosity (gm/cm sec)	2.82 x 10 ⁻³	10.05 x 10 ⁻³	3.16 x 10 ⁻³	3.26 x 10 ⁻³
Surface tension (dyne/cm)	58.8	72.75	23.7	18.43

APPENDIX C

CALCULATION OF BUBBLE VOLUME

The volume of a bubble (at any instant during formation) was determined from the frames of high speed motion pictures in the manner described by L'Ecuyer and Murthy [26].

1. The picture frame from which the bubble volume was to be calculated was projected on a screen.

2. An enlarged tracing was obtained from the projected image.

3. The enlarged outline of the bubble was divided into a series of truncated cones by means of horizontal lines. Figure C.1 illustrates one such outline.

4. Assuming the bubble to be symmetrical with respect to the orifice axis, the 'enlarged bubble volume' was computed from the following expression. The meanings of the symbols are apparent from the figure.

$$V = \frac{\pi}{3} H_1 (3R_1 - H_1) + \sum_{i=1}^{n-1} \frac{\pi}{12} H_2 (d_i^2 + d_{i+1}^2 + d_i d_{i+1}) \\ + \frac{\pi}{12} H_3 (d_n^2 + d_{n+1}^2 + d_n d_{n+1})$$

5. The true bubble volume was computed from the

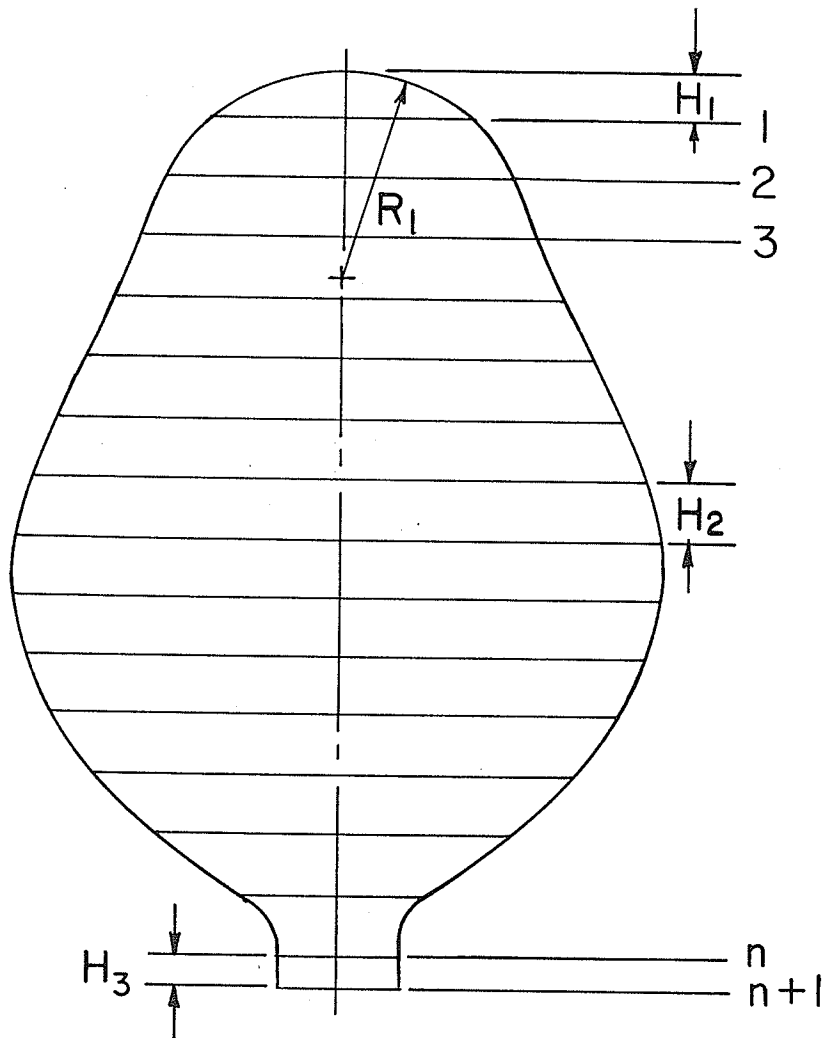


Fig. C.1 Enlarged bubble outline
for volume calculations

enlarged values by the application of an appropriate scale factor.†

† The scale factor was obtained from a picture of a scale in the plane of the orifice axis.

APPENDIX D

METHOD FOR FINDING THE TRUE FLOW RATE OF AIR THROUGH THE ORIFICE

Assumptions

1. Air is fully saturated when it leaves the saturator.
2. The pressure drop through the saturator is assumed to be negligible as compared to atmospheric pressure. Consequently, the pressure and temperature conditions are the same at the rotameter and the ante-chamber.

It is well known from thermodynamics that in a gaseous mixture, the volume fraction of one component is equal to the ratio of the partial pressure of that component at the temperature of the mixture to the total pressure of the mixture. That is,

$$\frac{V_{\text{vap}}}{V_{\text{mix}}} = \frac{V_{\text{vap}}}{V_{\text{vap}} + V_{\text{air}}} = \frac{p_v}{p_{\text{total}}} \quad \text{D.1}$$

where V_{air} , V_{vap} and V_{mix} are the volumetric flow rates of air, vapour and mixture, respectively, at the total pressure while p_v is the partial pressure of the vapour in the ante-chamber and p_{total} is the total pressure (same in ante-

chamber and rotameter).

Example:

Let the liquid be hexane. The manometer reading is 2.5 inches of liquid. The temperature of the system is 72°F and the flowmeter reading is 552.5 cm³/min. From tables, the vapour pressure of hexane at 72°F is 133.5 mm of mercury absolute. Substituting the relevant values into Eqn. D.1 we have,

$$\frac{V_{\text{vap}}}{V_{\text{vap}} + V_{\text{air}}} = \frac{133.5 \times 13.6}{2.5 \times 25.4 \times 0.827 + 760 \times 13.6}$$

$$= 0.1745$$

Therefore

$$V_{\text{vap}} = 0.1745 V_{\text{vap}} + 0.1745 \times 552.5$$

Solving for V_{vap} ,

$$V_{\text{vap}} = 117 \text{ cm}^3/\text{min}$$

Thus, the total flow through the orifice is

$$\begin{aligned} \text{Flowmeter Reading} + V_{\text{vap}} &= 552.5 + 117 \\ &= 669.5 \text{ cm}^3/\text{min} . \end{aligned}$$

APPENDIX E

BUBBLE GROWTH RATE DATA

This appendix presents tabulated data for the bubble growth rates obtained during the experimental investigation in the present work. Three bubbles were analysed for each test liquid for each flow rate. Data were obtained for three such flow rates for each liquid, giving a total of 27 bubbles. The systems for which data were collected are summarised in Table 3.1. The profiles of bubbles during growth are presented after the tabulated data (Figs. E.1 to E.9).

Bubble Identification

Each bubble analysed is identified by a code in the following tables. The first letter in the code refers to the first letter in the name of the liquid tested. The three air flow rates for which bubbles were analysed are classified as low, medium and high in the increasing order, and are referred to by the middle letter in the code. The numbering in the code refers to the number of the bubble analysed. For example, W-L-2 refers to the second bubble analysed for the low flow rate ($4.07 \text{ cm}^3/\text{sec}$) for water.

Symbols indicated alongside the codes are used for identifying bubble numbers on the graphs.

Zero Time

Reference is made to the explanation given for zero time under Sec. 3.4.4. According to this, a bubble for which the starting frame number is other than zero belongs to Category I and a bubble for which the frame number is zero to start with belongs to Category II.

Symbol

The symbol '→' which one encounters while progressing along the frame numbers indicates that the frame number at which it is pointing is the frame corresponding to the end of the formation of the primary bubble (i.e. end of 'neck' formation) and the beginning of the appearance of the secondary bubble. As explained in Chapter 3 the growth rate curves presented in Figs. 3.10 through 3.18 were plotted taking this frame as the one corresponding to the end of the formation period. The last frame in the series for each bubble corresponds to the time at which the secondary bubble, which rises as part of the primary bubble, actually severs its connection with the hemispherical interface at the orifice. For a further discussion in this regard, reference is made to Appendix F.

Table E.1. Bubble growth data for water

Symbol, Identifi- cation Code	Frame Number (Counted from zero time)	Air Flow Rate 4.07 cm ³ /sec		Bubble Volume cm ³	Bubble Equiv. Radius cm	t^* $\left(\equiv \sqrt{\frac{\sigma}{\rho_L R_0^3}} \right)$	R* ($\equiv R/R_0$)
		Time t, Sec x 10 ³	Bubble Volume cm ³				
⊙ W-L-1	0	0.000	0.0000	0.0000	0.0000		
	3	5.930	0.0037	0.0037	0.0963		
	6	11.860	0.0228	0.0228	0.1758		
	9	17.790	0.0897	0.0897	0.2776		
	12	23.720	0.2494	0.2494	0.3905		
	15	29.650	0.5060	0.5060	0.4943		
	18	35.580	0.8660	0.8660	0.5913		
	21	41.510	1.2362	1.2362	0.6658		
	24	47.440	1.6439	1.6439	0.7321		
	→ 26	51.400	1.9131	1.9131	0.7701		
	29	57.400	2.0116	2.0116	0.7880		
	32	63.300	2.3174	2.3174	0.8240		
	34	67.250	2.3632	2.3632	0.8280		
	▽ W-L-2	0	0.000	0.0047	0.0047	0.1042	
4		7.900	0.0050	0.0050	0.1061		
8		15.800	0.0097	0.0097	0.1325		
12		23.700	0.0323	0.0323	0.1975		
16		31.600	0.1347	0.1347	0.3180		
20		39.500	0.3749	0.3749	0.4473		
24		47.400	0.7402	0.7402	0.5611		
28		55.300	1.2077	1.2077	0.6606		
→ 31		61.250	1.6472	1.6472	0.7326		
34		67.100	1.8359	1.8359	0.7610		
37		73.100	1.8426	1.8426	0.7630		
45		89.000	2.4930	2.4930	0.8470		

Table E.1 (continued)

Symbol, Identifi- cation Code	Frame Number (counted from zero time)	Time t, Sec x 10 ³	Air Flow Rate 4.07 cm ³ /sec		Bubble Equiv. Radius cm	t*	R*
			Bubble Volume cm ³	Bubble Radius cm			
W-L-3 X	0	0	0.0051	0.1070	0	0.86	
	4	7.900	0.0110	0.1381	1.52	1.10	
	8	15.600	0.0303	0.1934	3.04	1.54	
	12	23.700	0.1171	0.3035	4.56	2.43	
	16	31.600	0.3353	0.4310	6.08	3.45	
	20	39.500	0.7331	0.5594	7.60	4.48	
	24	47.400	1.2079	0.6607	9.12	5.30	
	→28	55.300	1.5011	0.7100	10.64	5.70	
	32	63.200	1.7454	0.7470	12.16	6.00	
	36	71.100	1.9073	0.7710	13.07	6.16	
	W-L-4	0	0	0	0	0	
		4	7.900	0.0020	0.0781		
		8	15.600	0.0069	0.1179		
12		23.700	0.0355	0.2039			
16		31.600	0.1793	0.3498			
20		39.500	0.4986	0.4919			
24		47.400	0.9168	0.6026			
28		55.300	1.4357	0.6998			
→30 *		59.250	1.7542	0.7482			
W-L-5		0	0	0	0	0	
		3	5.930	0.0042	0.1000		
		6	11.860	0.0137	0.1483		
		9	17.790	0.0632	0.2471		
	12	23.720	0.1839	0.3528			
	15	29.650	0.4227	0.4656			
	18	35.580	0.7399	0.5611			
	21	41.510	1.1099	0.6423			
	24	47.440	1.5289	0.7146			
	→27 *	53.500	1.9266	0.7719			

* Bubble analysed till the formation of neck only.

Table E.1 (continued)

Symbol, Identification Code	Frame Number (counted from zero time)	Air Flow Rate 4.07 cm ³ /sec		Bubble Equiv. Radius cm	t*	R*
		Time t, sec x 10 ³	Bubble Volume cm ³			
W-L-6	0	0	0.0049	0.1052		
	3	5.930	0.0063	0.1144		
	6	11.860	0.0080	0.1241		
	9	17.790	0.0099	0.1331		
	12	23.720	0.0251	0.1816		
	15	29.650	0.0682	0.2535		
	18	35.580	0.1784	0.3492		
	21	41.510	0.3684	0.4447		
	24	47.440	0.6299	0.5318		
	27	53.500	0.9656	0.6131		
	→ 31 *	61.250	1.5567	0.7190		
W-M-1 □	0	0	0.0038	0.0971		
	10	5.550	0.0108	0.1372		
	20	11.110	0.0464	0.2229		
	30	16.650	0.1756	0.3474		
	40	22.200	0.4160	0.4631		
	50	27.750	0.6645	0.5413		
	60	33.300	1.1521	0.6503		
	70	38.850	1.6066	0.7266		
	→ 80	44.400	2.1730	0.8035		
	90	49.950	2.2439	0.8150		
	100	55.500	2.5652	0.8500		
106	58.900	2.7217	0.8660			

Table E.1 (continued)

Symbol, Identifi- cation Code	Frame Number (counted from zero time)	Time t , sec x 10^3	Air Flow Rate 32.5 cm ³ /sec			R*
			Bubble Volume cm ³	Bubble Equiv. Radius cm	t^*	
W-M-2 ▽	0	0	0.0044	0.1014	0	0.81
	10	5.550	0.0257	0.1831	1.07	1.46
	20	11.110	0.0849	0.2727	2.14	2.18
	30	16.680	0.2832	0.4074	3.21	3.26
	40	22.200	0.5353	0.5037	4.28	4.03
	50	27.750	0.9725	0.6146	5.35	4.92
	60	33.300	1.3773	0.6902	6.42	5.52
	70	38.850	1.7808	0.7519	7.49	6.01
	→ 75	41.600	2.0003	0.7816	8.02	6.25
	85	47.200	2.1497	0.8150	9.10	6.50
	97	53.900	2.3873	0.8330	10.40	6.66
W-M-3 ⊙	0	0	0.0027	0.0864		
	9	5.000	0.0081	0.1244		
	18	10.000	0.0212	0.1716		
	27	15.000	0.0734	0.2597		
	36	20.000	0.2029	0.3645		
	45	25.000	0.4141	0.4624		
	54	30.000	0.6997	0.5507		
	63	35.000	0.9865	0.6175		
	72	40.000	1.3360	0.6832		
	→ 82	45.600	1.7263	0.7442		
	92	51.100	1.8706	0.7650		
102	56.600	2.0891	0.7940			
116	64.500	2.7538	0.8720			

Table E.1 (continued)

Symbol, Identification Code	Frame Number (counted from zero time)	Time t , $\text{sec} \times 10^3$	Air Flow Rate $60.5 \text{ cm}^3/\text{sec}$ Bubble Volume cm^3	Bubble Equiv. Radius cm	t^*	R^*
W-H-1 □	0	0	0.0140	0.1495	0	1.20
	9	5.050	0.0581	0.2403	0.97	1.92
	18	10.100	0.2494	0.3905	1.94	3.12
	27	15.150	0.6705	0.5430	2.91	4.30
	36	20.200	1.2234	0.6635	3.88	5.30
	45	25.250	1.8035	0.7551	4.85	6.04
	54	30.300	2.3732	0.8275	5.82	6.62
	63	35.350	2.9108	0.8857	6.79	7.10
	→ 71	39.900	3.4269	0.9353	7.66	7.50
	81	44.900	3.4901	0.9435	8.62	7.54
	91	51.000	3.7193	0.9640	9.80	7.70
	96	53.900	4.0056	0.9870	10.35	7.90
	W-H-2 ▽	0	0	0.0246	0.1805	
9		5.050	0.0994	0.2874		
18		10.100	0.3337	0.4303		
27		15.150	0.8005	0.5760		
36		20.200	1.3086	0.6785		
45		25.250	1.8935	0.7675		
54		30.300	2.4607	0.8375		
63		35.350	2.8864	0.8832		
→ 67		37.600	3.0477	0.8994		
77		43.250	3.0796	0.9050		
87		48.750	3.5144	0.9450		
97		54.500	4.1312	0.9960		
101		56.600	4.5744	1.0500		

Table E.1 (continued)

Symbol, Identifi- cation Code	Frame Number (counted from zero time)	Air Flow Rate 60.5 cm ³ /sec Time t, sec x 10 ³	Bubble Volume cm ³	Bubble Equiv. Radius cm	t*	R*
W-H-3	0	0	0.0223	0.1746		
	8	4.500	0.0870	0.2748		
	16	9.000	0.2398	0.3854		
	24	13.500	0.5009	0.4927		
	32	18.000	0.8819	0.5949		
	40	22.500	1.3120	0.6791		
	48	27.000	1.7719	0.7507		
	56	31.500	2.2941	0.8132		
	64	36.000	2.7587	0.8700		
	+ 69	38.900	2.8245	0.8769		
	79	44.500	3.0996	0.9068		
	89	50.000	3.5641	0.9490		
	99	55.600	4.2086	1.0000		

Table E.2. Bubble growth data for acetone

Air Flow Rate 8.64 cm³/sec

Symbol, Identifi- cation Code	Frame Number (counted from zero time)	Time t, sec x 10 ³	Bubble Volume cm ³	Bubble Equiv. Radius cm	t*	R*
A-L-1 □	0	0	0.0061	0.1135	0	0.95
	5	4.680	0.0100	0.1338	0.714	1.16
	10	9.360	0.0124	0.1438	1.428	1.37
	15	14.040	0.0158	0.1557	2.142	1.67
	20	18.720	0.0299	0.1925	2.856	2.10
	25	23.400	0.0569	0.2386	3.570	2.72
	30	28.080	0.1083	0.2957	4.284	3.34
	35	32.760	0.2198	0.3744	4.998	3.94
	40	37.440	0.3533	0.4386	5.580	4.30
	45	42.120	0.5272	0.5011	5.950	4.40
	→50	46.800	0.7031	0.5516	6.300	4.53
	55	51.480	0.8114	0.5800	6.660	4.72
	60	56.160	0.9694	0.6160	7.030	4.90
62	58.000	1.1700	0.6540			
A-L-2 ▽	0	0	0.0069	0.1182	0	0.95
	6	5.630	0.0127	0.1447	0.714	1.16
	12	11.260	0.0213	0.1721	1.428	1.37
	18	16.890	0.0380	0.2086	2.142	1.67
	24	22.520	0.0767	0.2636	2.856	2.10
	30	28.150	0.1633	0.3394	3.570	2.72
	36	33.780	0.3038	0.4170	4.284	3.34
	42	39.410	0.5002	0.4924	4.998	3.94
	→47	44.100	0.6540	0.5385	5.580	4.30
	50	46.900	0.6900	0.5470	5.950	4.40
	53	49.600	0.7630	0.5660	6.300	4.53
	56	52.500	0.8620	0.5900	6.660	4.72
	59	55.400	0.9500	0.6090	7.030	4.90

Table E.2 (continued)

Symbol, Identifi- cation Code	Frame Number (counted from zero time)	Time t , sec x 10^3	Air Flow Rate 8.64 cm ³ /sec		Bubble Equiv. Radius cm	R*	
			Bubble Volume cm ³	Bubble Equiv. Radius cm			
A-L-3 ⊙	0	0	0.0072	0	0.1198		
	6	5.630	0.0163	0	0.1574		
	12	11.260	0.0333	0	0.1996		
	18	16.890	0.0778	0	0.2648		
	24	22.520	0.1295	0	0.3139		
	30	28.150	0.2521	0	0.3919		
	36	33.780	0.4582	0	0.4783		
	42	39.410	0.6996	0	0.5507		
	→48	45.100	0.8063	0	0.5774		
	54	50.750	1.0989	0	0.6420		
	57	53.500	1.1977	0	0.6600		
	A-L-4	0	0	0	0	0	
		6	5.630	0.0021	0	0.0796	
12		11.260	0.0068	0	0.1177		
18		16.890	0.0294	0	0.1914		
24		22.520	0.0816	0	0.2691		
30		28.150	0.1972	0	0.3611		
36		33.780	0.3736	0	0.4468		
42		39.410	0.5879	0	0.5197		
48		45.100	0.8443	0	0.5863		
→52		49.000	1.0741	0	0.6353		
58		54.700	1.1285	0	0.6500		
64		60.500	1.3097	0	0.6800		

Table E.2 (continued)

Symbol, Identifi- cation Code	Frame Number (counted from zero time)	Air Flow Rate 19.65 cm ³ /sec			Bubble Volume cm ³	Bubble Equiv. Radius cm	t*	R*
		Time t, sec x 10 ³	Bubble Volume cm ³	Bubble Equiv. Radius cm				
A-M-1 □	0	0	0.0020	0.0777				
	6	5.930	0.0055	0.1094				
	12	11.860	0.0129	0.1456				
	18	17.790	0.0538	0.2342				
	24	23.720	0.1446	0.3256				
	30	29.650	0.2986	0.4146				
	36	35.580	0.5404	0.5053				
	42	41.510	0.7881	0.5730				
	→48	47.440	1.0412	0.6287				
	54	53.370	1.0794	0.6380				
	60	59.300	1.1696	0.6540				
A-M-2 ▽	0	0	0.0049	0.1060		0	0.89	
	6	5.930	0.0059	0.1123		0.76	0.90	
	12	11.860	0.0145	0.1512		1.52	1.20	
	18	17.790	0.0611	0.2444		2.28	1.96	
	24	23.720	0.1718	0.3449		3.04	2.76	
	30	29.650	0.3685	0.4447		3.80	3.55	
	36	35.580	0.5923	0.5210		4.56	4.20	
	42	41.510	0.8541	0.5886		5.32	4.70	
	→48	47.440	1.1985	0.6589		6.08	5.30	
	54	53.370	1.3105	0.6800		6.84	5.44	
	64	63.300	1.5303	0.7150		8.11	5.72	

Table E.2 (continued)

Symbol, Identifi- cation Code	Frame Number (counted from zero time)	Air Flow Rate 19.65 cm ³ /sec			Bubble Equiv. Radius cm	R*
		Time t, sec x 10 ³	Bubble Volume cm ³	Bubble Equiv. Radius cm		
A-M-3 ⊙	0	0	0.0068	0.1177		
	6	5.930	0.0089	0.1287		
	8	11.860	0.0138	0.1488		
	1	17.790	0.0428	0.2169		
	24	23.720	0.1212	0.3070		
	30	29.650	0.2783	0.4050		
	36	35.580	0.5326	0.5028		
	42	41.510	0.7503	0.5637		
	48	47.440	1.0707	0.6346		
	→ 50	49.400	1.1765	0.6549		
	55	54.400	1.2550	0.6700		
	60	59.300	1.5000	0.7100		
	66	65.230	1.6530	0.7320		
A-H-1 □	0	0	0.0106	0.1364		
	8	5.550	0.0520	0.2316		
	16	11.100	0.1324	0.3162		
	24	16.550	0.2612	0.3966		
	32	22.200	0.4310	0.4686		
	40	27.750	0.6413	0.5350		
	48	33.300	0.9180	0.6029		
	56	38.850	1.1923	0.6578		
	→ 64	44.400	1.5042	0.7108		
	68	47.300	1.5800	0.7240		
	76	52.800	1.7500	0.7490		
	89	61.750	2.0900	0.7940		
						t*

Table E.2 (continued)

Symbol, Identification Code	Frame Number (counted from zero time)	Time t , sec x 10^3	Air Flow Rate $32.4 \text{ cm}^3/\text{sec}$	Bubble Volume cm^3	Bubble Equiv. Radius cm	t^*	R^*
A-H-2 ▽	0	0		0.0075	0.1214		
	8	5.550		0.0183	0.1636		
	16	11.100		0.0517	0.2311		
	24	16.550		0.1380	0.3205		
	32	22.200		0.2985	0.4146		
	40	27.750		0.5377	0.5044		
	48	33.300		0.7857	0.5724		
	56	38.850		0.9843	0.6171		
	→ 64	44.400		1.2558	0.6693		
	74	51.300		1.5195	0.7150		
	84	58.400		1.5208	0.7310		
	92	63.900		1.7886	0.7550		
	96	66.500		1.9076	0.7720		
A-H-3 ⊙	0	0		0.0130	0.1459	0	1.17
	8	5.550		0.0297	0.1920	0.72	7.54
	16	11.100		0.0680	0.2532	1.44	2.02
	24	16.550		1.1735	0.3460	2.16	2.77
	32	22.200		0.3270	0.4274	2.88	3.42
	40	27.750		0.5592	0.5110	3.60	4.44
	48	33.300		0.8098	0.5782	4.32	4.63
	56	38.850		1.0131	0.6230	5.04	4.98
	→ 64	44.400		1.2670	0.6713	5.76	5.37
	70	48.600		1.4415	0.7008	6.30	5.61
	79	54.750		1.5178	0.7130	6.90	5.70
	90	62.500		1.8404	0.7630	8.11	6.10

Table E.3. Bubble growth data for hexane

Symbol, Identifi- cation Code	Frame Number (Counted from zero time)	Air Flow Rate 8.1 cm ³ /sec		Bubble Volume cm ³	Bubble Equiv. Radius cm	t*	R*	
		Time t, 10 ³ Sec x 10 ³	Bubble Volume cm ³					
H-L-1 □	0	0	0.0040	0.0040	0.0987			
	3	6.000	0.0073	0.0073	0.1201			
	6	12.000	0.0245	0.0245	0.1802			
	9	18.000	0.0484	0.0484	0.2260			
	12	24.000	0.1088	0.1088	0.2962			
	15	30.000	0.2234	0.2234	0.3764			
	18	36.000	0.3839	0.3839	0.4508			
	+21	42.000	0.5747	0.5747	0.5157			
	24	48.000	0.6198	0.6198	0.5289			
	27	54.000	0.7593	0.7593	0.5670			
	30	60.000	0.8547	0.8547	0.5970			
	H-L-2 ▽	0	0	0.0079	0.0079	0.1234		
		3	6.000	0.0094	0.0094	0.1311		
6		12.000	0.0448	0.0448	0.2202			
9		18.000	0.1344	0.1344	0.3177			
12		24.000	0.2300	0.2300	0.3801			
15		30.000	0.3889	0.3889	0.4528			
+20		40.000	0.7579	0.7579	0.5656			
23		46.000	0.7641	0.7641	0.5100			
26		52.000	1.0319	1.0319	0.6280			

Table E.3 (continued)

Symbol, Identifi- cation Code	Frame Number (counted from zero time)	Time t , Sec x 10^3	Air Flow Rate 8.1 cm ³ /sec		Bubble Equiv. Radius cm	t^*	R*	
			Bubble Volume cm ³	Bubble Equiv. Radius cm				
H-L-3 ⊙	0	0	0.0085	0	0.1266	0	1.013	
	3	6.000	0.0113	0	0.1391	0.72	1.113	
	6	12.000	0.0317		0.1964	1.44	1.571	
	9	18.000	0.0899		0.2779	2.16	2.223	
	12	24.000	0.2043		0.3654	2.88	2.920	
	15	30.000	0.3922		0.4541	3.60	3.630	
	18	36.000	0.6063		0.5250	4.32	4.200	
	→20	40.000	0.7543		0.5647	4.80	4.520	
	23	46.000	0.8643		0.5900	5.52	4.720	
	27	54.000	1.1300		0.6400	6.48	5.120	
	H-L-4	0	0	0	0	0	0	
		3	6.000	0.0030		0.0893		
		6	12.000	0.0070		0.1187		
9		18.000	0.0295		0.1917			
12		24.000	0.0901		0.2781			
15		30.000	0.2047		0.3656			
18		36.000	0.3482		0.4364			
→21		42.000	0.5370		0.5042			
24		48.000	0.7073		0.5527			
27		54.000	0.7925		0.5740			
30		60.000	0.9047		0.6000			

Table E.3 (continued)

Symbol, Identifi- cation Code	Frame Number (counted from zero time)	Time t, Sec x 10 ³	Air Flow Rate 15.6 cm ³ /sec			t*	R*
			Bubble Volume cm ³	Bubble Equiv. Radius cm	Bubble Volume cm ³		
H-M-1 □	0	0	0.0074	0.1208	0	0.966	
	9	5.000	0.0200	0.1683	0.60	1.350	
	18	10.000	0.0403	0.2128	1.20	1.700	
	27	15.000	0.1049	0.2926	1.80	2.340	
	36	20.000	0.2029	0.3645	2.40	2.916	
	45	25.000	0.3804	0.4495	3.00	3.600	
	54	30.000	0.6146	0.5274	3.60	4.220	
	→ 63	35.000	0.8628	0.5906	4.20	4.720	
	71	39.500	0.9067	0.602	4.74	4.820	
	81	45.000	1.1189	0.660	5.40	5.300	
	H-M-2 ▽	0	0	0.0108	0.1372		
		9	5.000	0.0297	0.1921		
		18	10.000	0.0645	0.2488		
27		15.000	0.1120	0.2990			
36		20.000	0.2255	0.3776			
45		25.000	0.3933	0.4545			
54		30.000	0.6154	0.5277			
→ 63		35.000	0.9026	0.5995			
71		39.500	1.1063	0.6420			
79		44.000	1.1600	0.6520			
87	48.400	1.3400	0.6860				

Table E.3 (continued)

Symbol, Identifi- cation Code	Frame Number (Counted from zero time)	Air Flow Rate 15.6 cm ³ /sec		Bubble Volume cm ³	Bubble Equiv. Radius cm	t*	R*
		Time t, Sec x 10 ³	Bubble Volume cm ³				
H-M-3 ⊙	0	0	0.0051	0.0051	0.1066		
	9	5.000	0.0132	0.0132	0.1464		
	18	10.000	0.0402	0.0402	0.2126		
	27	15.000	0.0921	0.0921	0.2801		
	36	20.000	0.2043	0.2043	0.3654		
	45	25.000	0.3749	0.3749	0.4473		
	54	30.000	0.5928	0.5928	0.5211		
	→63	35.000	0.8260	0.8260	0.5821		
	68	37.800	0.8632	0.8632	0.5920		
	77	42.800	0.9258	0.9258	0.6060		
	86	47.800	1.1522	1.1522	0.6520		
H-H-1 □	0	0	0.0026	0.0026	0.0851		
	8	5.000	0.0121	0.0121	0.1424		
	16	10.000	0.0343	0.0343	0.2015		
	24	15.000	0.0801	0.0801	0.2674		
	32	20.000	0.1609	0.1609	0.3374		
	40	25.000	0.2998	0.2998	0.4152		
	48	30.000	0.4518	0.4518	0.4760		
	56	35.000	0.6960	0.6960	0.5497		
	64	40.000	0.9136	0.9136	0.6019		
	→70	43.800	1.0477	1.0477	0.6301		
	76	47.500	1.1268	1.1268	0.6440		
	84	52.500	1.2490	1.2490	0.6680		
92	57.500	1.4009	1.4009	0.6940			

Table E.3 (continued)

Symbol, Identifi- cation Code	Frame Number (counted from zero time)	Time t , Sec x 10^3	Air Flow Rate 30.4 cm ³ /sec			Bubble Equiv. Radius cm	t^*	R*
			Bubble Volume cm ³	Bubble Radius cm	Bubble Equiv. Radius cm			
H-H-2 ⊙	0	0	0.0067	0.1172	0	0.94		
	8	5.000	0.0312	0.1953	0.60	1.56		
	16	10.000	0.0721	0.2582	1.20	2.06		
	24	15.000	0.1508	0.3302	1.80	2.64		
	32	20.000	0.2730	0.4024	2.40	3.22		
	40	25.000	0.4267	0.4670	3.00	3.74		
	48	30.000	0.5871	0.5194	3.60	4.15		
	56	35.000	0.8341	0.5839	4.20	4.67		
	64	40.000	1.0471	0.6299	4.80	5.04		
	+67	42.000	1.1578	0.6514	5.04	5.21		
	75	46.900	1.2275	0.6660	5.63	5.33		
	83	52.000	1.2994	0.6780	6.24	5.42		
	91	57.000	1.4313	0.7000	6.84	5.60		
	102	63.600	1.5424	0.7180	7.63	5.74		
H-H-3 ▽	0	0	0.0053	0.1082	0	0.94		
	8	5.000	0.0075	0.1217	0.60	1.56		
	16	10.000	0.0171	0.1599	1.20	2.06		
	24	15.000	0.0488	0.2266	1.80	2.64		
	32	20.000	0.1023	0.2902	2.40	3.22		
	40	25.000	0.2165	0.3725	3.00	3.74		
	48	30.000	0.3526	0.4382	3.60	4.15		
	56	35.000	0.5415	0.5056	4.20	4.67		
	64	40.000	0.7158	0.5549	4.80	5.04		
	+70	43.900	0.9097	0.6011	5.04	5.21		
	78	48.800	0.9446	0.6100	5.63	5.33		
	86	53.800	1.1536	0.6510	6.24	5.42		
	92	57.500	1.2010	0.6630	6.84	5.60		
					7.63	5.74		

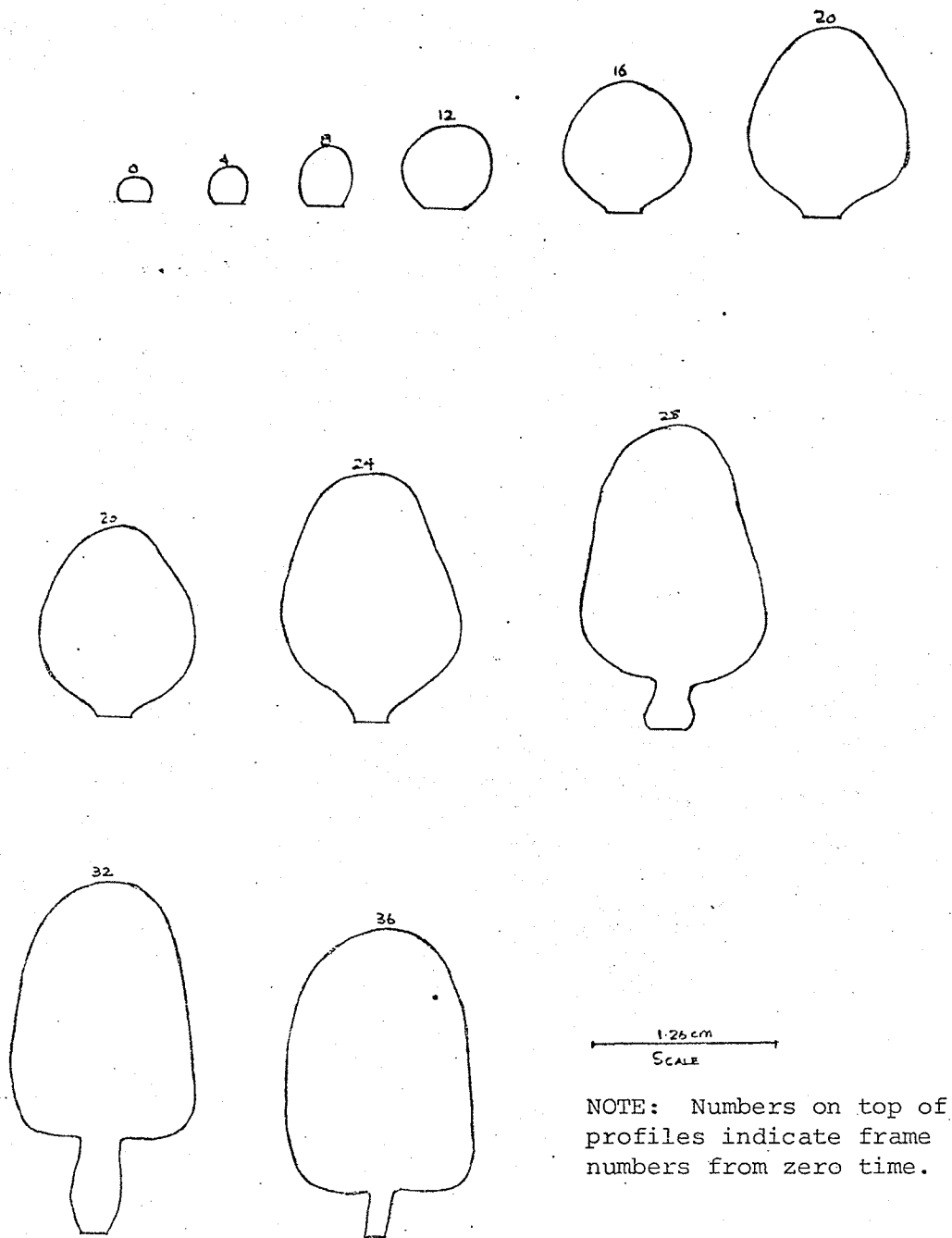


Fig. E.1 Growth profiles for bubble W-L-3

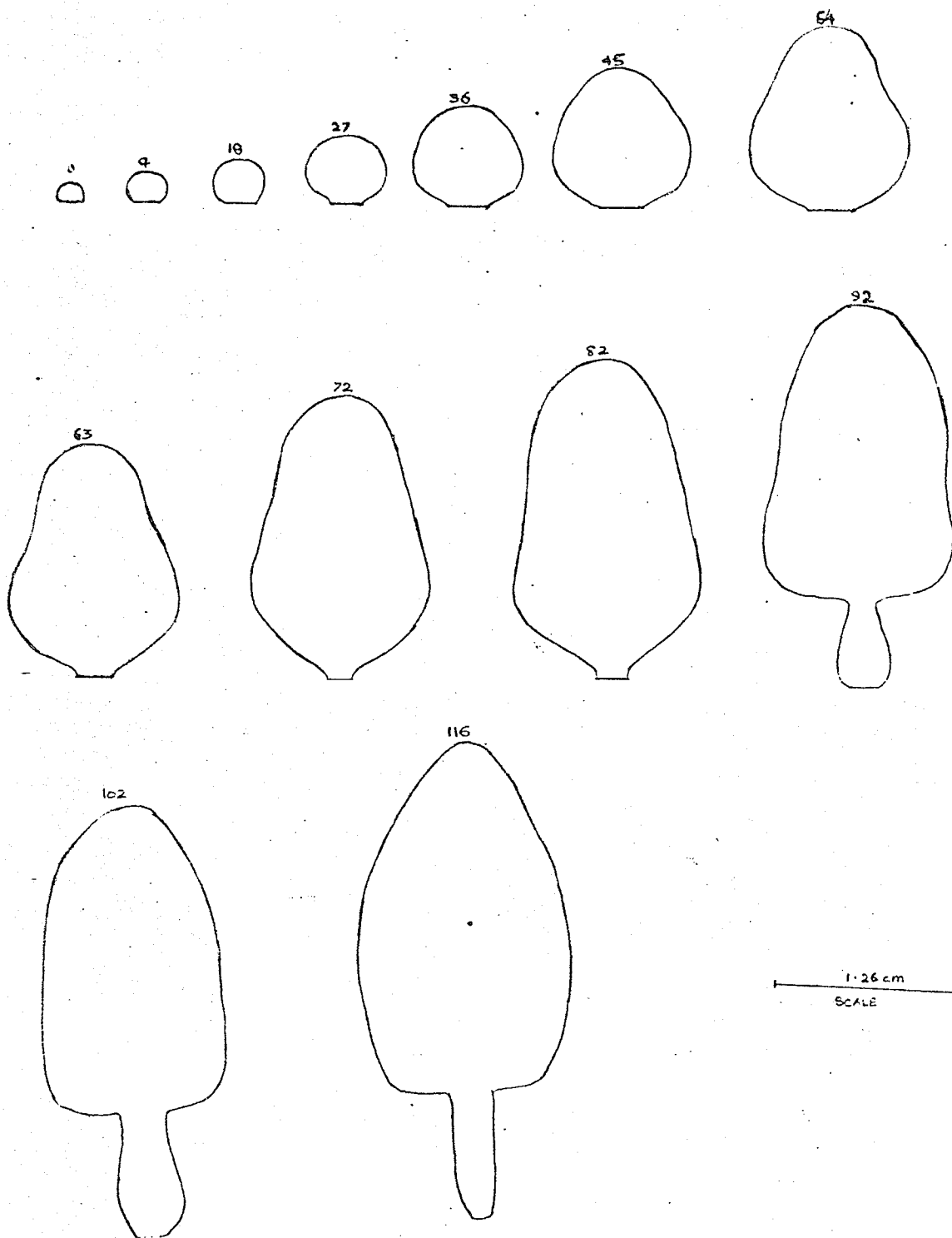


Fig. E.2 Growth profiles for bubble W-M-3

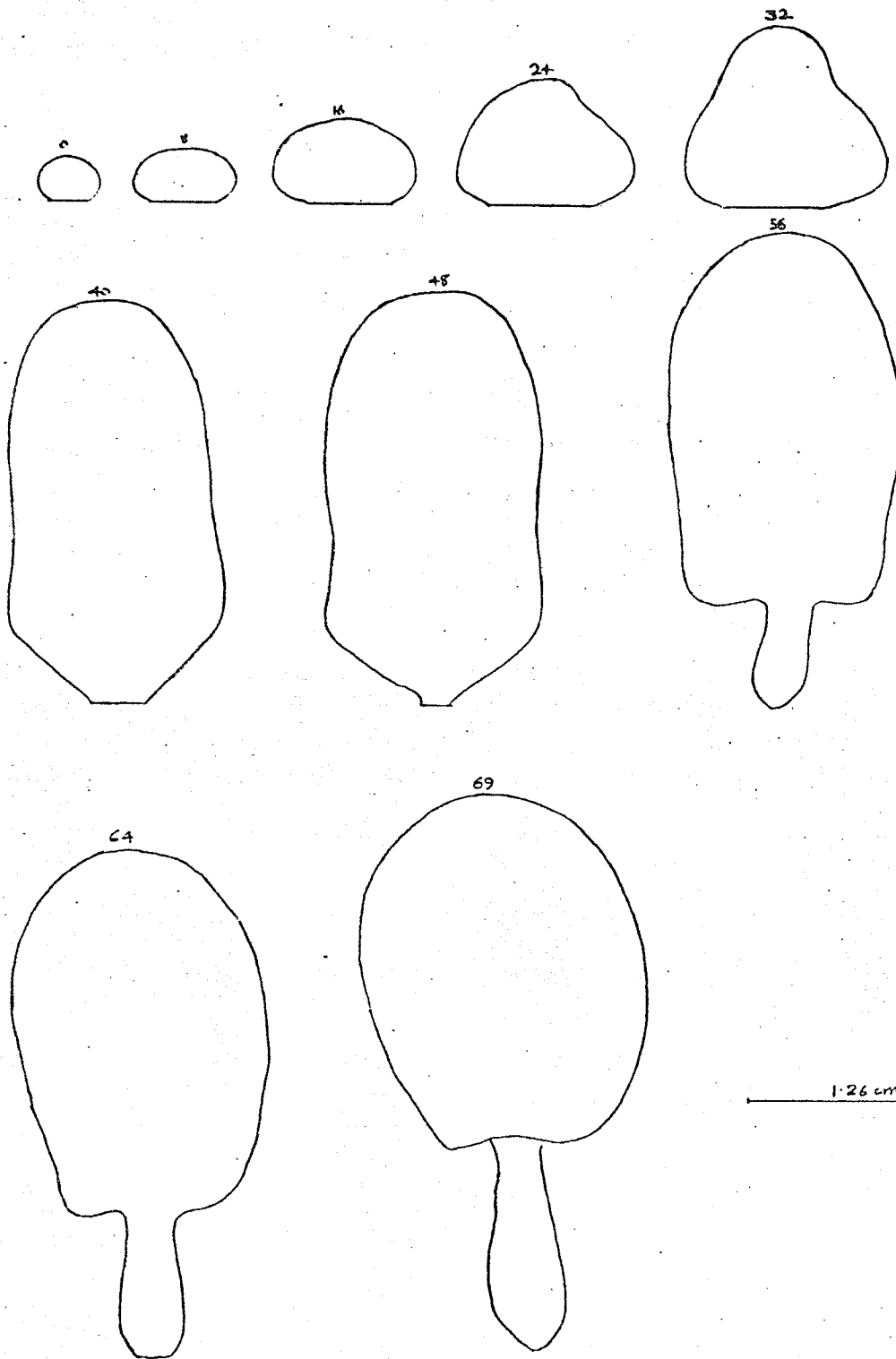


Fig. E.3 Growth profiles for bubble W-H-3

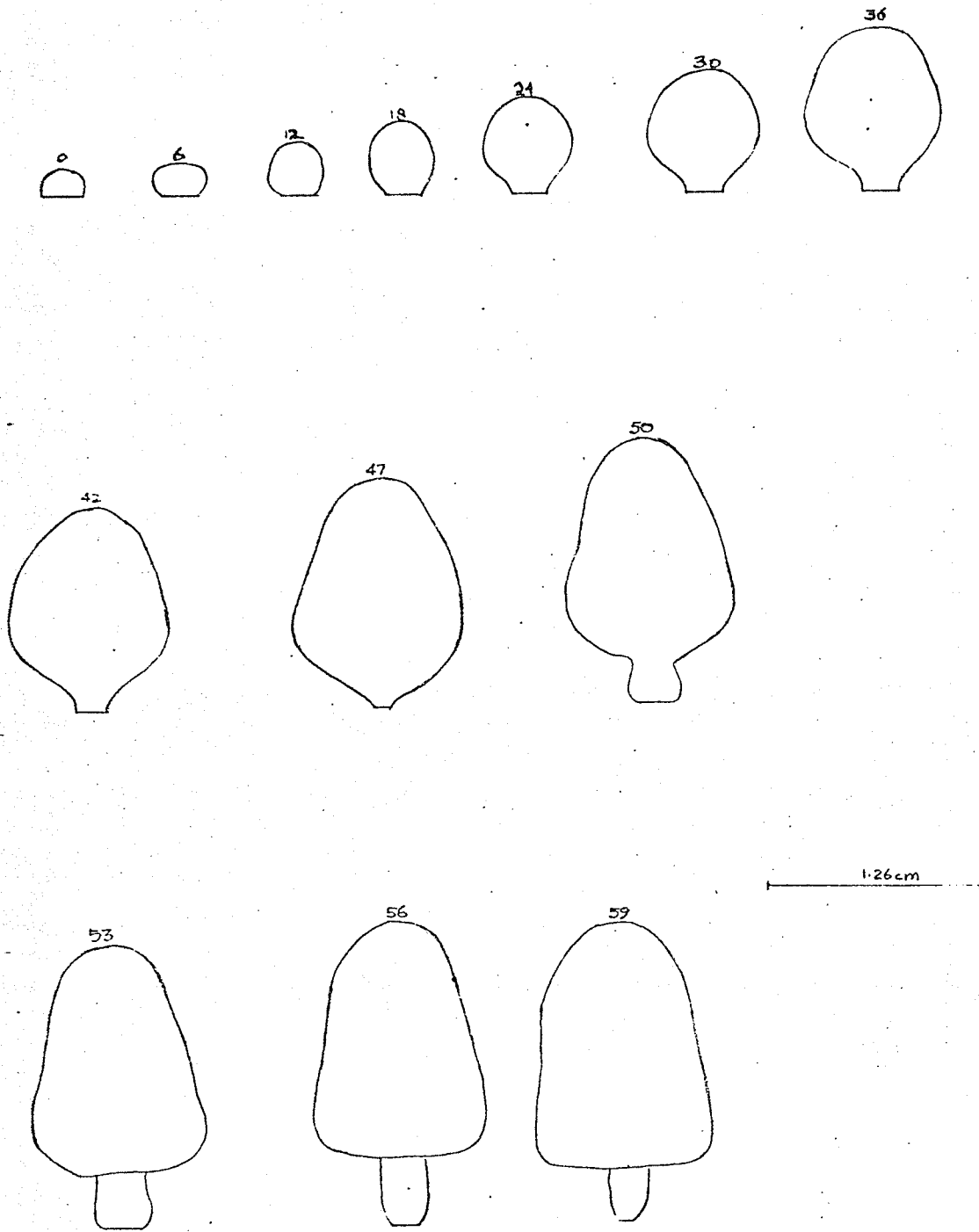


Fig. E.4 Growth profiles for bubble A-L-2

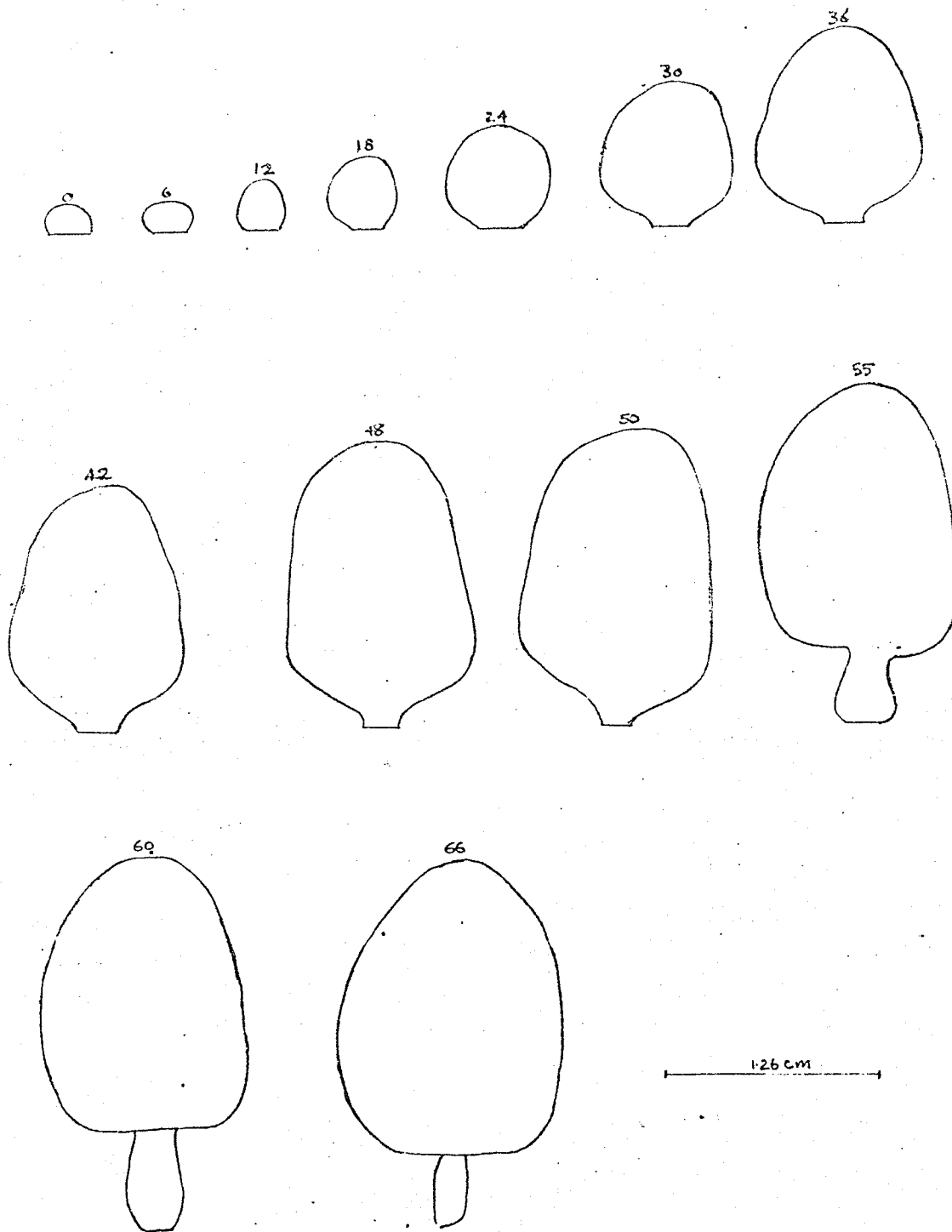


Fig. E.5 Growth profiles for bubble A-M-3.

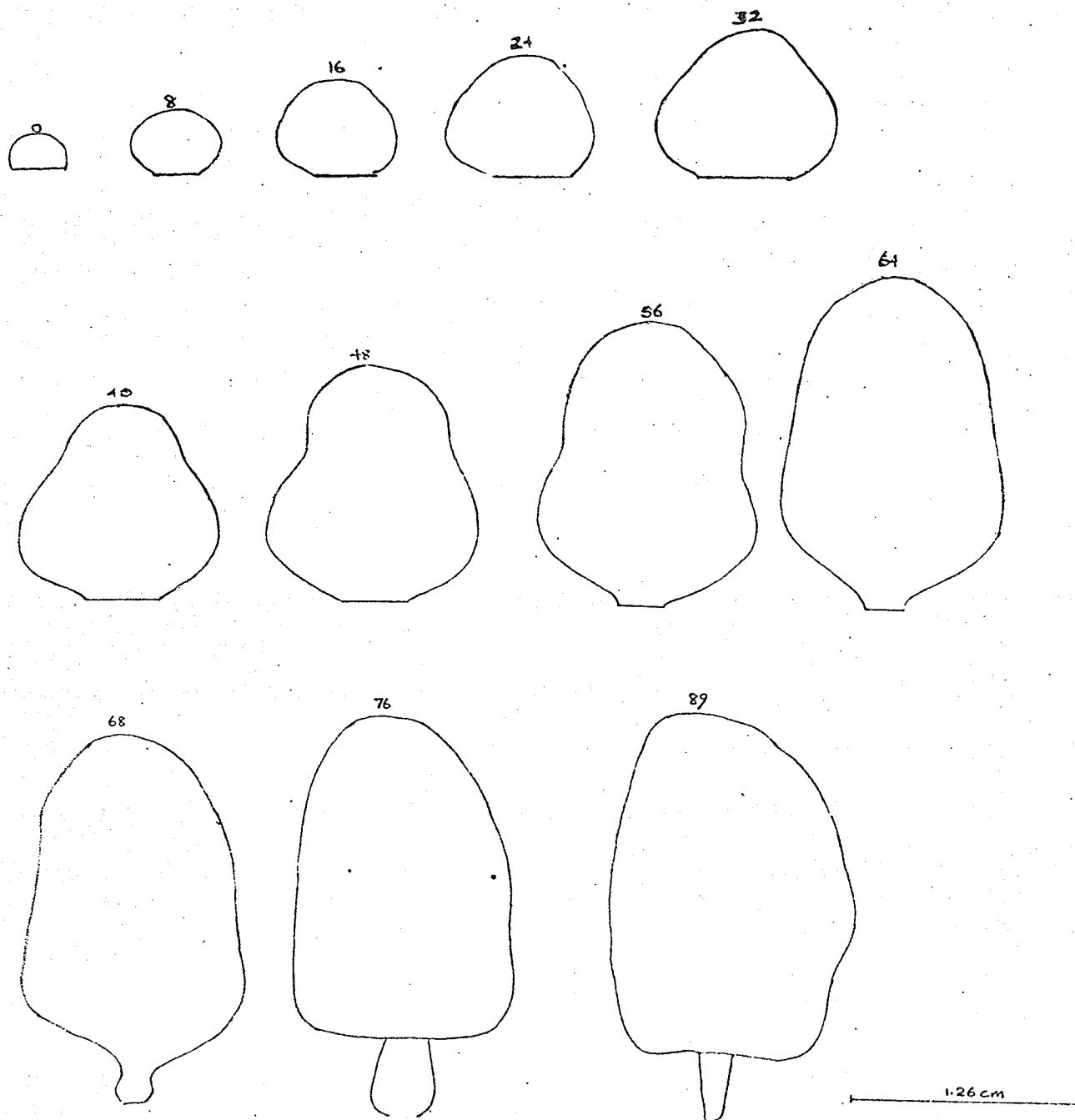


Fig. E.6 Growth profiles for bubble A-H-1

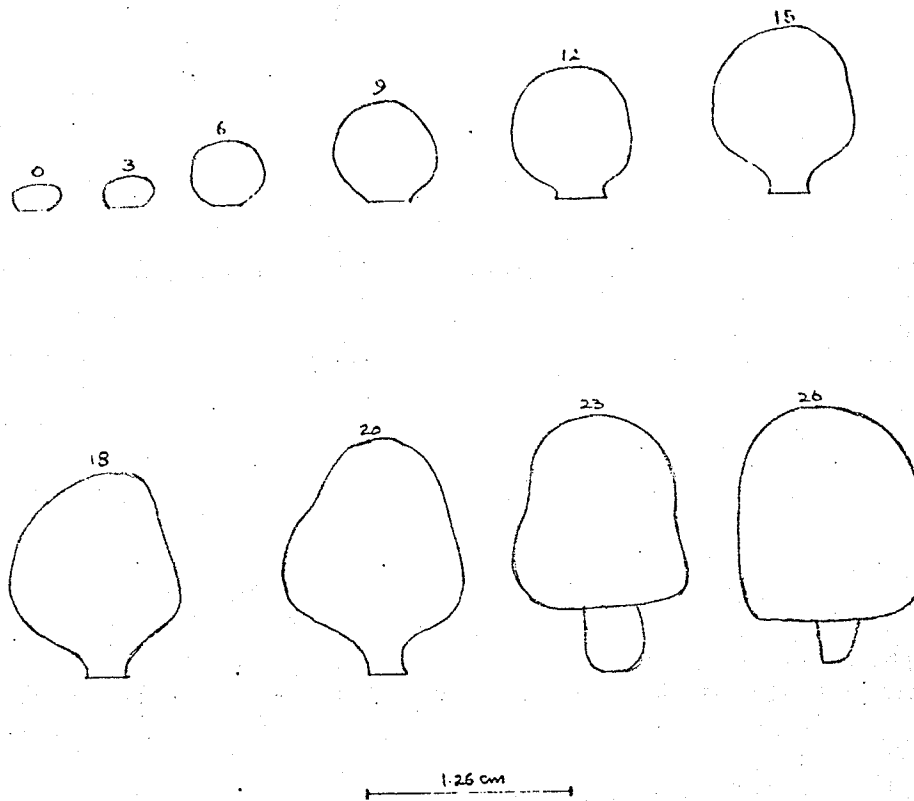


Fig. E.7 Growth profiles for bubble H-L-2

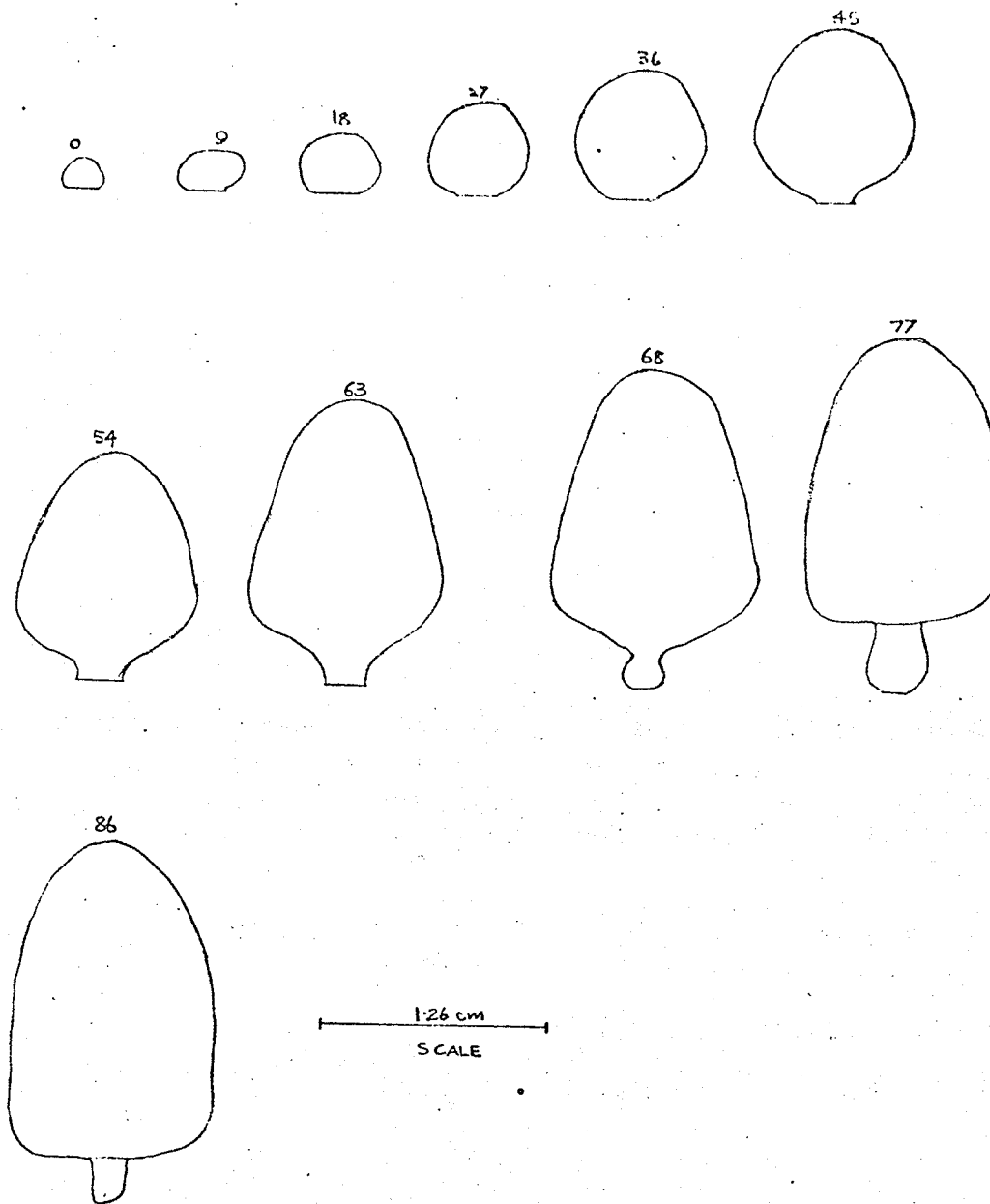


Fig. E.8 Growth profiles for bubble H-M-3

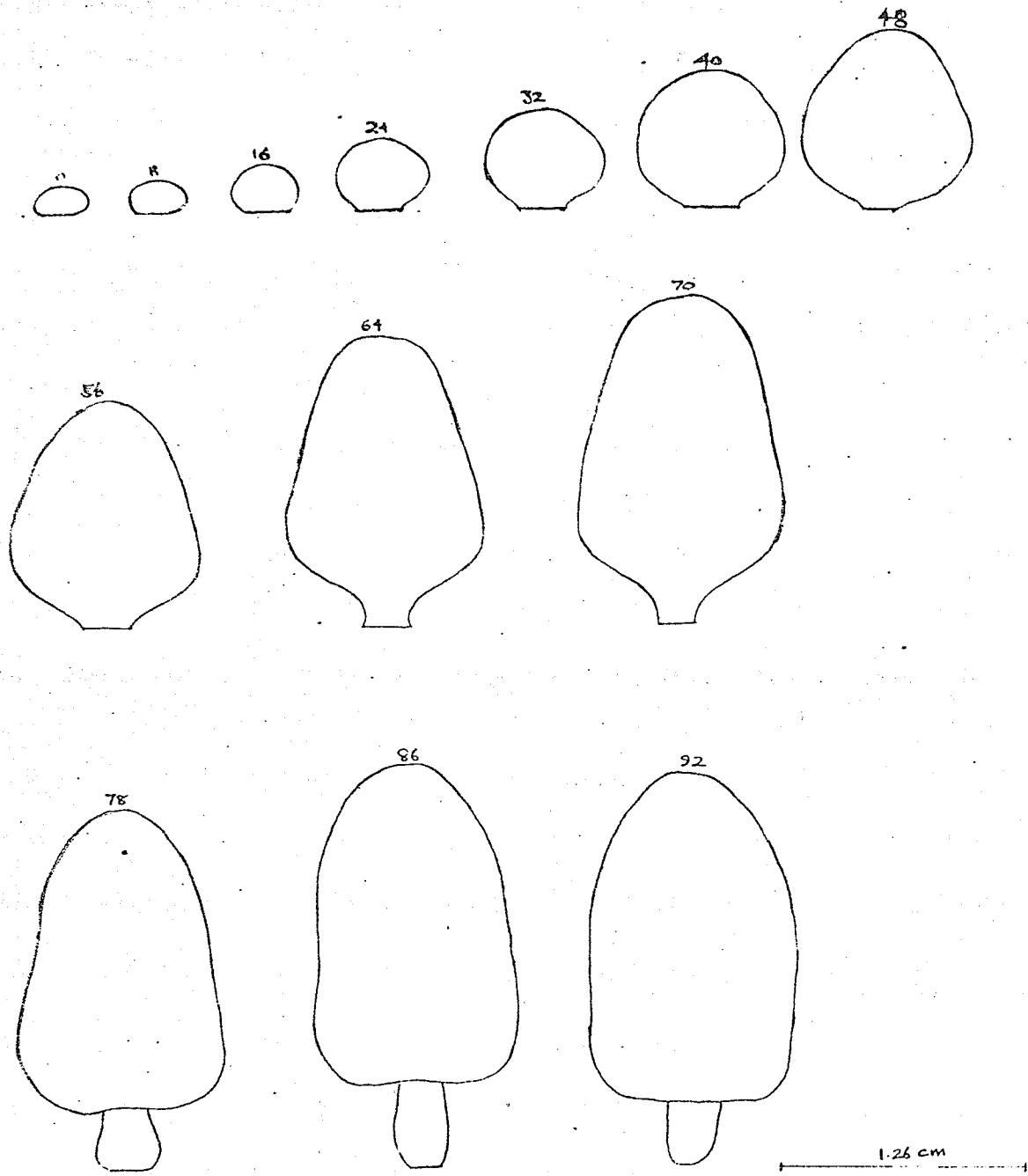


Fig. E.9 Growth profiles for bubble H-H-3

APPENDIX F

FURTHER DISCUSSION ON BUBBLE GROWTH RATES

In Sec. 3.4.4 it was observed that a bubble appearing at the orifice after a definite 'waiting period' has a growth curve essentially the same as that of a bubble that begins its life period as an approximately hemispherical interface (waiting period equal to zero). It was also pointed out that there is no significant variation in the shapes of the growth curves of any particular bubble plotted according to the following two different criteria with regard to the end of the formation period:

1. The life cycle of a bubble ends with the formation of a neck (see Fig. 3.6) just prior to the appearance of a secondary bubble.

2. The life cycle ends when the bubble (primary plus secondary) just severs its connection with the orifice and departs.

This appendix presents evidence for the above observations in the form of Figs. F.1 through F.6. Figures F.1 through F.3 are basically reproductions of Figs. 3.10, 3.13 and 3.16 giving typical growth curves for bubbles starting

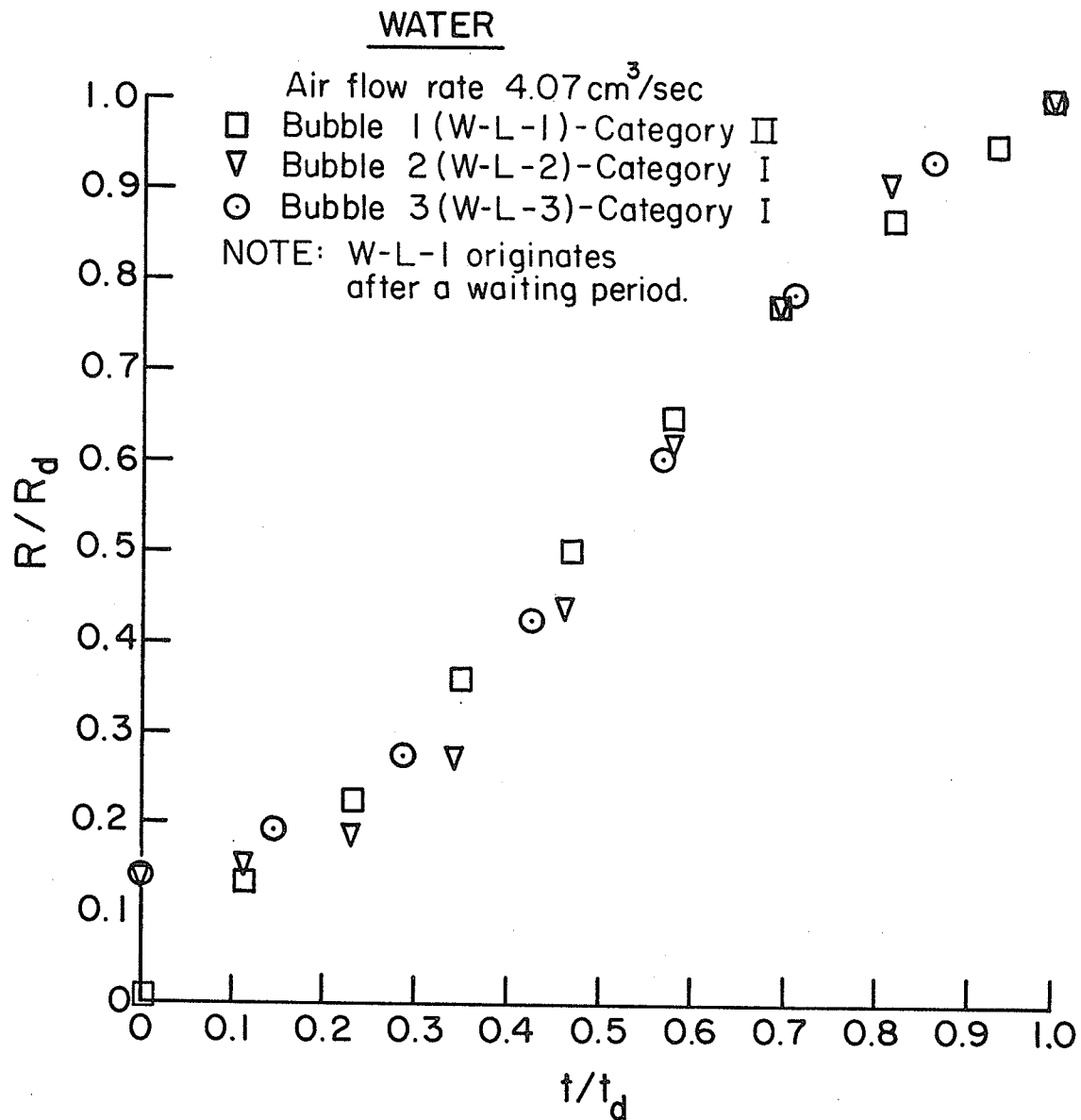


Fig. F.1 Bubble growth curves of Category I and Category II bubbles (water)

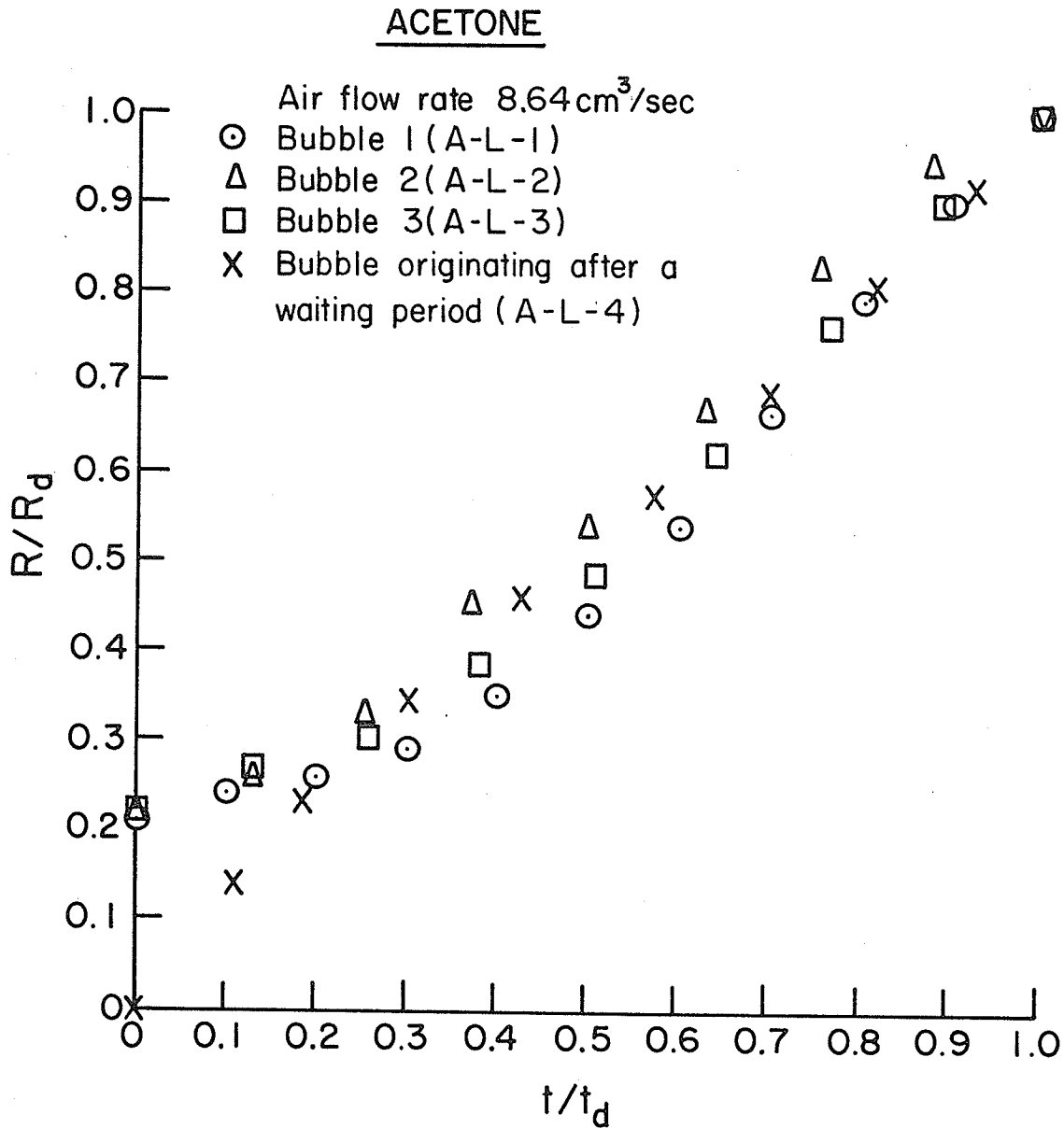


Fig. F.2 Bubble growth curves of Category I and Category II bubbles (Acetone)

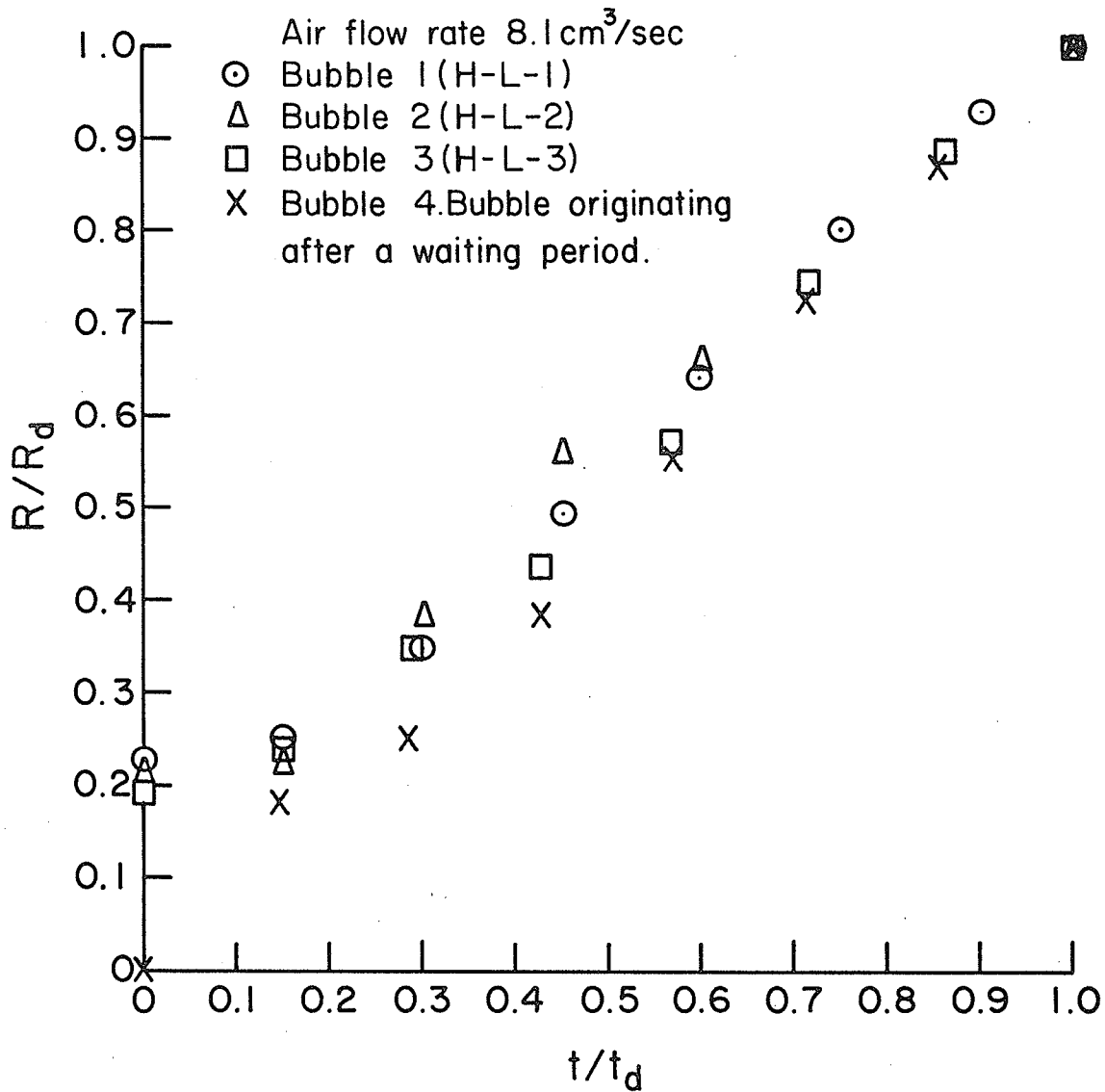
HEXANE

Fig. F.3 Bubble growth curves of Category I and Category II bubbles (hexane)

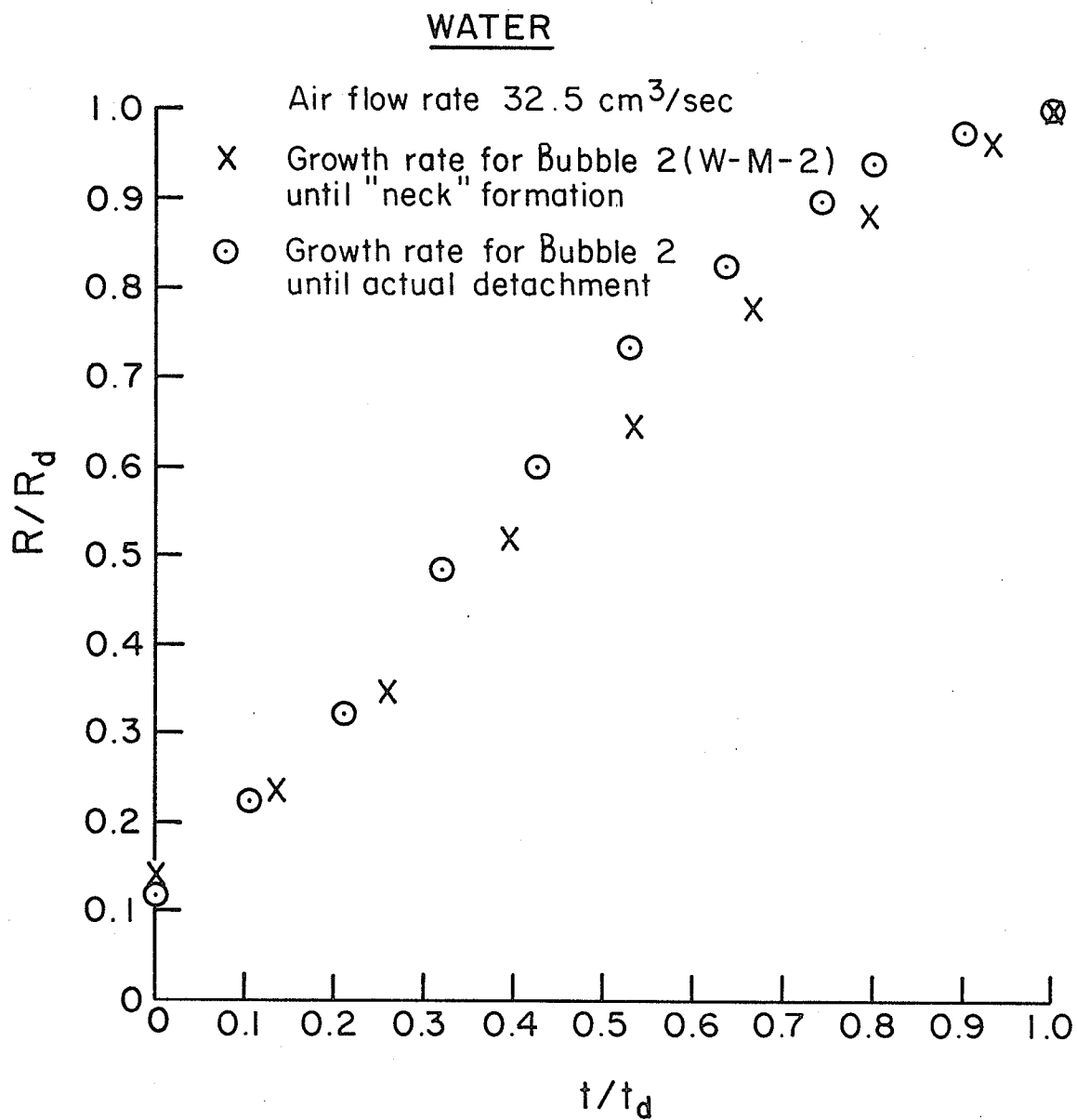


Fig. F.4 Bubble growth curves corresponding to the two departure criteria (water)

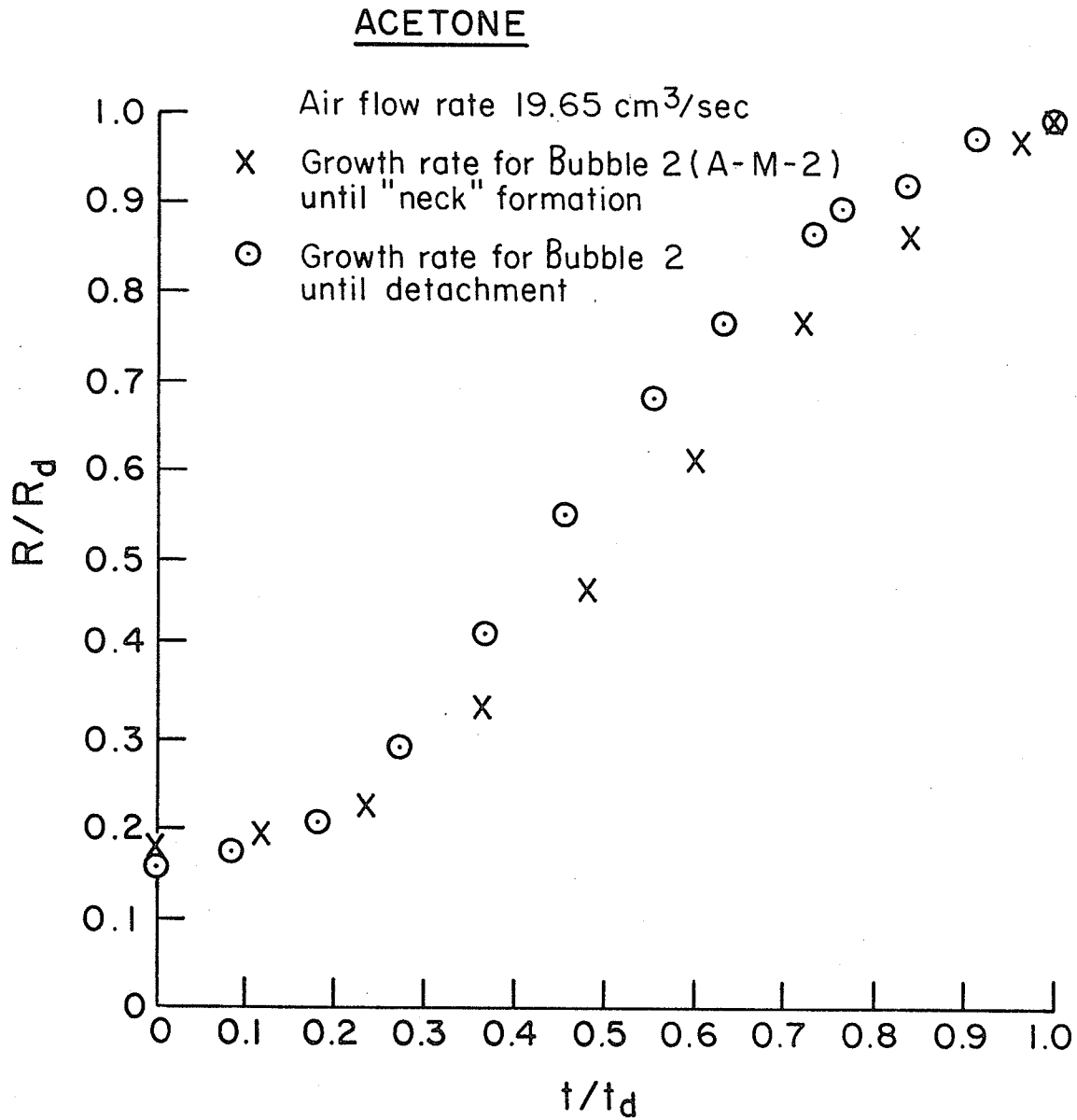


Fig. F.5 Bubble growth curves corresponding to the two departure criteria (acetone)

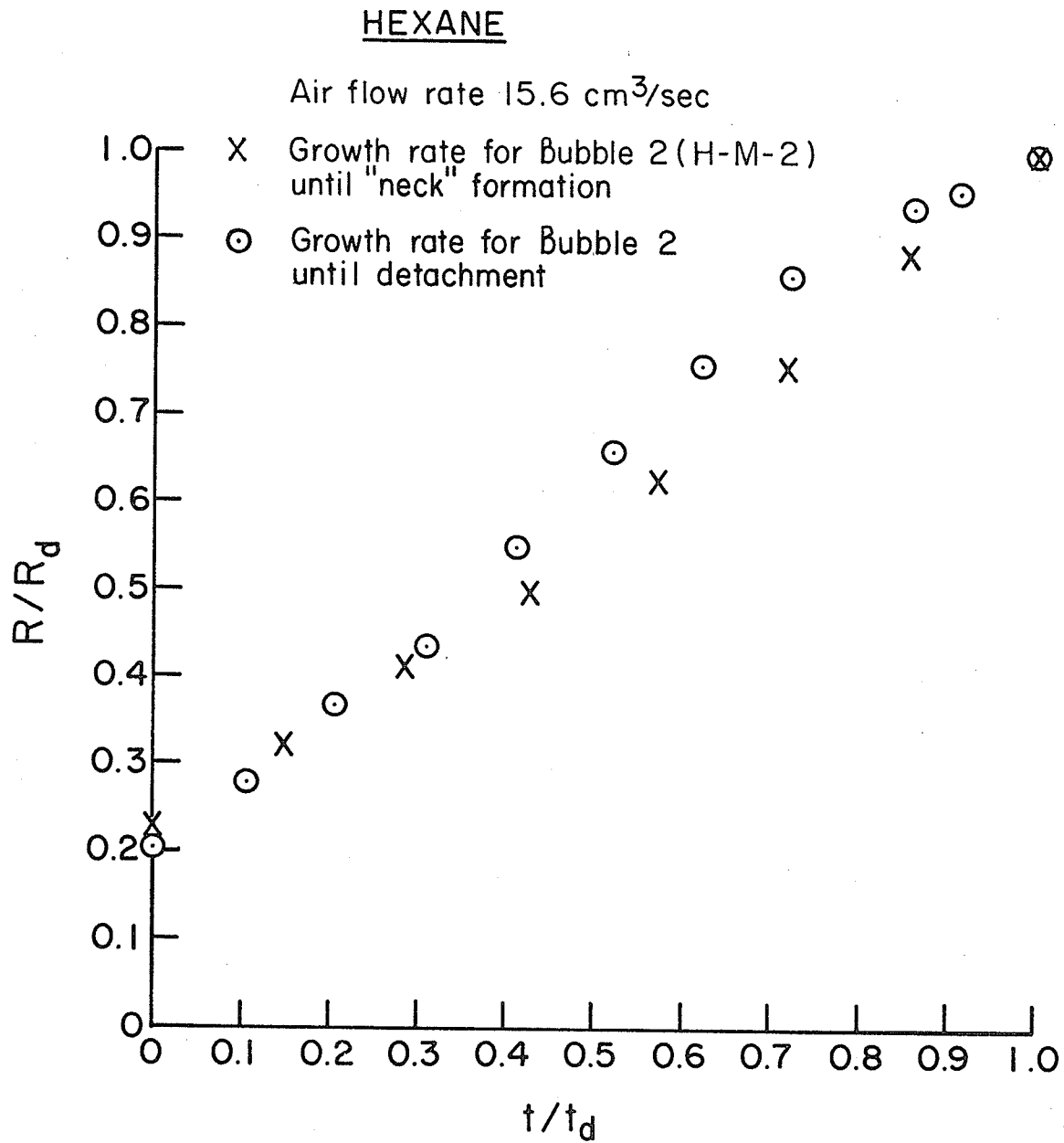


Fig. F.6 Bubble growth curves corresponding to the two departure criteria (hexane)

with a zero waiting time (at the flow rates quoted therein), but superimposed on these graphs are the growth curves of bubbles that originate after a waiting period. The end point for these curves again corresponds to the 'necking' point. A growth plot of one such bubble is given for each liquid and it is readily evident that the growth curves of the latter show no significant variation when compared with the rest.

Figures F.4 to F.6 present the growth curves of typical bubbles, each plotted according to the two different criteria above for the end of the life period of a bubble. It is apparent that differences in the growth curves arising from these two different criteria are not significant, especially when one considers the stochastic nature of bubble growth as evidenced, for instance, in Figs. 3.10, 3.13 and 3.16. Table F.1 gives the values of growth exponent n (method described in Sec. 3.4.4) for the two cases. It is seen that the values are very close.

Table F.1. Values for bubble growth exponents 'n' for the two cases discussed in Appendix F.

Liquid	Air Flow Rate cm ³ /sec	Bubble Growth Exponent 'n'	
		Till 'Neck' Formation	Till Detachment
water	32.50	0.75	0.71
acetone	19.65	0.83	0.82
hexane	15.60	0.62	0.60

APPENDIX G

GROWTH EQUATION $R^* = \theta^n$ USED

FOR BARBOTAGE DATA

It was stated in Sec. 3.4.4 that in order to compare barbotage and boiling growth rate data, the barbotage data was recast to fit a growth equation of the form $R^* = \theta^n$, where $R^* \equiv R/R_d$, $\theta \equiv t/t_d$, and n is the growth exponent.

Now, the above equation implies that the R^* vs θ curve passes through the point (0,0) in rectangular coordinates, whereas the bubble growth curves in Figs. 3.10 through 3.18 are seen to possess finite ordinate values at zero time. An estimate of the error introduced in the average growth exponent n due to this discrepancy was determined in the following manner.

Let V_0 be the volume of the bubble at zero time and V the volume at any time t during the growth period. $V - V_0$ then gives the increase in volume in time $t - t_0$ ($=t$) and if one were to plot the equivalent radius corresponding to $V - V_0$ vs t over the whole growth time in rectangular coordinates, one obtains a curve that passes through (0,0). A best fit growth equation of the form $R = at^n$ or $R^* = \theta^n$

(in the non-dimensional form) can then be applied 'with rigour' to describe the data. Applying this procedure together with the least squares fit, values of growth exponent n were obtained for one bubble for each liquid for each flow rate and compared with the n values obtained originally (i.e., without any modification to data as described above and given in Table 3.5). Table G.1 compares these values of n obtained with and without recasting the data as described above. The worst case seems to be that of hexane at the lowest flow rate, where the percentage variation is 28. However, considering the statistical variation of about 20 per cent existing in the growth rate of individual bubbles for any one flow rate, the above variation is not considered to be significant. Further, in spite of the individual variations existing in the two methods described, it is noteworthy that no value of n obtained by the method described in this appendix falls outside the range of n given in Table 3.5 for the barbotage data. In view of the above considerations it was decided to retain application of the equation $R^* = \theta^n$ to barbotage data obtained in the present work in its original form.

Table G.1. Growth exponents for barbotage bubbles obtained by the two methods discussed in Appendix G.

Liquid	Flow Rate cm ³ /sec	Range of 'n' For 3 Bubbles	'n'		
			Method I* (Average for 3 Bubbles)	Method II** (1 Bubble)	$\frac{\text{'n' Method II}}{\text{'n' Method I}}$ (Average)
water	60.5	0.56 - 0.67	0.60	0.70	1.16
	32.5	0.75 - 0.88	0.83	0.93	1.12
	4.07	0.97 - 1.2	1.10	1.00	0.91
acetone	32.4	0.55 - 0.71	0.63	0.72	1.14
	19.65	0.85 - 0.92	0.89	1.07	1.20
	8.64	0.66 - 0.67	0.67	0.80	1.19
hexane	30.4	0.59 - 0.78	0.69	0.62	0.90
	15.6	0.59 - 0.72	0.66	0.80	1.21
	8.1	0.76 - 0.77	0.77	0.99	1.28

* Method I - Values of 'n' obtained without modification of data and given in Table 4.2 (i.e., at time $t=0$; $V_b=V_0$; at time $t=t$, $V_b=V$).

** Method II - Values of 'n' obtained by method suggested in Appendix G. (i.e., at time $t=0$, $V_b=0$; at time $t=t$, $V_b=V-V_0$).

APPENDIX H

EQUATION OF MOTION FOR AN EXPANDING BUBBLE

The equation of motion for an expanding spherical bubble boundary can be derived by considering the motion of the liquid surrounding the bubble. Consider a spherical bubble in an incompressible liquid of infinite extent and let the origin of co-ordinates be at the bubble centre which is at rest. The radius of the bubble at any time t is R , and r' is the radius to any point in the liquid. Then, if in addition it is assumed that the liquid flow is irrotational, the velocity of the liquid can be derived from a velocity potential ϕ given by

$$\phi = R^2 \dot{R} / r' \quad (\text{H.1})$$

and the Bernoulli integral of the motion is,

$$-\frac{\partial \phi}{\partial t} + \frac{1}{2}(\nabla \phi)^2 + \frac{p(r')}{\rho_L} = p_\infty / \rho_L \quad (\text{H.2})$$

where $\dot{R} = \frac{dR}{dt}$; $p(r')$ is the pressure at r' and p_∞ is the pressure at a large distance from the bubble. Also, from Eqn. H.1,

$$(\nabla \phi)^2 = R^4 \dot{R}^2 / r'^4 \quad (\text{H.3})$$

$$\frac{\partial \phi}{\partial t} = \frac{1}{r'} (2R\dot{R}^2 + R^2\ddot{R}) \quad (\text{H.4})$$

Equation H.4 will be applied at $r' = R$ so that the equation of motion for the bubble radius is determined. Now,

$$\left(\frac{\partial \phi}{\partial t}\right)_{r'=R} = 2\dot{R}^2 + R\ddot{R} \quad (\text{H.5})$$

$$(\nabla \phi)_{r'=R}^2 = \dot{R}^2 \quad (\text{H.6})$$

so that Eqn. H.2 becomes

$$\frac{p(R) - p_{\infty}}{\rho_L} = \frac{3}{2}\dot{R}^2 + R\ddot{R} \quad (\text{H.7})$$

Equation H.7 is the general equation of motion for a spherical bubble in a liquid and with the pressure at the bubble boundary $p(R)$. Now, the instantaneous pressure $p_b(t)$ of the gas in the bubble can be obtained from Eqn. H.7 by accounting for the increase in pressure across the gas-liquid interface due to the surface tension along the interface. That is,

$$p_b(t) - \frac{2\sigma}{R} = p(R) \quad (\text{H.8})$$

Substituting Eqn. H.8 into Eqn. H.7 one obtains

$$\frac{p_b - p_{\infty}}{\rho_L} = R\ddot{R} + \frac{3}{2}\dot{R}^2 + \frac{2\sigma}{\rho_L R}$$

This equation is used further in Chapter 5.